DEVELOPMENT OF AN ARTIFICIAL MENISCUS IMPLANT

A Thesis
Presented to
The Academic Faculty

by

Trent Gardner Callcott

In Partial Fulfillment
of the Requirements for the Degree
Master of Science in the
School of Mechanical Engineering

Georgia Institute of Technology
May 2020

DEVELOPMENT OF AN ARTIFICIAL MENISCUS IMPLANT

Approved by:

Dr. David N. Ku, Advisor
School of Mechanical Engineering
Georgia Institute of Technology

Dr. Richard Neu
School of Mechanical Engineering
Georgia Institute of Technology

Dr. Kyle Hammond
School of Medicine
Emory University

Date Approved: April 20, 2020

ACKNOWLEDGEMENTS

I would like to thank Dr. David Ku for inviting me to join his lab and providing this opportunity to experience the initial stages of research and development of a device across multiple components of its design, verification, and validation. His expertise and guidance across these areas taught me more than I could have imagined and resulted in me becoming a far more comprehensive, strategic, and innovative engineer. These, among other skills I learned through this opportunity, are directly applicable to the career interests we discussed before I even started the project, and I will use them throughout all aspects of my future career. I will always be thankful for his mentorship and my experience in his lab.

I would also like to thank my past and present lab mates for their help throughout my project. Because the lab is diverse, we worked on very different projects; however, I greatly appreciated the help and advice as well as the opportunity to learn about fields outside of my own project. I enjoyed the lab environment created by you all and wish you all the best of luck with the rest of your projects and future endeavors.

I would like to thank my friends outside of the lab as well. Spending time with them provided a great outlet from my thesis work and into other activities that I enjoy.

Finally, I would like to thank my parents, Frank and Donna, and my sisters Lauren and Lea for always supporting me and remaining positive throughout my entire project. I wouldn't be where I am today without their love and drive for me to do my best. I am very lucky to have the support of such a great family always there for me.

TABLE OF CONTENTS

LIST OF TABLES

LIST OF FIGURES

SUMMARY

The menisci protect the knee by distributing the compressive loads experienced across the joint. They are able to accomplish this because of their wedge shape that conforms to the femur and tibia and their strong yet compliant structure. Meniscus lesions are among the most common orthopedic injuries, but all current treatments are only applicable to a limited number of tears or have poor clinical outcomes. The majority of the meniscus is avascular and has limited healing capacity. As a result, removal of the meniscus after a tear is the most common treatment but has shown development of osteoarthritis, increase in pain, and mechanical impairment of the joint. Accordingly, there is a need to develop a meniscus replacement. The work of this thesis developed an artificial meniscus implant with a similar shape, strength, compliance, and contact mechanics as the natural meniscus. Previous work on this implant showed that PVA gave the desired compressive properties and reinforcing Kevlar fibers had the desired strength. These materials needed to be designed into a composite implant and then tested for its durability and functionality.

In order to design the implant, design specifications were established from mechanical properties of the natural menisci and loads experienced in the knee joint. One design aspect of interest was the spacing of the fibers within the hydrogel. FEA was performed to observe trends between fiber spacing on implant deformation and stresses. The remaining design variables were chosen to either resemble the structure of the natural meniscus or ease manufacturing. The easier to manufacture variables represented design choices made by previous implants in order to see if they could be improved. The best implant design was chosen based on compression and delamination durability as well as contact stress functionality tests.

Once the best design was chosen, it underwent further durability and functionality testing. Tests focused on the strength and compliance of the overall implant and durability of the implant over prolonged use. Accordingly, compressive modulus and fiber tear out strength testing was performed where the design passed if it was at least as strong and compliant as the natural meniscus. High impact and cyclic compression and shear tests were performed to simulate the higher loads experienced in the knee across a year of use. After these tests, tibial contact pressure and radial extrusion testing was performed to evaluate the prolonged functionality of the implant.

All design specifications were met by the chosen implant design. The tests showed that the implant can provide the mechanical properties and functionality needed to serve as a meniscus replacement. To validate this, an animal study was designed to access durability as well as the biocompatibility and chondroprotection of the implant. A sheep shaped implant was designed for this test and cadaveric work was performed to provide a final design with proper fit and fixation within the knee. This animal study was not finished before this work was concluded so the results are not reported, but they should give insight into the effectiveness the implant and which future steps should be taken.

CHAPTER 1. INTRODUCTION AND BACKGROUD

1.1 Meniscus Structure and Function

The primary functions of the meniscus are load transmission and shock absorption within the knee. In doing this, its goal is to mitigate the compressive stress transferred through the knee by distributing this load across a large area. They absorb 50%–70% of the load across the knee and increase the tibiofemoral contact area by two to three times [1, 2]. Accordingly, the menisci are located between the femur and tibia with one on the lateral and one on the medial side of the knee, as seen in Figure 1. To allow for the greatest possible stress transfer, the meniscus has a curved superior surface to conform to the femoral condyle and a flatter inferior surface to align with the tibial plateau. However, the lateral and medial menisci have different shapes and dimensions. While they both conform to their interacting surfaces, the lateral meniscus is more circular and nearly encompasses the femoral condyle whereas the medial meniscus resembles a crescent shape and is larger. This may be because the medial side experiences more of the load in the knee. They are attached to the tibia at each horn, which provides semi-constrained mobility across the tibial plateau to allow for meniscus deformation and load dissipation.

In addition to its shape and position, the structure of the meniscus helps with its ability to dissipate compressive loads and survive the environment of the knee. About 72% of its weight is water, 21% is collagen (90% of this is type I collagen), and the remaining weight is primarily composed of fibrochondrocyte cells, proteoglycans, glycoproteins, and elastin [3-5]. The collagen fibers contribute directly to the strength and tensile stiffness of the meniscus and are organized in the network shown in Figure 2. The majority of the fibers are oriented circumferentially within the body of the meniscus as a primary component of its function, which is depicted in Figure 3.

Because of the wedged shape of the meniscus, it extrudes radially when compressed. However, excessive radial extrusion is prevented because of these circumferentially oriented fibers and ligaments that attach the horns to the tibia. This results in tensile hoop stresses in these fibers [6-8]. Radially oriented fibers encompass the bulk of the meniscus. A few radially oriented fibers also appear in the bulk of the meniscus woven through the circumferential fibers. Together, all of these radial fibers help to tie the meniscus together and prevent separation of the circumferential fiber network [9]. Exterior to this layer, the surfaces of the meniscus are composed of a random mesh of fibers that aid in low friction articulation with the contacting articular cartilage [10-12].

Even though the collagen structure of the meniscus is fairly uniform across its width, this is not the case for its vascularity. The meniscus contains blood vessels and nerves only in the peripheral 10-25 % of the tissue, as seen in Figure 4 [3-5]. This vascular and neural region is referred to as the red zone and the avascular and aneural region is referred to as the white zone. The healing capacity of each region is directly related to its blood circulation, which results in the majority of the meniscus being susceptible to permanent injury.

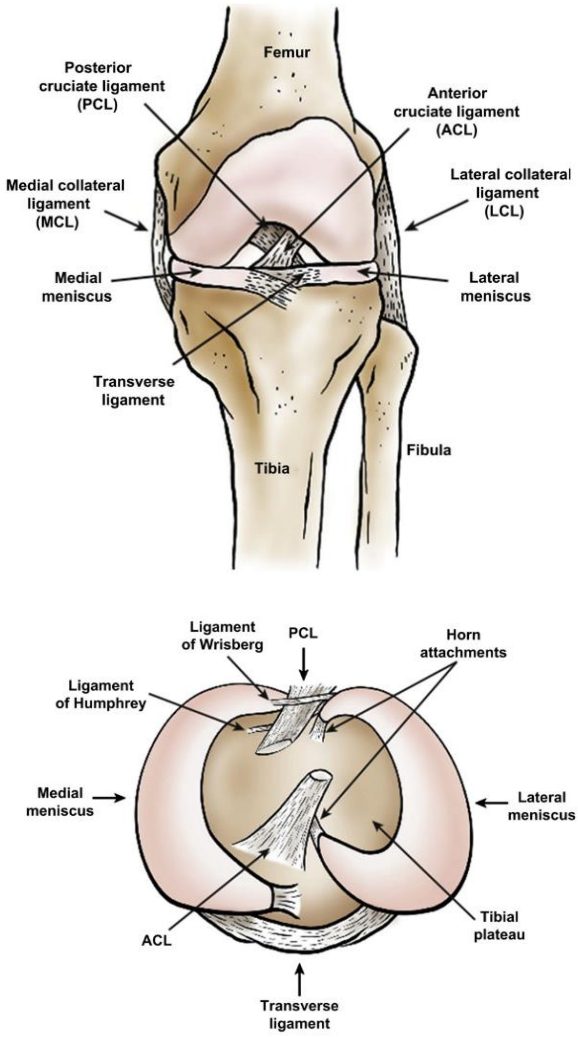

Figure 1: The anatomy of the knee (top) and the menisci with their horn attachments (bottom). [5]

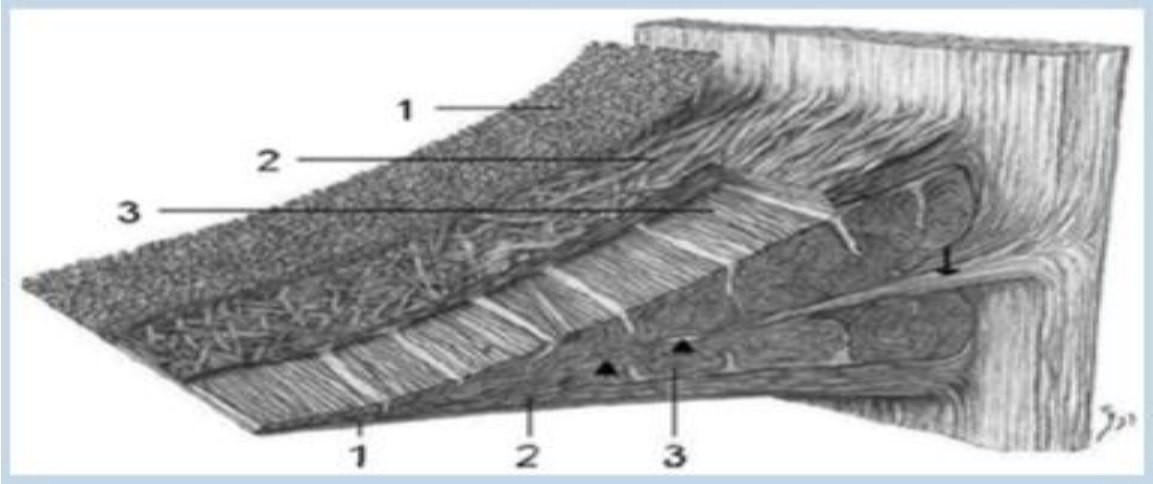

Figure 2: The ultrastructure and orientation of collagen fibers within the meniscus: the superficial network (1), radial layer (2), circumferential body (3). [13]

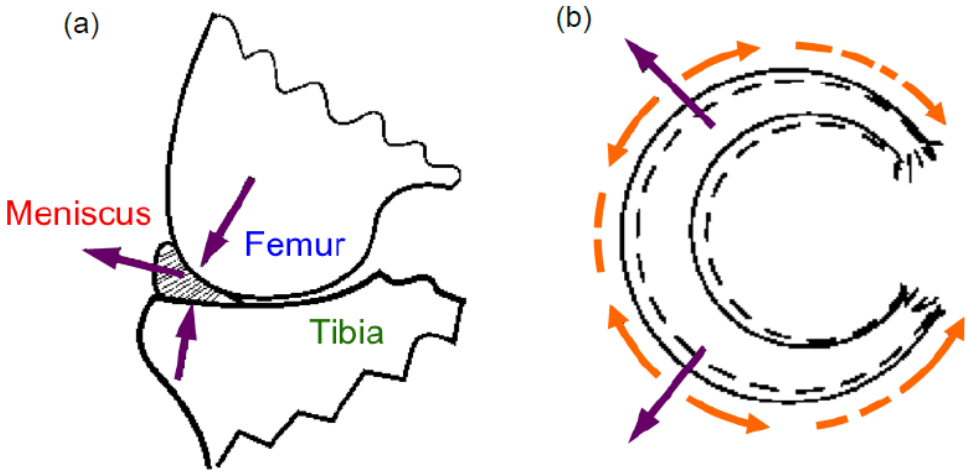

Figure 3: The loading and movement of the meniscus as the knee is compressed from a side view (a) and the hoop stresses created in the circumferential direction from resisting this radial extrusion (b). [14]

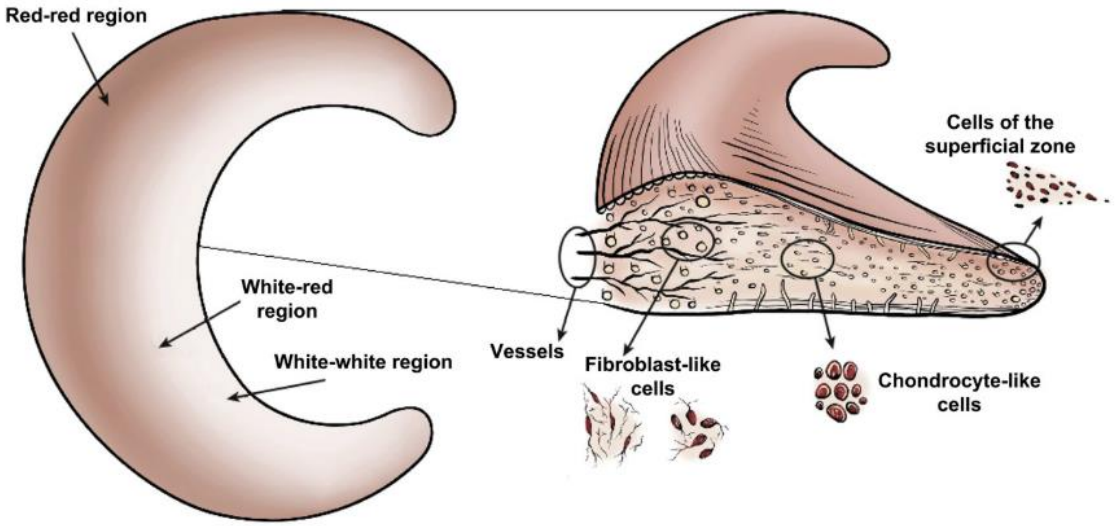

Figure 4: The vasculature of the meniscus including where vessels and certain cells are located. [5]

1.2 Meniscus Injuries

1.2.1 Prevalence

Meniscus injuries commonly result in knee pain, swelling, tenderness, and mechanical impairment. They occur in approximately 60-70 per 100,000 people annually [4, 5]. This incidence is increased to 8.27 per 1,000 for military service members and 145 per 1,000 for athletes [15, 16]. As a result, around 850,000 meniscus injury related surgeries occur in the USA every year, which makes up 10-20% of orthopaedic surgeries [16-19]. This number is on the incline as focus on youth sports grows and people retain increased levels of activity at higher ages [20, 21]. These injuries are three to four times more likely in men with peak incidence occurring between 20-29 years of age [4, 5]; however, people over 40 are reported to be four times more at risk of tearing a meniscus [18]. The

medial meniscus is injured four times more often than the lateral meniscus with the majority of these occurring in the right knee [4, 5].

1.2.2 Types of Injuries

There are two categories of lesions the meniscus can experience. Nearly 30% of lesions are degenerative tears. These are a result of cumulative stresses on aged tissue and are most commonly found in patients 40-70 years of age [22]. Traumatic tears make up the remaining lesions and are more prevalent among the youth [23]. They occur during sports, exercise, and nonactivity (the patient could not identify any specific incident that resulted in injury) in nearly equal proportions [24]. Despite the differences in injury method, it has been shown that these tears result from axial and shear loads within the knee [23]. When looking at traumatic tears resulting from a known injury, soccer, basketball, and skiing resulted in the highest number of lesions with the largest tears found in skiers [25]. Figure 5 shows examples of the most common types of traumatic tears. Overall, the most common tear types are the bucket handle (23.1%), longitudinal (18.2%), and horizontal (17.4%) [25]. Bucket handle and longitudinal tears occur between parallel circumferential fibers. Horizontal tears are thought to result from shear forces between the superior and inferior surfaces and tend to initiate within the body of the meniscus [22]. Longitudinal (22.1%), bucket-handle (32.4%), and oblique (16.8%) tears are the most common for the medial meniscus [25]. Radial (32.7%) and horizontal (25.8%) tears are the most frequent for the lateral meniscus [25]. Figure 6 shows the most common location of tears circled in red. Over 70% and 90% of traumatic tears occur in the 2 and 3 circumferential zones on the figure for the medial and lateral menisci respectively [25]. That means the majority of traumatic tears occur at least partially in the avascular and aneural white zone that greatly limits healing potential. In addition to tears, a relationship has been clinically shown between pain and both increased contact pressure on the

tibial plateau and excessive radial extrusion into the knee cavity [26-28]. Contact pressure and radial extrusion are related within themselves because as the meniscus extrudes, it covers a smaller area of the tibial plateau which results in increased contact pressures [29, 30]. Additionally, both excessive radial extrusion and increased contact pressure can indicate tearing of the meniscus.

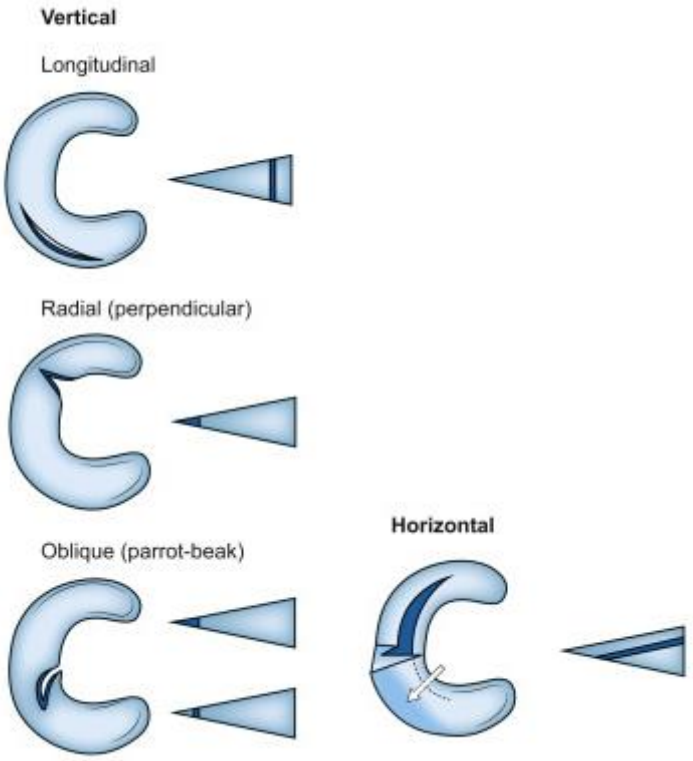

Figure 5: Common traumatic tear types. [31]

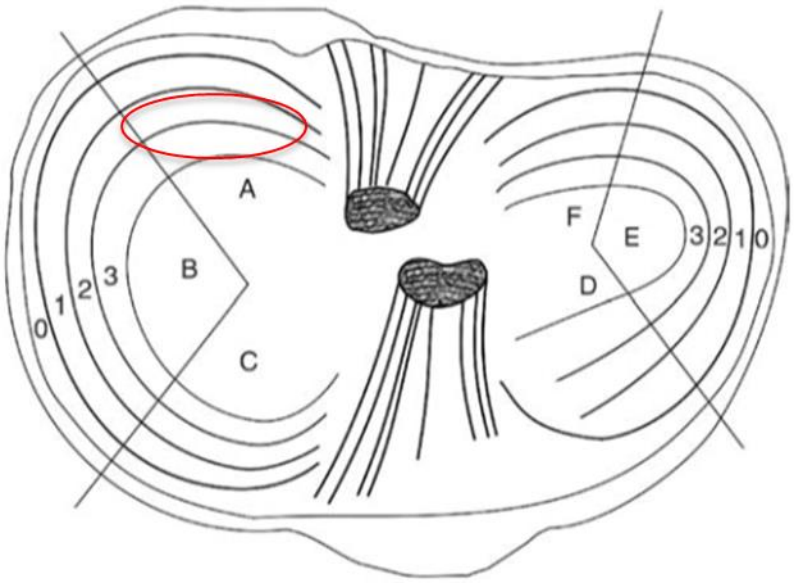

Figure 6: Most traumatic tears occur in the inner posterior region of the medial meniscus shown by the red circle. [25]

1.3 Current Treatments

1.3.1 Surgical Techniques

1.3.1.1 Repair

Surgical repair of a meniscus lesion involves adhering the edges of a tear with sutures or other similar methods. It is an attractive treatment because it can be done arthroscopically and has positive clinical outcomes. These outcomes range from a 50-90% clinical success rate depending on age of the patient, location, size, type of tear, and if additional knee repairs were performed [32-35]. However, in the largest data set found from this decade, repair was only used in about 4% of meniscus related surgeries because it is only effective for tears within the vascularized region

that can heal [36]. As discuss before, because over 70-90% of traumatic tears occur in the white zone, this overlap is not very common [25].

1.3.1.2 Meniscectomy

Meniscectomy is the partial or total removal of the meniscus depending on the severity of the tear. It is the most common treatment and makes up 96% of meniscus related procedures [36]. This treatment is so common because it is applicable to all lesion types and was traditionally recommended because the meniscus was thought to be a "functionless remnant vestige" [4]. However, the necessity of the meniscus has become apparent in the last few decades. Contact stresses have been shown to increase proportionally with the amount of meniscus removed, with an increase of 200-300% following a total meniscectomy due to a reduction of contact area up to 40-50% [2, 37, 38]. Figure 7 displays this relationship. Clinically, this has led to femoral condylar flattening and narrowing of the joint space [4]. Patients have shown a 14 time increase in the risk of radiographic osteoarthritis (OA) with 50% of patients experiencing symptomatic OA and a significantly higher incidence of knee pain compared to matched controls long term [28, 39].

1.3.1.3 Allograft

Meniscal allografts replace the patient's natural meniscus with one from a donor and are most often used for young to middle-aged patients presenting moderate to severe pain post-meniscectomy. They are implanted by either open surgery or arthroscopy and use sutures attached to the horns of the allograft to secure the implant by pulling these sutures through drilled bone tunnels in the tibia and then tying them together on the distal end as seen in Figure 8. Other methods leave blocks of donor bone attached to the allograft that are then secured to the patient's tibia using a similar bone tunnel approach. Sometimes, additional sutures are used to attach the peripheral

edge of the allograft to the tibial plateau or joint capsule. Typically, allografts are matched to the anterior-posterior (A-P) and medial-lateral (M-L) lengths of the patient's native meniscus with a 5% tolerance [40]. They have consistently better outcomes than repair with 75-90% of patients experiencing fair to excellent functional results following implantation [41]. However, allografts are known to shrink and undergo collagen remodelling and degeneration which can diminish their mechanical strength over time [41]. Between 2 and 10 years of use, around 30-46% of them failed, typically by tearing [42-45]. At 15 years of use, a study found the failure rate of allografts increased to 60% [20]. Furthermore, there is no level I evidence to support their role in halting the progression of osteoarthritis [46, 47]. Additional drawbacks include the limited number of available grafts, cost, graft sizing, immunological concerns, and the risk of disease transmission [18, 48, 49]. Currently, allografts are still the best treatment method but are used in less than 0.1% of meniscus related surgeries because of their limited availability [36].

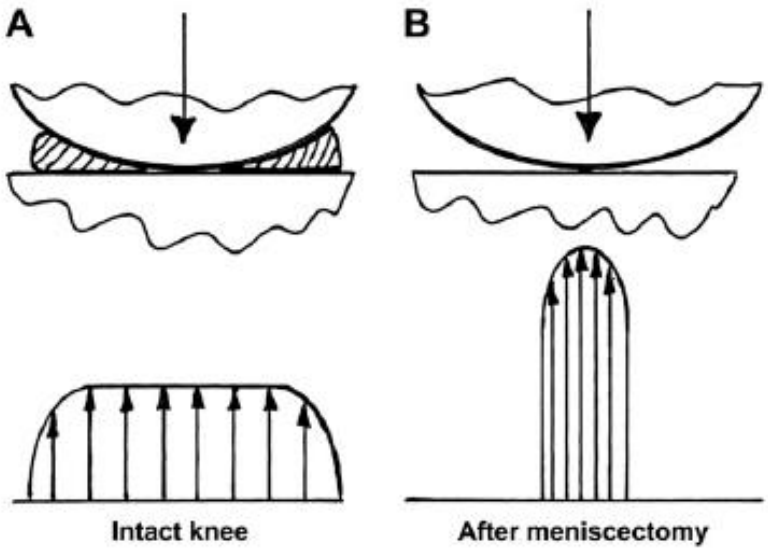

Figure 7: The contact area and stress for an intact knee (A) and following a meniscectomy (B). [10]

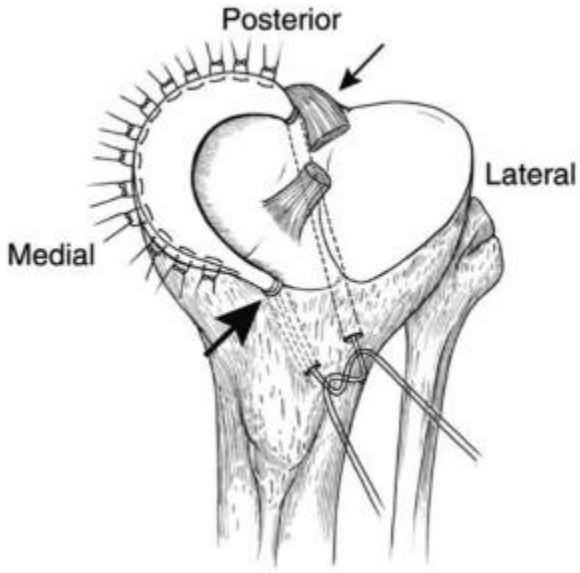

Figure 8: Attachment method of a meniscus allograft. [4]

1.3.2 Commercial Implants

1.3.2.1 Collagen Meniscus Implant

The Collagen Meniscus Implant (CMI) is a Food and Drug Administration (FDA) and Conformitè Europëenne (CE) approved scaffold intended to help regenerate the natural meniscus. It was designed to be implanted within the remaining portion of the meniscus after a partial meniscectomy and is shown in Figure 9. For this design to work, it is only intended for patients who have lost more than half of their meniscus but still retain an intact peripheral rim of the meniscus with secure attachment at both horns [20]. The scaffold is made of type I collagen, which is the bulk of the dry weight of the natural meniscus. The largest clinical study reported a reoperation rate of 9.5% at a mean follow-up of 5 years [50]. However, shrinkage and extrusion of the implant was observed during follow-up and persistent pain was noted in 12% of patients [51-54]. When compared to partial meniscectomy, acute patients were shown to experience no additional benefits and chronic patients experienced a 13% improvement on an activity index but not for any other clinical outcomes [55].

1.3.2.2 Actifit

Actifit is a CE mark approved synthetic scaffold comprised of polyurethane segments. It was originally designed as a total meniscus replacement but was not strong enough to resist the shear forces in the knee joint, so it was adapted to aid with tissue regeneration [56, 57]. It is implanted in a similar manner as the CMI and also requires a secure peripheral rim for attachment. The primary difference is that the scaffold is biodegradable. The scaffold fully degrades in 5 years and tissue in-growth is apparent after 12 months of implantation [58]. However, the in-growth does not resemble the tissue of the native meniscus even after 10 years of implantation. Recent clinical

trials have shown that the scaffold is not strong enough and fails within two years in 25% of cases. Additionally, they show that the regenerated meniscus is not fully mature by the time the scaffold fully degrades, leading to late failures and post-meniscectomy symptoms in nearly all cases [54, 58-61].

1.3.2.3 NUsurface

NUsurface has received FDA breakthrough device designation (prioritized devices with more efficient development, assessment, and review by the FDA) and is a CE mark approved meniscus replacement. It is made of polycarbonate urethane (PCU) and reinforced with polyethylene around its circumference, likely chosen in part because they are both already FDA approved materials. Similar to the CMI and Actifit, it is implanted in patients with an intact peripheral rim. However, it is disc shaped instead of resembling the shape of the natural meniscus. Because of the unique shape, the implant is free floating and positioned in the knee as seen in Figure 10. Clinical trials reported that 46% of patients with a NUsurface implant required removal of the device at 2 to 26 months with the most common complications being radial tears and dislocation of the device [59]. Additional complications including inflammation, effusion, and squeaking occurred in 78% of patients [59].

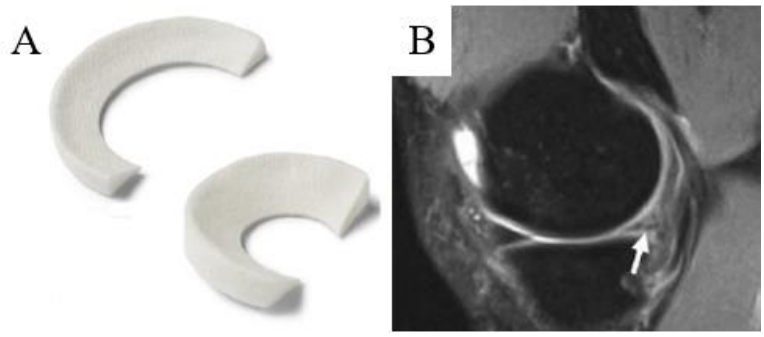

Figure 9: The CMI for medial and lateral implants (A) and an MRI showing implant placement and shrinkage indicated by the white arrow (B). [18]

Figure 10: NUsurface meniscal implant and positioning. [62]

1.3.3 Experimental Implants

1.3.3.1 Trammpolin

Trammpolin has received FDA breakthrough device designation and is a total meniscus replacement. Similar to NUsurface, it is made of PCU, but it is an anatomically shaped, does not require an intact peripheral rim, and is unreinforced. It is fixed to the tibia using custom screws as seen in Figure 11. Clinical trials have begun, but there are currently no reported results. A 12-month caprine study was performed with a goat shaped implant that used sutures for fixation in a similar manner to allograft fixation. The chondroprotective score for the implant was not statistically different than the allograft but was also not statistically different than meniscectomy and was significantly worse than the control. The implants experienced notable deformation with nearly a 5% increase in length and 11% decrease in posterior area, which is a greater difference in size than is recommended when matching allografts to patients. Along with the deformation, the implants exhibited twice the radial extrusion as the control meniscus. Of the seven implants tested, one implant experienced a complete tear of the posterior horn [63].

1.3.3.2 Polyvinyl Alcohol Implants

Kobayashi et al. developed polyvinyl alcohol (PVA) implants because of their compressive strength and viscoelastic behavior that mimicked that of the natural meniscus even after two years of implantation in a rabbit [64, 65]. However, when used in a large animal, the implants experienced severe damage primarily by radial tearing [66]. Holloway developed a PVA implant reinforced with a weave of polyethylene fibers to strengthen the device while maintaining the desired compressive and viscoelastic properties. However, the implant experienced delamination

of the fibers from the PVA in 2 of the 3 cases and excessive radial extrusion of all implants in an ovine model. The implant and failure mode are shown in Figure 12 [67].

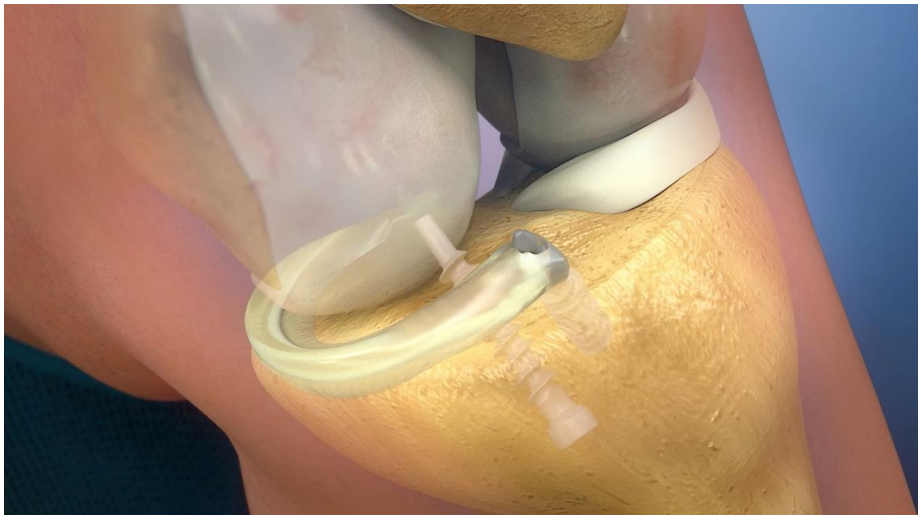

Figure 11: Trammpolin implant and fixation. [68]

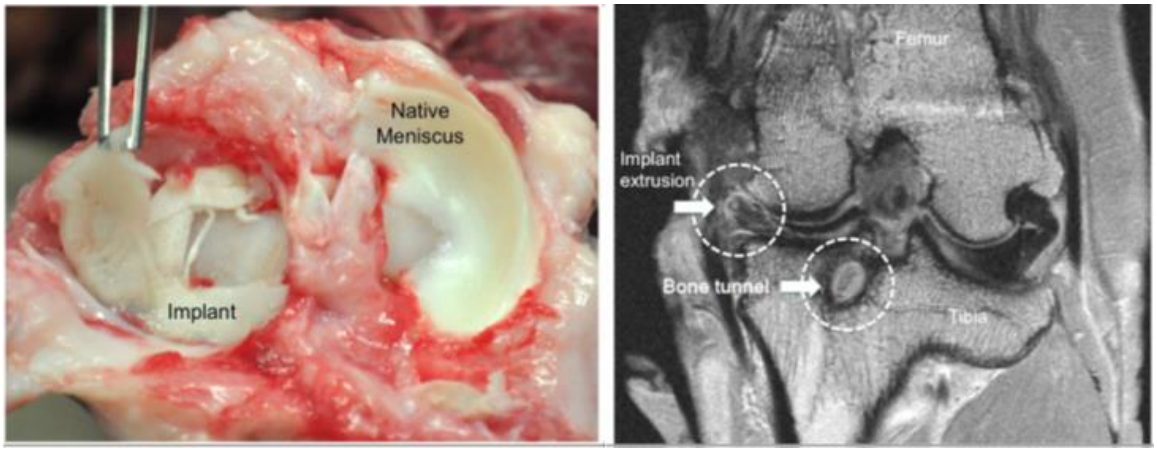

Figure 12: Holloway PVA implant and failure modes. [67]

1.4 Previous Work on the Proposed Implant

1.4.1 Material Selection

A prosthetic meniscus implant must be durable yet compliant to exhibit the strength and pressure distribution functionality of the native meniscus. This can be accomplished by a composite implant comprised of a flexible bulk material and a strong reinforcing material. Previous work in the Biofluids and Medical Device Research Group was done to test PVA as the bulk material for its compressive properties and Kevlar as the reinforcement for its tensile properties [69]. PVA is a hydrogel that can be made with varying amounts of solution and freeze/thaw cycling that allow its mechanical properties to be tuned [67, 70-73]. This hydrogel was chosen because it can be adjusted to closely mimic the compressive and viscoelastic properties of meniscus tissue [65, 74-78]. Additionally, PVA has already received FDA approval for use as a cartilage replacement device in joints and has positive clinical results [79-81]. Kevlar is an aramid fiber with high strength and stiffness. Additionally, Kevlar was shown to be as safe and biocompatible as FDA approved nylon sutures in a tendon cell model [82]. These fibers were chosen because they incorporate well with the hydrogel due to their hydrophilicity and can be easily manipulated to mimic the orientation, positioning, and function of the fibers in the native meniscus. The design that resulted from combining these materials in this work is shown in Figure 13. It incorporated a weave of Kevlar fibers parallel to the inferior surface and one grouping of circumferential fibers following the peripheral edge of the implant. This is referred to as the weave design throughout the rest of this thesis.

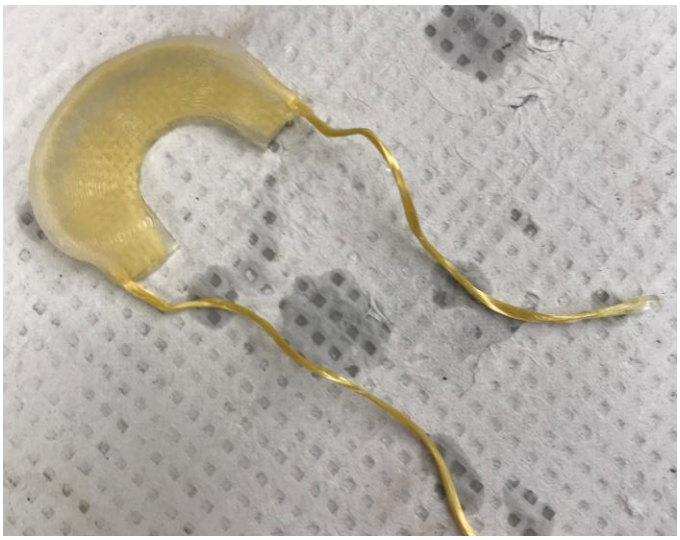

Figure 13: PVA and Kevlar weave design. [69]

1.4.2 Material Property Tests

1.4.2.1 Tensile Properties

The tensile properties of the Kevlar fibers are important because they function as both the circumferential and radial fibers of the meniscus. This means they help convert the compressive loads on the implant into tensile hoop stresses, strengthen the bulk of the implant, limit radial extrusion and implant mobility, and are used for implant fixation. Accordingly, the tensile properties of interest were ultimate tensile strength and modulus of the composite material.

The ultimate tensile strength and tensile modulus of the Kevlar circumferential fiber composite samples were compared to those of the native meniscus. It was shown that by using at least four fiber bundles, the composite was within the strength range of the native meniscus in the circumferential direction. An additional strength test was performed to evaluate the force required

to tear a four fiber bundle grouping out of the hydrogel when integrated into a full implant, but the nonembedded portion of the fibers failed before there was any PVA/Kevlar separation. This test showed that using the four fiber bundles extending from the implant for fixation was as strong as the average sectioned/repaired meniscus roots but was weaker than healthy ones [83]. Composite samples with four fiber bundles were then tested to a max physiological circumferential tensile strain of 5% to evaluate the material stiffness. This yielded a higher tensile modulus than seen in the natural meniscus of 589 MPa instead of 50-300 MPa [84, 85]. However, this was acceptable because the tensile stiffness was only being considered to ensure the material was not too compliant and result in excessive implant deformation or extrusion. Additionally, metal spacer devices used in the knee have a modulus around 200 GPa, whereas the material of the implant has a modulus on the same order of magnitude as the native meniscus [86].

In order to observe how well these tensile properties are maintained, a composite sample with four fiber bundles was cyclically pulled in tension 1,000 times to 1.5 times the maximum tension experienced by the meniscus during gait. The ultimate tensile strength and modulus were retested after the cycling to identify any changes in these properties. After the cycling, there was an increase in strength from 20.2 MPa to 21.9 MPa and modulus from 589 MPa to 709 MPa. The stiffening was shown to happen progressively over time and believed to be caused by the hydrogel losing water during stretching. However, in the knee environment, this same drying out effect seen in an open-air environment would not occur. Even with these value changes, the tensile properties of the composite material stayed above the threshold values which may even be considered an improvement.

The importance of tensile strength and stiffness of the implant were expressed in a tibial contact pressure distribution test. A PVA only implant and a PVA/Kevlar composite implant of the same

shape were inserted in a Somso NS 50 bone model (Marcus Sommer SOMSO Modelle GmbH, Coburg, Germany) and compressed to the load experienced when standing on two legs. From literature, the peak tibial pressure experienced in this test is 3 MPa for a native meniscus and 6 MPa for a meniscectomy [37, 87]. The PVA/Kevlar implant had a peak and average contact pressure of 2.82 MPa and 0.80 MPa respectively; whereas, the unreinforced implant resulted in an increased peak and average contact pressure of >3.06 MPa (the peak pressure exceeded the upper limit of the pressure film) and 1.10 MPa respectively.

1.4.2.2 Shear Properties

The shear properties of the bulk of the implant are important to ensure it can survive the environment of the knee during daily activities. Accordingly, the shear property of interest was the shear strength of the PVA material.

The shear strength of the PVA samples was compared to the maximum shear experienced in the knee during daily activities. The samples were tested to failure and survived to a force 2.6 times higher than what was seen in vivo. Even though this was not a cyclic test and did not integrate the Kevlar fibers, it still provided confidence that the PVA could survive the daily shear force experienced in the knee.

1.4.2.3 Compressive Properties

The compressive properties of the PVA are important because they incorporate the pressure dissipation and shock absorption functions of the meniscus. Accordingly, the compressive property of interest was the compressive modulus of the composite material.

The compressive modulus of the PVA/Kevlar composite samples was compared to that of the native meniscus. Even though the strength and stiffness of the meniscus in the radial direction is less than those in the circumferential direction, a weave of Kevlar fibers was implemented as the radial fibers [85]. This was because the primary concern of the tensile properties is ensuring the implant is strong enough to survive the environment of the knee and stiff enough to not excessively deform or radially extrude. Composite samples were cyclically compressed to find their moduli and yielded a slightly higher compressive modulus of 1.63 MPa than the modulus range 0.30-1.16 MPa seen in the natural meniscus [88].

In order to observe how well these compressive properties are maintained, a composite sample with a fiber weave was monotonically compressed to the maximum stress experienced in the knee during common daily activities and was cyclically compressed 1,000 times to the stress experienced during gait. The modulus and sample height were remeasured after one and three daily activity compressions, an additional 1,000 gait cycles, followed by another daily activity compression, an overnight recovery period, and a final daily activity compression. The moduli decreased to around 1.2 MPa for the one through five daily activity compressions. The greatest change in modulus was seen after the additional 1,000 gait cycles, which decreased the modulus to 0.94 MPa. This may prove to be a beneficial characteristic of the composite since the natural meniscus modulus has been shown to decrease after cycling as well [89]. Additionally, the heights of the samples did not decrease by more than 5% after the three daily activity compressions and the 1,000 gait cycles, expressing the material's resistance to plastic deformation. After allowing the sample to rest overnight, the composite recovered to a modulus that was not statistically different from the initial modulus.

The importance of compliance of the implant was expressed in a tibial contact pressure distribution test. A stiffer Somso NS 50 meniscus model and the PVA/Kevlar implant of the same shape were inserted in a Somso NS 50 bone model and compressed to the load experienced when standing on two legs. The PVA/Kevlar implant had a peak and average contact pressure of 2.82 MPa and 0.80 MPa respectively; whereas, the stiffer implant resulted in an increased peak and average contact pressure of 3.04 MPa and 1.09 MPa respectively.

1.4.3 Implant Geometry

The wedged shaped of the meniscus largely contributes to its proper function. The curved superior surface not only adheres to the shape of the femur and increases its contact area, but it also converts the compressive force into the hoop stresses that help reduce radial extrusion and contact pressure on the tibia. As a result, the implant shape was designed to also incorporate a curved superior surface with a similar overall geometry and size as the native meniscus.

The importance of implant shape was expressed in a tibial contact pressure distribution test. An implant shape modelled after generic native meniscus dimensions found in literature and an implant with the proposed shape that was modelled after a Somso NS 50 meniscus model with slightly larger dimensions that increased its contact area were both made of PVA and Kevlar and inserted in a Somso NS 50 bone model and compressed to the load experienced when standing on two legs. The proposed implant shape had a peak and average contact pressure of 2.50 MPa and 0.89 MPa respectively; whereas, the generic shape implant resulted in an increased peak and average contact pressure of >3.06 MPa (the peak pressure exceeded the upper limit of the pressure film) and 1.08 MPa respectively.

The material properties and contact pressure functionality of the materials and shape used for a meniscus implant were investigated and proven promising. As a result, these components laid the groundwork to design a final meniscus implant.

CHAPTER 2. IMPLANT DESIGN

2.1 Risk Management and Design Controls

2.1.1 Intended Use

The Artificial Implant is intended for replacement of the medial meniscus in the osteoarthritic knee, where substantial degeneration and/or injury associated with the medial meniscus has occurred resulting in moderate cartilage degeneration (grade III chondromalacia). The Artificial Implant is intended to be implanted in the knee as a fixated, intra-articular support with minimal movement of the device after implantation. The Artificial Implant is intended for patients of all ages who are moderately active but will not participate in activities classified as extreme sports/recreation and exercises following device implantation.

2.1.2 Risk Analysis

2.1.2.1 Methods

A Failure Modes, Effects, and Criticality Analysis (FMECA) was used to identify failure modes, their effects, and solutions for the weave design and previously described test methods. This standard is recognized by the FDA as relevant to medical devices because of its scientific and technical merit and because it supports existing regulatory policies. The process used was modeled after a method outlined to access failure mode severity, occurrence, and detectability [90]. Severity of failure modes is displayed in Table 1 and was rated based on safety and impact on device function. Occurrence is shown in Table 2 and was assigned based on the average failure rates for allografts with 20% as the moderate failure cutoff [91]. Within this, the different types of failure

modes were assigned an occurrence rating in accordance with the frequency that each type of tear is experienced in the natural meniscus. The breakdown of the incidence of each type of tear was detailed in the previous chapter. Detection ratings are displayed in Table 3 and were based on the previous weave implant design and test methods used for its development. For each risk, these three ratings were multiplied together to achieve a Risk Priority Number (RPN). Any failure mode with an RPN above 20 was deemed critical and required recommended actions to mitigate the risk.

2.1.2.2 Results

The FMECA generated is shown in Table 4. This FMECA is only intended for use during the feasibility stages of development. As a result, failure modes associated with manufacturing, packaging, and implementation were partially addressed and will need additional assessment of risk as those processes become well established in later development. The risks resulting from durability and performance of the implant were based on failures and effects seen with the natural meniscus, allografts, and other meniscus replacements that have undergone clinical or animal trials [63, 66, 67, 92-94]. In order to condense the length of the FMECA, each potential cause of failure was combined into one row after being introduced. All risks with an RPN above 20 received a recommended device design and/or test action highlighted in yellow. These recommended actions are elaborated in the design inputs and verification test methods sections.

Table 1: Severity ratings for risk analysis.

Rating	Meaning
1	No Effect – No reduction in safety or performance
2	Slight – Customer slightly annoyed. Slight effect on product performance
3	Moderate – Customer experiences some dissatisfaction. Moderate effect on product performance
4	Major – Customer dissatisfied. Product performance severely affected but functionable and safe. Product impaired
5	Hazardous – Safety related. Sudden failure. Non-compliance with government regulation

Table 2: Occurrence ratings for risk analysis.

Rating	Meaning
1	Almost Never – Failure unlikely. History shows no failure
2	Low Failures – <5% incidence
3	Moderate Failures – 5% to 20% incidence
4	High Failures – 20% to 50% incidence
5	Very High Failures – >50% incidence

Table 3: Detection ratings for failure analysis.

Rating	Meaning
1	Almost Certain– Tests are proven detection methods
2	High Detection – Tests are validated and/or worst-case scenario simulation and/or modelling of entire device and environment
3	Medium Detection – Tests are on individual components of device
4	Low Detection – Tests are on components similar to device. Tests only address short or long durability of device
5	Almost Impossible Detection – No known techniques available or used

Table 4: FMECA for the weave design.

Design Function	Potential Failure Mode	Potential Effect(s) of Failure	S	Potential causes of failure	O	Current Design Controls	D	RPN	Recommended actions
Bulk meniscus strength	Partial radial tear	Slight mechanical impairment (popping, catching) from unsmooth implant surface	3	Insufficient radial longevity	2	Fiber cyclic testing; Implant design with radial reinforcement	1	6	None
			3	Insufficient radial strength	2	Fiber strength testing; Implant design with radial reinforcement	1	6	None
		Propagation risk to large size	4	Insufficient radial reinforcements throughout hydrogel	2	Fiber cyclic testing; Implant design with radial reinforcement	3	24	Implant design with radial reinforcement near surface where tear originates; Implant compression and shear cyclic testing
	Large radial tear (90% or more)	Accelerated cartilage degeneration from increased contact pressure	4	Insufficient radial longevity/ strength/ reinforcement	2	Fiber cyclic and strength testing; Implant design with radial reinforcement	3	24	Implant design with radial reinforcement near surface where tear originates; Implant high impact testing
		Pain/tenderness from increased contact pressure	4	Insufficient radial longevity/ strength/ reinforcement	2	Fiber cyclic and strength testing; Implant design with radial reinforcement	3	24	Implant design with radial reinforcement near surface where tear originates; Implant high impact testing
		Mechanical impairment (locking, buckling)	4	Insufficient radial longevity/ strength/ reinforcement	2	Fiber cyclic and strength testing; Implant design with radial reinforcement	3	24	Implant design with radial reinforcement near surface where tear originates; Implant high impact testing
	Partial longitudinal tear	Slight mechanical impairment (popping, catching)	3	Insufficient longitudinal longevity/ strength	3	Circumferential cyclic and strength testing; Implant design with reinforcement	1	9	None
		Propagation risk to large size	4	Insufficient circumferential reinforcement throughout hydrogel	3	Circumferential cyclic and strength testing;	3	36	Implant design with circumferential

Table 4 Continued

						Implant design with reinforcement			reinforcement throughout hydrogel cross-section; Implant compression and shear cyclic testing
	Complete longitudinal tear (bucket handle)	Accelerated cartilage degeneration from increased contact pressure	4	Insufficient longitudinal longevity/ strength/ reinforcement	3	Circumferential cyclic and strength testing; Implant design with reinforcement	3	3 6	Implant design with circumferential reinforcement throughout hydrogel cross-section; Implant high impact testing
		Pain/tenderness from increased contact pressure	4	Insufficient longitudinal longevity/ strength/ reinforcement	3	Circumferential cyclic and strength testing; Implant design with reinforcement	3	3 6	Implant design with circumferential reinforcement throughout hydrogel cross-section; Implant high impact testing
		Mechanical impairment (locking, buckling)	4	Insufficient longitudinal longevity/ strength/ reinforcement	3	Circumferential cyclic and strength testing; Implant design with reinforcement	3	3 6	Implant design with circumferential reinforcement throughout hydrogel cross-section; Implant high impact testing
	Horizontal tear	Meniscal cysts and local swelling	3	Insufficient hydrogel longevity/ strength	2	Hydrogel shear strength testing	4	2 4	Composite shear cyclic testing
	Oblique tears	Mechanical impairment (flap catching)	4	Insufficient longitudinal or radial longevity/ strength/ reinforcement	3	Fiber cyclic and strength testing	2	2 4	Implant design with reinforcement spaced across hydrogel; Implant high impact testing
		Propagation risk to complete longitudinal	4	Insufficient longitudinal or radial reinforcement	3	Fiber cyclic and strength testing	2	2 4	Implant design with circumferential reinforcement throughout hydrogel cross-section; Implant compression and shear cyclic testing
	Compressive deformation	Joint space narrowing – potential increase in contact stress and cartilage damage	3	Insufficient hydrogel longevity/ compressive strength and stiffness	3	Compressive and cyclic testing for modulus and deformation	1	1 2	Compressive modulus and deformation will have to be reevaluated if weave design is changed

Table 4 Continued

	Reinforcement/ attachment fiber tear out (partial)	Slight mechanical impairment (popping, catching) from loose fibers	3	Insufficient strength or number of reinforcing fibers	2	Tensile strength testing of composites	1	6	None
			3	Improper layout of reinforcing fibers	2	Fiber tear out testing of implants	1	6	Fiber tear out will have to be reevaluated if circumferential fiber design is changed
		Reduced strength; risk of additional fibers breaking	4	Insufficient strength / number / improper layout of reinforcing fibers	2	Tensile strength and fiber tear out testing	2	16	None
	Reinforcement/ attachment fiber tear out (complete)	Mechanical impairment (locking, buckling) from implant dislocation	4	Insufficient strength or number of reinforcing fibers	2	Tensile strength testing of composites	1	8	None
	Delamination of composite	Reduced stress transfer – potential increase in contact stress, cartilage damage, and hydrogel tear	3	Insufficient interfacial adhesion of reinforcing fibers and hydrogel	3	Fiber tear out testing of implants; Hydrophilic fibers; Implant design with base weave reinforcement	3	27	Shear cyclic testing
			3	Improper integration of fibers into hydrogel matrix	2	Fiber tear out testing of implants	3	18	Optimize reinforcement to increase fiber/ hydrogel surface interaction; Shear cyclic testing
		Mechanical impairment from dislocation of hydrogel component	4	Insufficient interfacial adhesion of reinforcing fibers and hydrogel	3	Fiber tear out testing of implants; Hydrophilic fibers; Implant design with base weave reinforcement	3	36	Shear cyclic testing
			4	Improper integration of fibers into hydrogel matrix	2	Fiber tear out testing of implants	3	24	Optimize reinforcement to increase fiber/ hydrogel surface interaction; Shear cyclic testing
	Unnatural tibial pressure distribution	Accelerated cartilage degeneration from increased contact pressure	4	Insufficient tibial/femoral interfacing/strengths/fixation/geometry	3	Implant design with base weave reinforcement and anatomic geometry; Pressure distribution	2	24	Anatomic fiber orientation for pressure distribution and implant tensile properties

Table 4 Continued

						testing with reinforced/fixed implant			
		Pain/tenderness from increased contact pressure	4	Insufficient tibial/femoral interfacing/strengths/fixation/geometry	3	Implant design with base weave reinforcement and anatomic geometry; Pressure distribution testing with reinforced/fixed implant	2	24	Anatomic fiber orientation for pressure distribution and implant tensile properties
Fixation	Attachment tear at horns	Accelerated cartilage degeneration from insufficient tibial plateau coverage; Pain/tenderness from excessive extrusion	4	Insufficient attachment fiber strength	2	Attachment fiber tensile testing; Implant design with all circumferential fibers as attachment fibers	1	8	None
			4	Insufficient horn strength/reinforcement	3	Attachment fiber tensile testing; Implant design with slightly increased horn area	2	24	Implant high impact testing
	Radial extrusion	Accelerated cartilage degeneration from insufficient tibial plateau coverage; Pain/tenderness from excessive extrusion	4	Insufficient circumferential strength / reinforcement	3	Implant design with circumferential fibers; Tensile testing	1	12	None
			4	Improper layout of reinforcing fibers	3	Implant design with circumferential fiber bundle	3	36	Anatomic fiber orientation for implant tensile properties; Radial extrusion testing
	Bone tunnel widening	Slight fixation impairment	1	Insufficient implant anchoring stiffness	3	Surgical design option specs from literature	4	12	None
	Implant dislocation	Slight fixation impairment	2	Insufficient implant anchoring stiffness	3	Fix implant by tying the attachment fibers of each horn together on the distal side of the bone tunnels	4	24	Fix implant using interference screws; in vivo macroscopic dislocation analysis
		Accelerated cartilage degeneration from	4	Implant anchoring slippage	3	Fix implant by tying the attachment fibers of each	4	48	Fix implant using interference screws; in

Table 4 Continued

		insufficient tibial plateau coverage; Pain/tenderness from excessive extrusion				horn together on the distal side of the bone tunnels			vivo macroscopic dislocation analysis
			4	Improper implant geometry	2	Implant design with anatomic geometry; Pressure distribution testing with reinforced/fixed implant	2	16	None
Implant/cartilage interface	Extensive wear of implant	Joint space narrowing – potential increase in contact stress and cartilage damage	3	Insufficient contact stress distribution	2	Pressure distribution testing with reinforced/fixed implant; Implant design with maximized contact area (curvature)	2	12	None
			3	Insufficient shear/tensile strength near surface (of hydrogel only)	2	Tensile and shear strength testing of hydrogel	2	12	None
		Inflammation from wear particles	4	Excessive number of wear particles from composite roughness and lubricity	1	PVA literature wear rate values	4	16	None
			4	Excessive size of wear particles from composite roughness	2	PVA literature wear particle sizes and in vivo performances	4	32	In vivo inflammation analysis
	Extensive wear of articular cartilage	Accelerated cartilage degeneration from wear	4	Insufficient contact stress distribution	2	Pressure distribution testing with reinforced/fixed implant; Implant design – maximized contact area (curvature)	3	24	In vivo macroscopic and histological articular cartilage analysis
		Slight mechanical impairment (popping, catching) from unsmooth implant surface	3	Excessive implant surface roughness	2	PVA literature roughness values	3	18	None
	Increased joint friction	Slight motion impairment	2	Insufficient lubricity/excessive roughness and stiffness	2	Implant design with stiff reinforcements further from interface and hydrogel material to	3	12	None

Table 4 Continued

						maintain lubricity			
	Incompatible geometry with tibial and femoral surfaces	Excessive contact stresses from decreased contact area resulting in wear and accelerated cartilage degeneration	3	Inaccurate curvature of implant articulating surfaces.	2	Implant design with curved superior implant surface and hydrogel material will conform to interacting surface geometry	2	12	None
Compatibility	Host rejection	Inflammation from bulk composite	4	Insufficient biocompatibility of PVA	2	PVA literature in vivo results	2	16	In vivo inflammation analysis
		Bony reactions (Osteolysis)	4	Insufficient biocompatibility of PVA and Kevlar	2	PVA and Kevlar literature in vivo results	2	16	In vivo inflammation analysis
	Implant not compatible with adjunctive therapies	Altered physical properties or dimensional changes of implant	3	Inadequate labeling/training	2		4	24	Labeling/training
Packaging	Implant/package damaged during shipping	Procedure cannot be performed	2	Insufficient package strength/material	2		4	16	Sterilization validation, package testing
		Mechanically faulty implant inserted in patient	3	Insufficient package strength/material; insufficient fixation of implant in package	2		4	24	Sterilization validation, package testing
		Implant no longer sterilized	4	Insufficient package strength/material/insulation	2		4	32	Sterilization validation, package testing
	Packaging material contamination	Infection	4	Improper packaging material	2	Current packaging material literature review	3	24	Packaging must be EU accepted packaging
	No implant present in package	Procedure cannot be performed	2	Inadequate process qualification, inspection test plans	2		4	16	Process qualification and specifications, inspection test plans
	Implant package labeled incorrectly or wrong product in package	Improper implantation	4	Inadequate process qualification, inspection test plans	2		4	32	Process qualification and specifications, inspection test plans
	Package does not maintain shelf life	Implant performance degradation	3	Insufficient implant/package longevity	2		4	24	Implant/package mechanical aging studies
		Implant no longer sterilized	4	Insufficient package material/insulation longevity	2		4	32	Implant/package sterilization aging studies
	Implant installed following exposure to temperatures	Implant experiences degradation in performance	3	Inadequate labeling/training	2		4	24	Labeling/training

Table 4 Continued

	in excess of 49 C								
	Packaging labels fall off	Temperature: Implant experiences degradation in performance	3	Insufficient package with label longevity	2		4	24	Package with label aging studies
		Implant type: Improper implantation	3	Insufficient package with label longevity	2		4	24	Package with label aging studies
Sterilization	Implant not sterile	Infection	4	Implant material not compatible with sterilization	2	PVA literature sterilization results	3	24	Sterilization validation, package testing
			4	Insufficient sterilization	2	Literature general sterilization results	4	32	Sterilization validation, package testing
Implantation	Internal exposure to environment during surgery	Infection	4	Excessively invasive procedure	2	Implant design – flexible material	2	16	None
	Improper surgical technique - Physician damages implant during installation	Degradation of implant performance, premature failure	3	Inadequate training	2	Implant design – flexible, elastic material	3	18	Training
	Improper implant placement	Accelerated cartilage degeneration from insufficient tibial plateau coverage; Pain/tenderness from excessive extrusion	4	Incorrect surgical orientation/anchoring location	2		4	32	Adapt horn design to fit in desired location (bone tunnels); labeling/training
	Improper patient selection	Subjected to repetitive excessive loadings that could damage implant	3	Inadequate inspection test plans/labeling/training	2		4	24	Labeling/training
	Improper implant size selected	Pain/tenderness from excessive extrusion; limits range of motion	4	Implant size too large; inadequate training/labeling	2	Implant design - average meniscus geometry; Visualization during surgical procedure	4	32	Variety of size options; Labeling/training
		Accelerated cartilage degeneration from insufficient tibial plateau coverage; limits range of motion	4	Implant size too small; inadequate training/labeling	2	Implant design - average meniscus geometry	4	32	Variety of size options; Labeling/training

Table 4 Continued

	Physician modifies implant	Alters function of the device	3	Inadequate labeling/training	2		4	24	Labeling/training
	Osteophytes not properly removed	Unable to place device; premature implant compromise	3	Inadequate training	2		4	24	Training

2.1.3 Design Inputs

Design inputs were identified to verify that the implant is strong enough to survive the environment of the knee during daily use while maintaining proper functionality. These were categorized into material properties and durability.

2.1.3.1 Material Properties

The implant must be as strong and compliant as the natural meniscus if it is expected to survive in the same environment and function properly. As discussed before, some of the implant material properties were previously tested when developing the weave design and reappear in the design inputs to ensure any new designs still encompass these properties.

Ultimate Tensile Strengths

The circumferential and radial fibers play crucial roles in the proper function and durability of the meniscus. The meniscus dissipates loads in the knee by converting some of that force into hoop stresses that are then withstood by the circumferential fibers. It is able to survive this compression because of the strength of the circumferential fibers themselves and the radial fibers that prevent tears between them [95]. For these fibers to maintain the integrity of the implant, they must be as strong as the fibers of the natural meniscus in both directions. The average human meniscus has

an ultimate tensile strength of 11-19 MPa in the circumferential direction and 2-4 MPa in the radial direction, so these are the minimum strengths the implant should have in each orientation [85, 96].

Compressive Modulus

While ensuring the implant is as strong as the natural meniscus, it must remain compliant. As described previously, the compressive nature of the meniscus is an essential part of its functionality and allows for dissipation of the compressive load on the knee resulting in reduced contact stresses on the tibia. In order to mimic this function, the implant must have the same compressive modulus. The average natural meniscus has a compressive modulus ranging from 0.30 to 1.13 MPa when compressed in an unconfined environment to the 12% strain experienced during gait, so the implant must have a compressive modulus within these bounds [88, 97, 98].

Fiber Tear Out Force

The circumferential fibers exit the horns of the implant and are then used for attachment within the patient. The portion of these fibers extending outside of the hydrogel, referred to as attachment fibers, should be as strong as the ligament attachments (roots) of the average human meniscus. As identified in the FMECA, these fibers can fail by either tearing or delaminating from the hydrogel. As a result, both failure modes must be at least as strong as 660 N, which is the average strength of native meniscus roots [83]. A force is used for this criterion instead of a stress because the attachment fibers without the hydrogel have a smaller cross-sectional area than the natural meniscus roots.

2.1.3.2 Durability

Once it is known that the different components of the implant represent the strength and stiffness of the natural meniscus, durability tests must be conducted to ensure the implant survives the environment of the knee when used as indicated. As discussed before, both excessive radial extrusion and increased tibial contact pressure clinically have a relationship with knee pain, so the implant must function properly to avoid these failures. Accordingly, the implant should withstand the highest loads experienced during a year of daily use without tearing or losing functionality.

Daily Compression

Axial compression is the largest force experienced by the knee and has been identified in the FMECA as an essential test to mitigate multiple failure modes including several types of tearing, excessive radial extrusion, and excessive tibial contact stresses. It has been seen in vivo that the highest axial compressive force experienced in the knee during common daily activities occurs while descending stairs and is 3.46 times the person's bodyweight [99, 100]. By assuming the medial side of the knee takes up to 80% of the total load during heavily loaded times, a 50^{th} percentile body mass male above the age of 20 corresponds to a compressive force of 2,300 N using Equation 1 [101, 102]. Assuming the patient descends/ascends 9 flights of stairs a day, this equates to 40,000 cycles a year using Equation 2. This is an overestimate according to studies reporting an average number closer to 4 flights of stairs taken a day [103]. It is important to note that the 0.5 leg compressions per step is included because only one leg is taking a step at a time. Also, there are two force spikes per step with the largest being then the leg is straight and contacting the step below [99].

After completion of the cycles, radial extrusion and tibial contact pressure performance must be evaluated. It was observed in vivo that the natural medial meniscus extrudes in the medial direction

an average of 2 mm beyond the tibial plateau during static/standing loads [104, 105]. Standing results in a load 1.16 times the person's bodyweight acting within the knee [99]. By replacing 3.46 in Equation 1 with 1.16, this results in a force of 800 N that should be used to compare the implant extrusion to the protrusion values found in literature. A similar approach is used to compare implant performance to literature values for evaluating pressure distribution functionality. The peak contact pressure on the tibial plateau for the natural meniscus when subject to static/standing loading conditions is around 3 MPa [37, 87]. The design passes the input if there are no macroscopically observable tears, radial extrusion is less than or equal to 2 mm, and peak tibial contact pressure is below or equal to 3 MPa following completion of the compression cycles.

Extreme Compression

The implant is intended for use during daily activity but not extreme activities. As a result, even though the implant must survive a year of the peak loads experienced during daily activities, the implant is not intended to survive the high compression during extreme sports or exercises. The compressive force experienced carving down slopes while skiing was found to be the highest across several different sports and exercises. As discussed before, skiing also leads to the largest number of bucket-handle tears (large longitudinal tears) [16]. This load is 4.30 times the person's bodyweight [106]. By replacing 3.46 in Equation 1 with 4.30, this results in a force of 3,000 N. In order to ensure the implant will survive a worse case compressive load, the implant must survive at least one extreme compressive load without any tearing.

After completion of the test, radial extrusion and pressure distribution performance must be evaluated the same way outlined in the section above. The design passes the input if there are no

macroscopically observable tears, radial extrusion is less than or equal to 2 mm, and peak tibial contact pressure is below or equal to 3 MPa following completion of the extreme compression test.

Daily and Extreme Shear

Shear, particularly parallel to the tibial plateau, is commonly experienced in the knee and has been identified using the FMECA as an avenue for failure modes including horizontal tearing and delamination. Accordingly, the weakest region of the design should be tested in shear to observe if any tearing or delamination occurs. It was seen in vivo that the highest shear experienced by the knee during both common daily activities and recreation and exercise activities occurs while descending stairs or performing a leg press and knee extension exercise and is 0.35 times the person's bodyweight [99, 106]. No literature was found stating how much of the implant absorbs the shear load in vivo, so this test overestimates this ratio by assuming the meniscus transmits all of the shear force within the knee. Therefore, a 50^{th} percentile body mass male above the age of 20 corresponds to a shear force of 290 N using Equation 3 [101, 102]. By using the area of the inferior surface of the implant (793 mm^2) and the area of the cylindrical sample used for this test (78.5 mm^2), this force was then converted to a shear stress of 30 N using Equation 4. Similar to the maximum daily activity compressive force, the maximum daily activity shear force is seen while descending stairs, so the test will be conducted for 40,000 cycles to simulate a year of use. The design passes the input if there is no macroscopically observable tearing or delamination following completion of the shear cycles.

$$m\ x\ g\ x\ BW\ x\ MSL = \ 2{,}300\ N$$

Mass of Average Male: m = 85 kg; Acceleration of Gravity: g = 9.8 $\frac{m}{s^2}$; Body Weight Multiplier: BW = 3.46; Medial Side Load Transmission: MSL = 0.8

Equation 1: Daily compression force.

$$12\ \frac{steps}{flight}\ x\ 9\ \frac{flights}{day}\ x\ 365\ \frac{days}{year}\ x\ 0.5\ \frac{leg\ compression}{step}\ x\ 2\ \frac{force\ spikes}{leg\ compression}$$

$$= \ 40{,}000\ force\ spikes$$

Equation 2: Daily compression cycle number.

$$m\ x\ g\ x\ BW = \ 290\ N$$

Mass of Average Male: m = 85 kg; Acceleration of Gravity: g = 9.8 $\frac{m}{s^2}$; Body Weight Multiplier: BW = 0.35

Equation 3: Daily and extreme shear force in knee.

$$\frac{S}{A}\ x\ R^2\ x\ \pi = \ 30\ N$$

Shear Force in Knee: S = 290 N; Implant Inferior Surface Area: A = 793 mm^2; Cylindrical Sample Radius: R = 5 mm

Equation 4: Shear force in knee conversion to shear force on sample.

Table 5: Design Inputs.

Metric	*Test Spec*
Mechanical Properties	
Ultimate tensile strength – circumferential	>19 MPa
Ultimate tensile strength – radial	>4 MPa
Fiber tear out force	>660 N
Compressive modulus	0.35 – 1.13 MPa at 12% strain
Durability	
Primary Tests	
Implant high impact compression	Implant must survive without any macroscopically observable tears (larger than 1 mm) when loaded to 3,000 N No excessive radial extrusion (see sub-tests) or excessive peak contact pressure (see sub-tests) following the high impact
Implant compression longevity	Implant must survive without any macroscopically observable tears (larger than 1 mm) when loaded to 2,300 N for 40,000 cycles No excessive radial extrusion (see sub-tests) or excessive peak contact pressure (see sub-tests) following the cycles
Sample shear longevity	20% PVA/40% PVA/Kevlar interface must survive without any macroscopically observable tears (larger than 1 mm) when loaded to 30 N for 40,000 cycles
Sub-Tests	
Tibial contact pressure	Peak tibial contact pressure <3 MPa when loaded to 800 N
Implant radial dislocation and extrusion	Implant extrusion <2 mm in the medial direction when loaded to 800 N

2.2 Preliminary Fiber Design Study

2.2.1 Objectives

Finite element analysis (FEA) was used to observe the effects of circumferential fiber spacing on implant stresses and deformation that may indicate impacts on implant durability and performance. This was a design area of interest because the native meniscus has circumferential fibers across its entire width and nearly the entire height; however, the only commercial synthetic meniscus replacement, NUsurface, has all of the circumferential fibers located along the peripheral edge and resulted in tears and the Holloway PVA implant had reinforcement throughout the implant that resulted in delamination. This layout must be optimized so the design encompasses the preferable durability and functionality outcomes of the natural meniscus.

The two variables tested were the number of spaced fiber groupings and the fiber placement within the hydrogel. As discussed previously, it was shown that four Kevlar fiber bundles resembled the strength of the natural meniscus, so four fiber bundles were evenly dividing amongst 1 to 4 groupings in this study. Fiber placement was varied between fibers that spanned the height of the implant cross section (peripheral fibers) and fibers that spanned the base of the cross section (bulk fibers) as seen in Figure 14. In order to get insight about durability of the implant, the maximum von Mises stresses and A-P/M-L plane shear stresses were evaluated. Additionally, the shear stress in the A-P/M-L plane may give insight into delamination between the hydrogel and fibers. However, the survival of the implant is not all that is necessary. The implant must function properly by not excessively extruding into the knee cavity or exerting excessive stresses on the articular cartilage contacting the base of the implant. For the simulation, deformation in the medial direction

and the stress normal to the base of the implant were evaluated that may give insight into trends of implant performance.

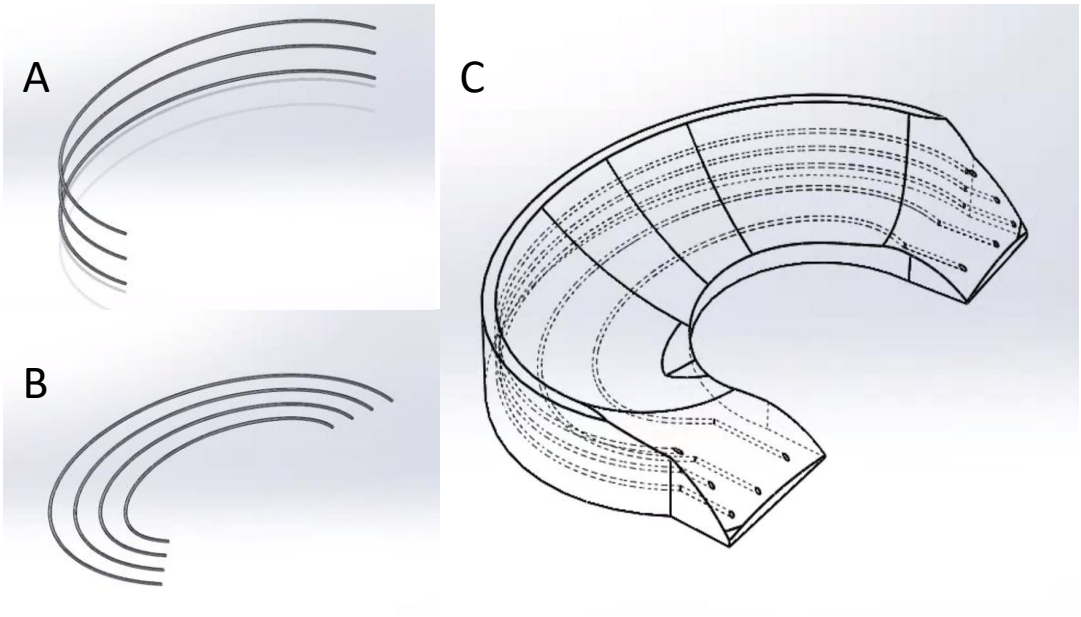

Figure 14: Layout and shape of the maximum number of peripheral fiber groupings (A) and bulk fiber groupings (B). An example of each fiber placement within the implant (C).

2.2.2 Modelling

2.2.2.1 Geometry

The implant consisted of a hydrogel and embedded fibers. The geometries were designed in SolidWorks and imported to ANSYS 19.1 for analysis. The implant geometry was the same as that of the proposed implant. An individual fiber bundle was measured to be 0.75 mm in diameter and approximately 50 mm of its length was embedded in the hydrogel. The diameter of each fiber grouping was adjusted depending on the number of fiber bundles in each grouping. For example, if the fibers were spaced across four groupings, each grouping would have a diameter of 0.75 mm,

but if the fibers were all placed in one grouping, the cross-sectional area of that grouping would be four times larger, resulting in a diameter of 1.5 mm (double the individual fiber bundle diameter). For the bulk fibers, the first fiber was located 1 mm above the base of the implant and in the middle of the width of the implant. As additional fibers were added, the fibers were spaced so they evenly spanned the width. For the peripheral fibers, the first fiber was located 1 mm inward of the peripheral edge of the implant and in the middle of the height of the peripheral edge. This 1 peripheral fiber grouping placement was similar to the weave implant design excluding the radial fibers. The peripheral fibers were evenly divided into 1 to 3 groupings instead of 4 like the bulk fibers because of the limited space across the height of the implant. Spanning fibers into 4 groups across the height of the implant would not only be difficult to manufacture but also would lead to 43% of the peripheral height of the implant being composed of fibers, which is far greater than the 21% of the native meniscus being composed of collagen [3-5]. The additional fibers were spaced so they evenly spanned the height of the implant. Figure 14 shows each of the fiber placements for the maximum number of fiber groupings with an example how these fibers were placed within the hydrogel to make the composite meniscus.

2.2.2.2 Material Properties

The implant is a composite comprised of a 40% PVA hydrogel and reinforcing Kevlar fibers. The hydrogel is a viscoelastic material, making it nonlinear. In order to model this behavior in Ansys, uniaxial and shear test data was obtained from the previous work on the weave design. In order to curve fit the data, a Mooney-Rivlin 3 parameter hyperelastic mathematical model (C10: 6.31e5 Pa, C01: -5.56e5 Pa, C11: 4.40e5 Pa, D1: 1 Pa^{-1}) was used as seen in Figure 15. This model was chosen because of its appropriate overall fit, overestimation in force at high strains, and accurate approximations at strains less than 45%, which was expected for all designs except the

unreinforced simulation. The Kevlar fibers were modeled using the material properties gathered from the previous work on the weave implant. In reality, these fibers are much weaker in the transverse direction than the axial; however, these fibers will always be in axial tension due to the hoop stresses experienced by opposing the radial expansion of the hydrogel part of the implant. As a result, they could be modeled as isotropic. These fibers are brittle, so they were modeled with a single, linear stress-strain slope. Because bone is several orders of magnitude stiffer than the meniscus, it has been shown that there is no significant difference between modeling the actual bone deformation, modeling the bone as rigid, and not modeling the bone at all in the simulation [107]. Based on these findings, the bone was not modeled in order to simplify the computation.

2.2.2.3 Loading Conditions

Data gathered while developing the weave design was used to validate the model. In the simulation, the implant was subjected to a load that could be used to compare against tests performed on the weave implant. Accordingly, load experienced in the knee while standing on two legs (1000 N) was applied to the implant as if the knee was at a 0° angle and the femur compressed directly downward [69, 99]. The sloped surface of both the meniscus and the femur result in this force acting normal to the surface of the implant, so this was chosen as the direction of the applied force in the simulation. Because the femur was not modeled, the contact area between the femur and implant was approximated to the region in Figure 17. This was chosen based on the interfacing area seen in SolidWorks. For this observation, the bone geometry from a MRI of a 74 kg male was imported. As seen in Figure 16, the femur primarily contacts the posterior and middle surfaces of the implant. As a result, these were the sections chosen for the force to act on in the simulation.

2.2.2.4 Analysis Type and Element Selection

Static structural analysis was used for all the simulations. Different types of element shapes and sizes were tested in order to obtain the best mesh. Because most of the contact region was on the posterior side of the implant, a higher density of elements was desired in this location. The best mesh for the hydrogel was obtained using tetrahedrons with quadratic edges since this element shape gave the best element ratio and most uniform mesh distribution as seen in Figure 18. The fibers were meshed using the cubic element with quadratic edges as shown in Figure 18. The same element size and edges for both the hydrogel and fibers were chosen for better interface compatibility. Figure 19 shows the plot of the mesh convergence study. The maximum von Mises stress as a function of mesh size was evaluated. After adjusting the mesh size several times, the von Mises stress converged for an element size of 1 mm. This mesh size was used for all further analysis.

2.2.2.5 Boundary Conditions

In order for the two separate materials to become a composite, they had to be bonded. The fiber/hydrogel interface was assumed to be fixed since the fiber pull out test for the weave design showed that the fibers would rupture before separating from the hydrogel when embedded in the implant [69]. The overall implant was bounded by a frictionless support along the base of the implant. This acted as the tibia and allowed the implant to freely deform and move along the tibial plane. This assumption has been used in validated FE models and was accurate because the compressed implant releases liquid that creates a lubricated and nearly frictionless sliding across the adjacent articular cartilage [108]. As seen in Figure 20, the edges of the horns of the implant were fixed. This was valid because there are attachment methods used in vivo for meniscus implants that involve pre-tensioning and have shown negligible movement or dislocation at the horns of the meniscus implant [109].

2.2.2.6 Model Validation

The simulation was validated experimentally by comparing the results of the 1 peripheral fiber implant's base contact stresses from the simulation with those found experimentally through mechanical testing of the weave implant [69]. The experimental test setup is shown below in Figure 21. The implant was uniaxially compressed between the Somso NS 50 bone model. A pressure film placed under the implant was used to acquire the stresses at the base of the implant. By incorporating the bone model in the experimental test, the force application region on implant simplification could be tested. Similar to the simulation, the implant was fixed at the horns, free to deform across the tibial plateau, and was compressed with 1000 N of force. Figure 22 shows the resulting experimental contact stresses and the simulation equivalent. The base contact stress from the simulation was around 5 MPa, which was 2 times the stress readings gathered experimentally. This may be a result of not including the radial fiber weave or by applying too high of a load in the simulation because it was unclear how much of the load was transmitted through the unphysiologically compliant bone model or the lateral meniscus model in the experimental setup. Even though the simulation value was higher than the experimental one, it was the same order of magnitude and an overestimate. The in-silico model was only used to observe trends between variables within the same model and not for any external comparisons or conclusions. It was seen that the experimental implant did have some gaps where the pressure was not distributed, but this difference in location was attributed to the bone model tibial plateau's uneven nature. Additionally, there was variability amongst the pressure distributions in the experimental tests, and when combining these test results, they roughly cover the whole implant base in a similar manner to the simulation results. Additionally, even though the internal implant stresses could not be gathered experimentally, it was noted that the implant did not tear, so the tensile and shear stresses must

have remained below the ultimate tensile stress and shear stress for failure of the composite, which was reflected in the simulation. The stress of the hydrogel of was around 30 Pa because nearly all of the stress was transferred to the fibers. The peak stress in the fibers reached 763 MPa; however, this was still around 5 times smaller than the strength of Kevlar.

An implant without any fibers was also experimentally tested and simulated. The experimental implant experienced a radial tear in the posterior region. This was reflected in the simulation since the posterior region of the implant without fibers extruded by nearly double the width of the implant before the deformation was too large for Ansys to continue the computation. The unreinforced simulation output is shown in Figure 23.

The Mooney-Rivlin 3 parameter mathematical model for the hydrogel was tested to see if it was applicable by calculating implant strain. This was essential because the chosen model was shown to have the strongest correlation with the test data up to 45% strain. As seen in Figure 24, the maximum strain of 18% remained well within the model's accurate range.

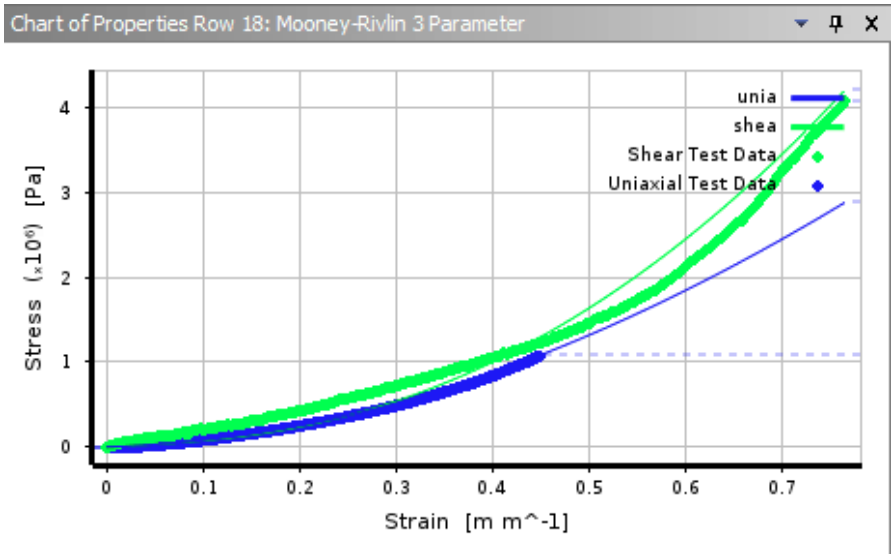

Figure 15: Mooney-Rivlin 3 parameter mathematical model curve fit for the PVA material properties.

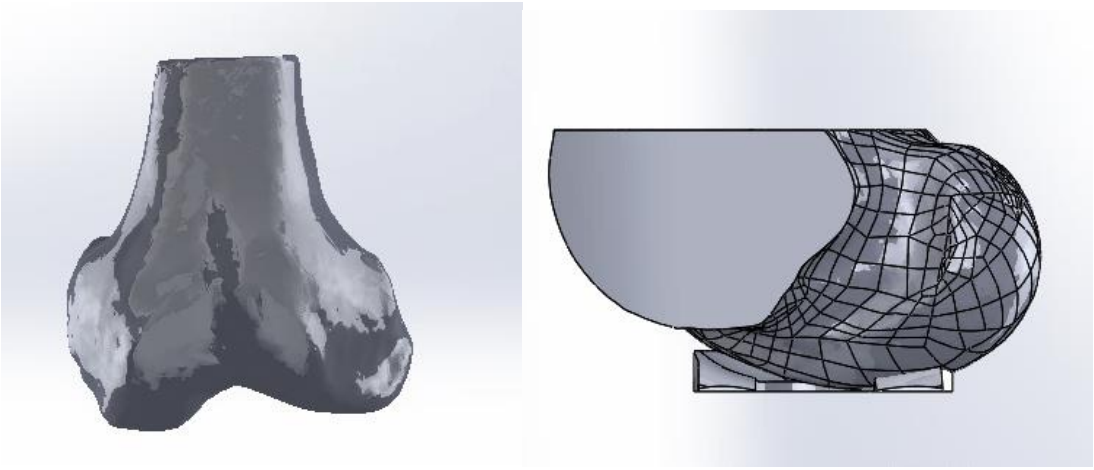

Figure 16: MRI of human femur in SolidWorks (left) and observation of femur/implant interface (right).

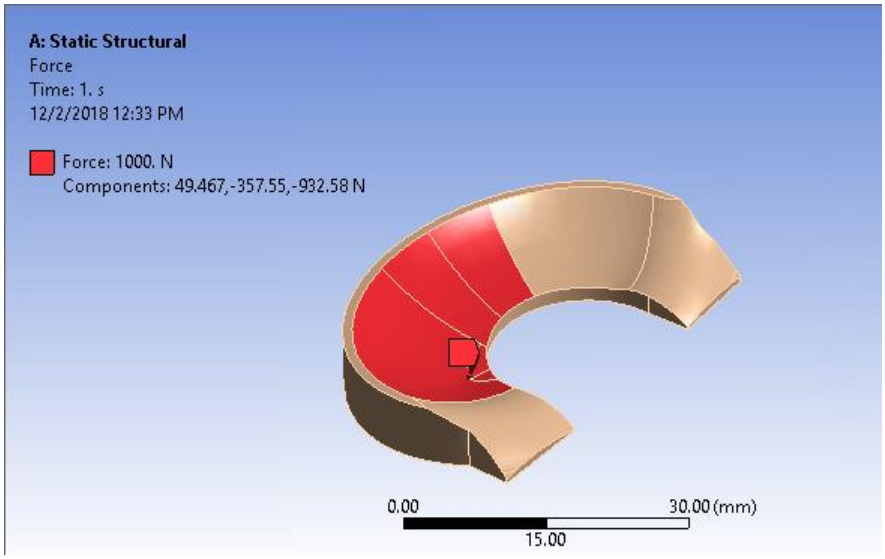

Figure 17: Location and magnitude of the applied force normal to the implant surface.

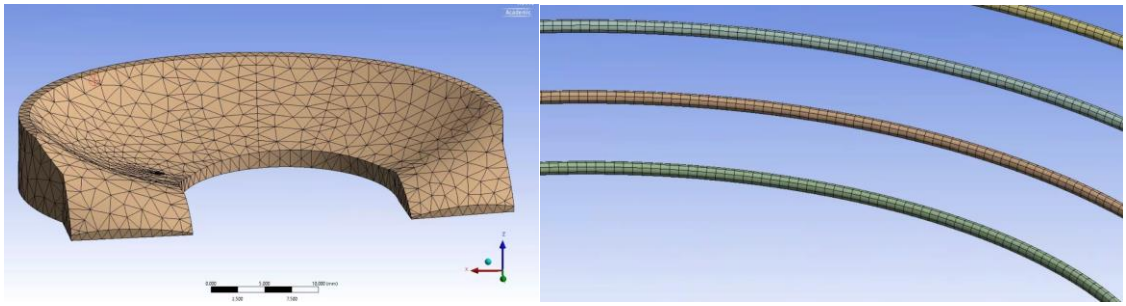

Figure 18: Hydrogel (left) and fiber (right) meshes.

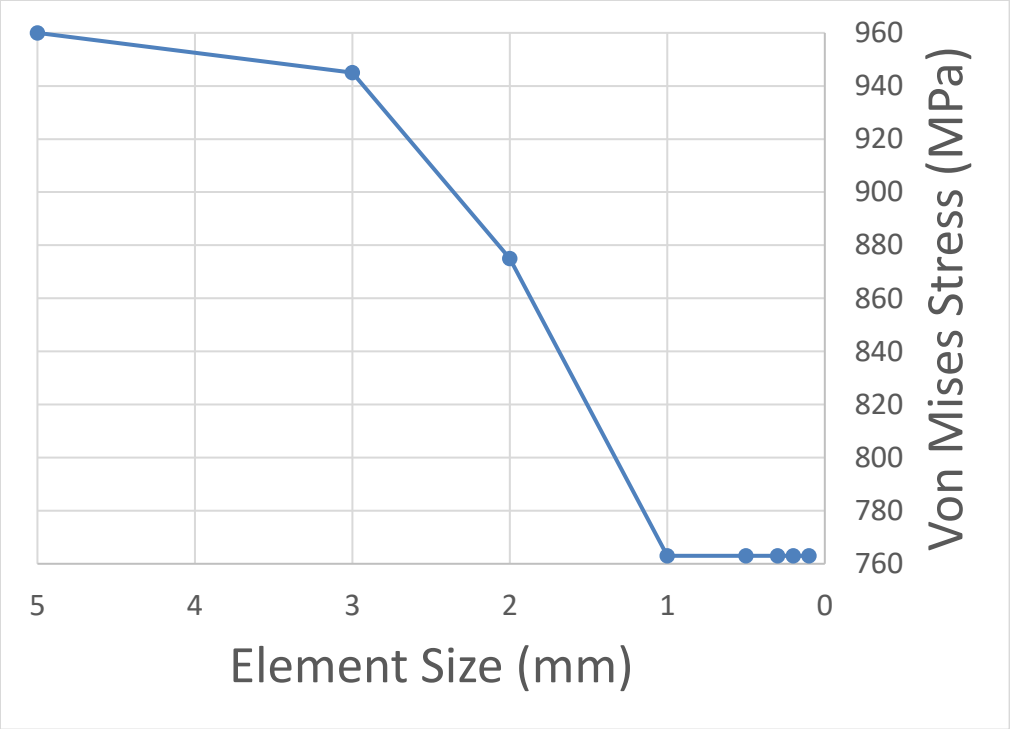

Figure 19: Mesh convergence study.

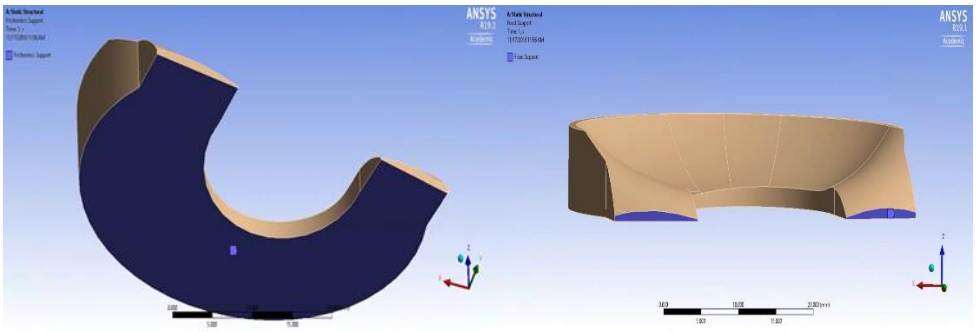

Figure 20: Frictionless boundary condition along base of implant (left) and fixed horn tips (right).

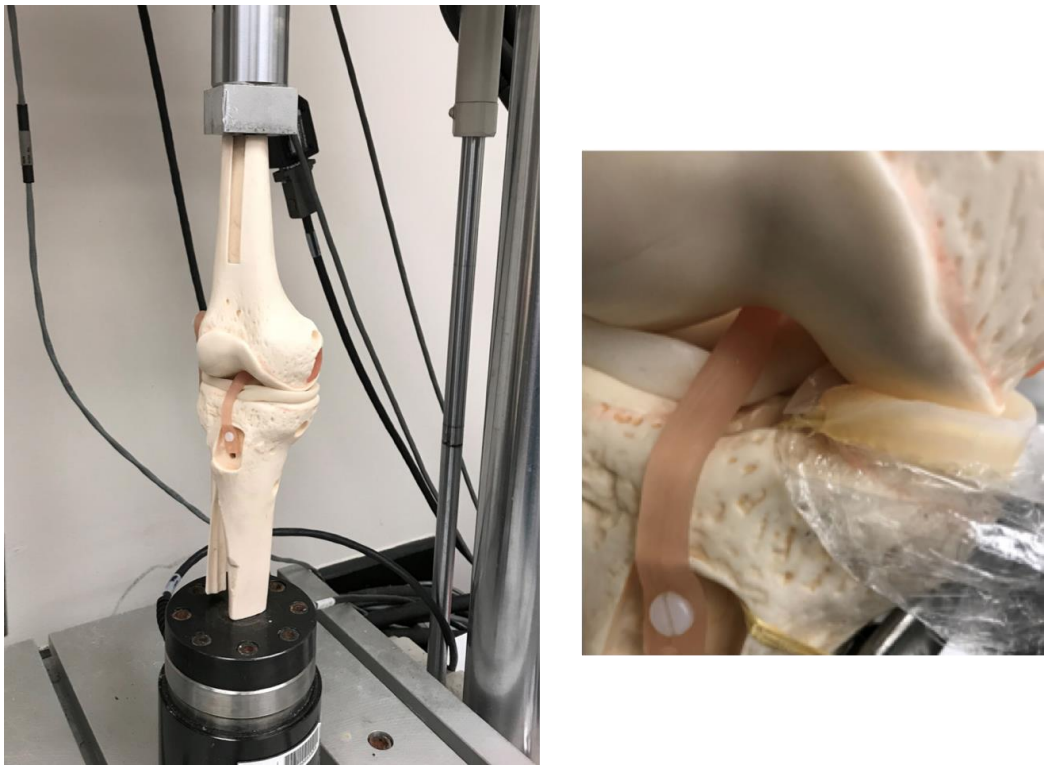

Figure 21: Experimental compression test with anatomically accurate geometry (left) and pressure film wrapped in plastic placed at base of implant (right). [69]

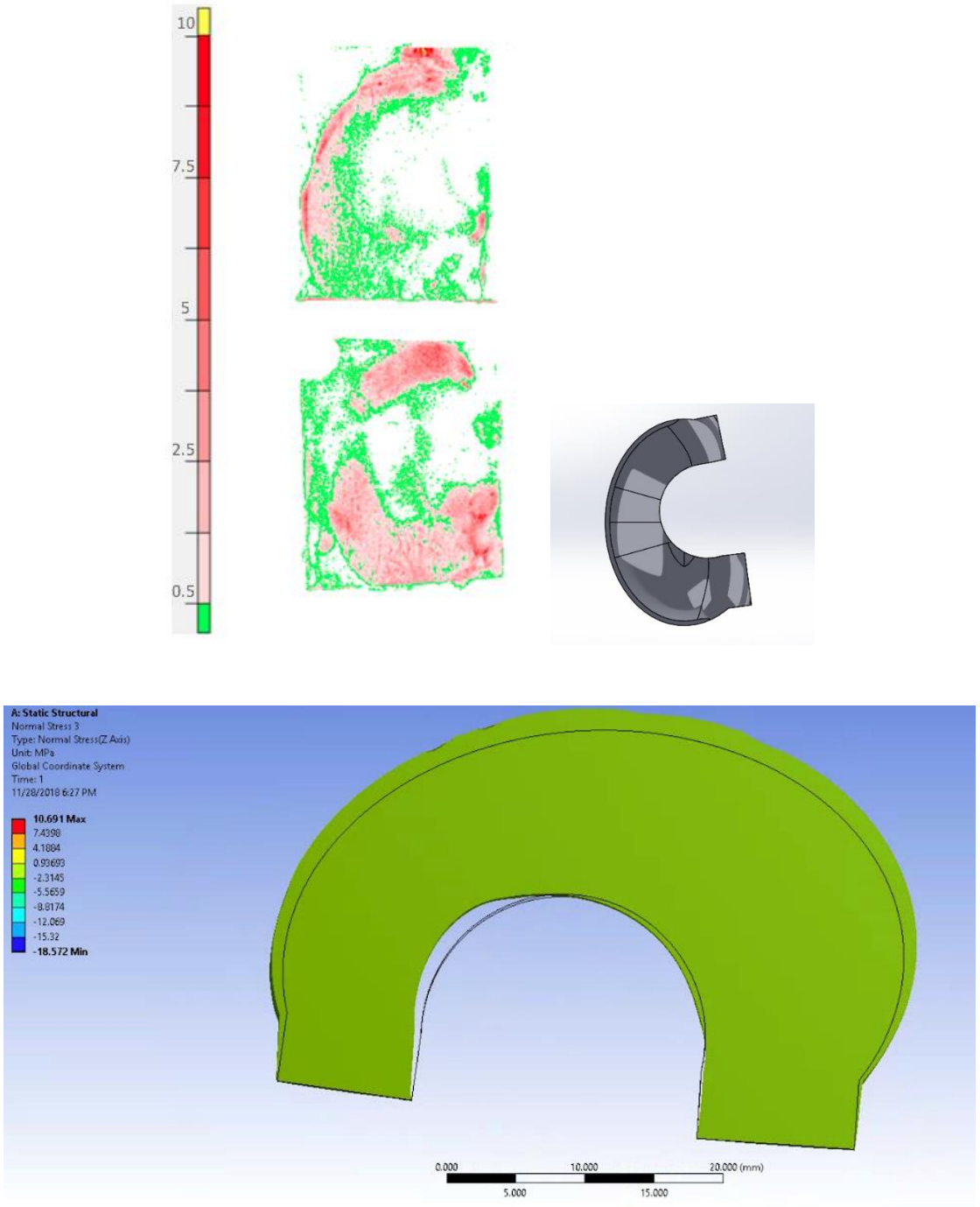

Figure 22: Experimental results from two compression tests of weave design (top left), implant orientation (top right), and simulated normal stress at inferior surface results for 1 peripheral fiber design (bottom). [69]

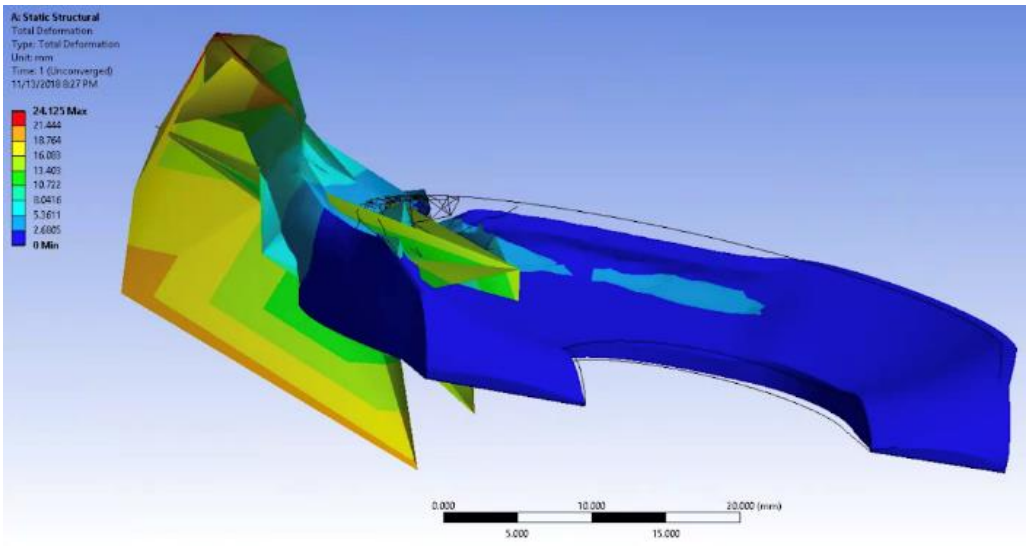

Figure 23: Deformation of hydrogel (0 fibers) in simulation up to computation error from large deformation.

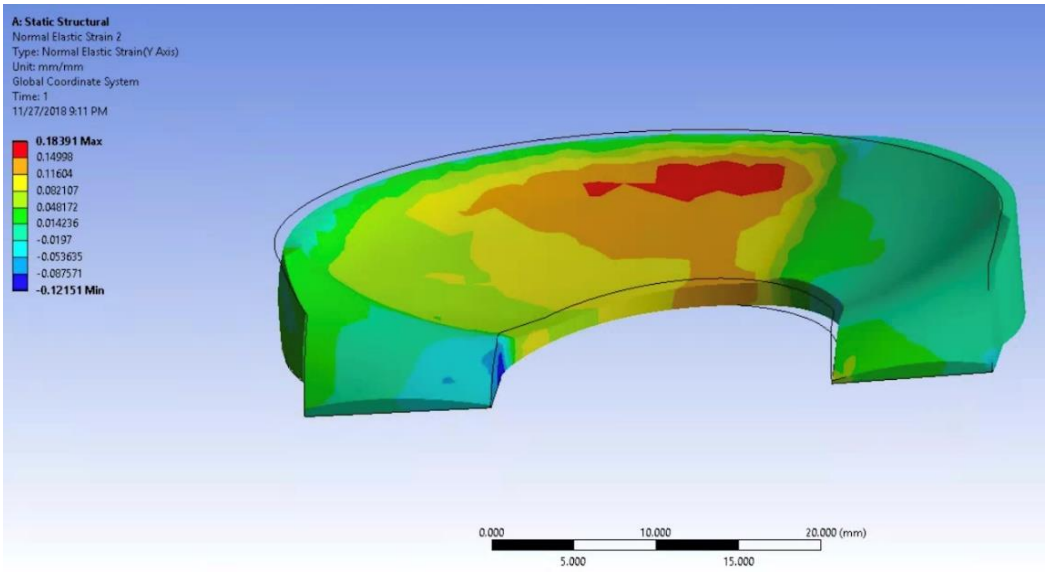

Figure 24: Maximum strain of 1 peripheral fiber implant (case with highest strain).

2.2.3 Design Trends

In order to evaluate the effects of the number of spaced fiber groupings and the fiber placement within the hydrogel on stress and deformation of the implant, simulations were run for each design change. Figure 25 shows the raw outputs for the 1 bulk implant design response under compression as an example.

2.2.3.1 Deformation

The deformation focused on was radial extrusion. The greatest deformation in the medial direction was consistently found in the outer periphery towards the base of the implant. The maximums of these deformations were compared across fiber grouping number and placement in Figure 26. The top chart including the implant with no fibers expresses the importance of reinforcing the hydrogel. As shown in the lower deformation chart, the fibers had a significant impact on radial extrusion of the implant. The fiber placement had a greater impact on deformation than fiber grouping number. This may be because deformation was along the width of the implant, so bulk fibers better resisted deformation at more locations along the width whereas the peripheral fibers were all placed at the same width location.

2.2.3.2 Stresses

Implant stresses were observed by looking at the equivalent and shear stresses of the implant and contact stresses were observed by looking at the stress normal to the base of the implant. The maximums of these stresses were compared across fiber grouping number and placement in Figure 27-29. The significance of the fibers was be noted by the consistent location of the maximum stresses in the fibers as opposed to the weaker hydrogel that the force was directly acting on. It is

also worth noting that the highest stresses were always found in the most peripheral fiber when varying bulk fibers and the fiber closest to the superior surface when varying peripheral fibers. This might lend some insight into why too many fibers in general may not be as beneficial since the energy is not dissipated throughout more of the implant, but instead becomes concentrated in the corners of implant. The implant internal von Mises stresses were highly dependent on number of groupings and position. Having 1 or 4 bulk implant fiber groupings resulted in higher stresses than the 2 or 3 bulk fiber groupings designs. Even though the increase caused by adding a fourth fiber grouping was surprising, this may be because adding too many fiber groupings caused too much of the implant to become stiff and did not allow for enough deformation and dissipation of the internal implant stresses. This was also seen when the peripheral fiber placement resulted in the lowest von Mises stresses but allowed the greatest deformation. When comparing implant shear stresses, the largest stresses were found parallel to the base of the implant. For these shear stresses, the number of fiber groupings and placement both had a big impact. Increasing the number of bulk fibers too high resulted in the lower part of the implant becoming far stiffer than the part of the implant above it. The hydrogel above these fibers deformed more than the stiff base and resulted in shear stresses parallel to the base. This was not the case for the perpendicular fibers. The contact stress seemed to be a factor of both number of fiber groupings and fiber placement as well. The base pressure results started at a similar value between the two fiber placements with just one fiber grouping but improved as more peripheral fiber groupings were added and became worse as more bulk fiber groupings were added. This may be because the peripheral fibers were added across the height of the implant, so the stress concentration was focused away from the base of the implant as opposed the bulk fibers which were placed closer and parallel to the base. It was interesting that

the contact pressure was uniformly distributed across the base of the implant for all of the bulk fiber designs; however, this was not the case for the 2 and 3 peripheral fiber designs.

Overall, it appeared that both peripheral and bulk fiber placements had benefits. Including two peripheral fiber groupings to span the height of the implant seemed to be better than bundling all of the fibers together, but this trend appeared to plateau as further fiber groupings were added. On the other hand, the trends with the bulk fibers proved to be beneficial as long as the implant was not over-reinforced with them. As a result, a spaced fiber design with 2 peripheral fiber groupings and 2 bulk fiber groupings was chosen as an implant variable in the design optimization section at the end of this chapter.

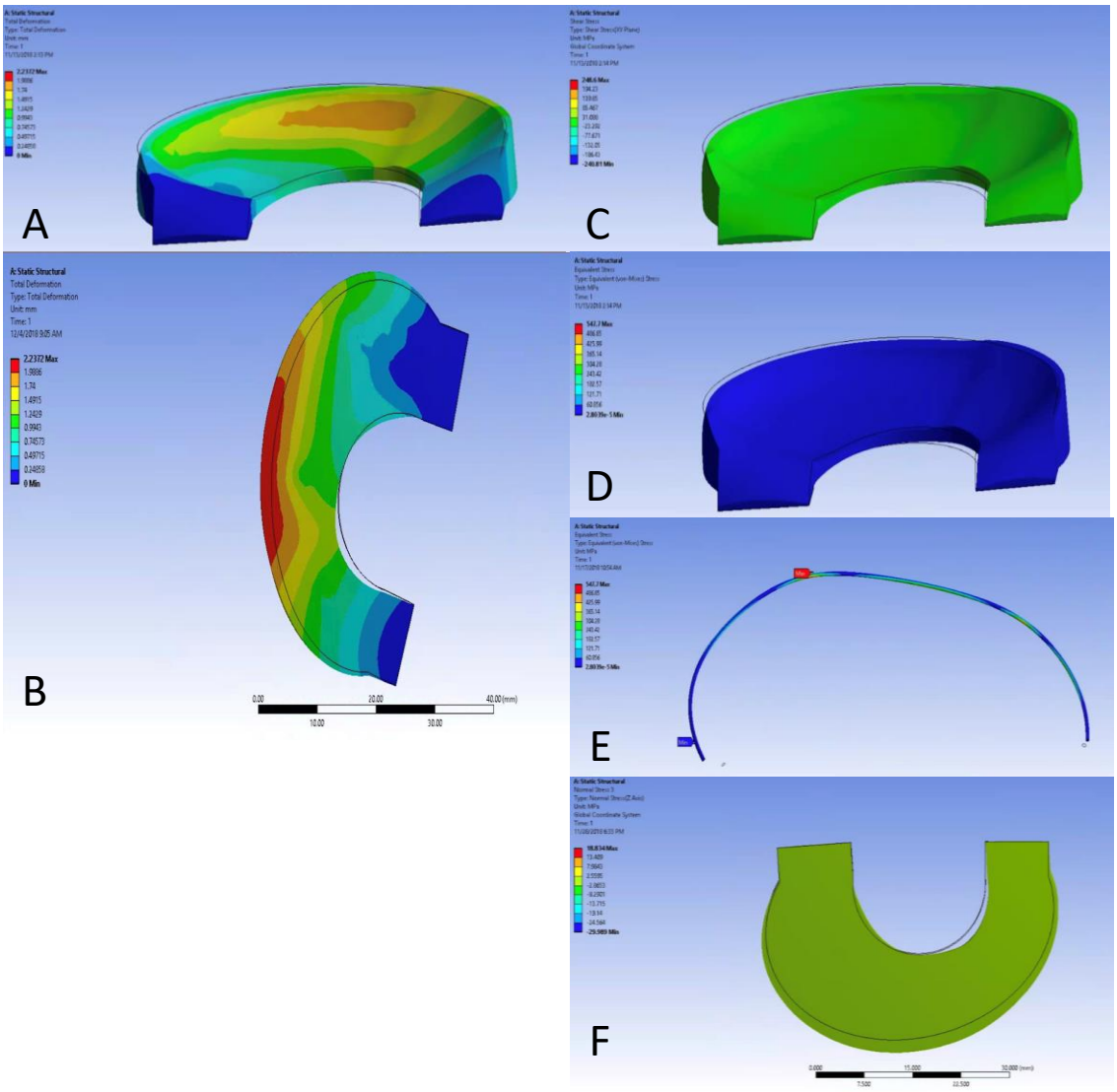

Figure 25: Deformation of the 1 bulk fiber implant at superior surface (A), and inferior surface (B). Shear stress of the implant (C). Equivalent stress of the hydrogel (D) and the fibers (E). Normal stress at the base of the implant (F).

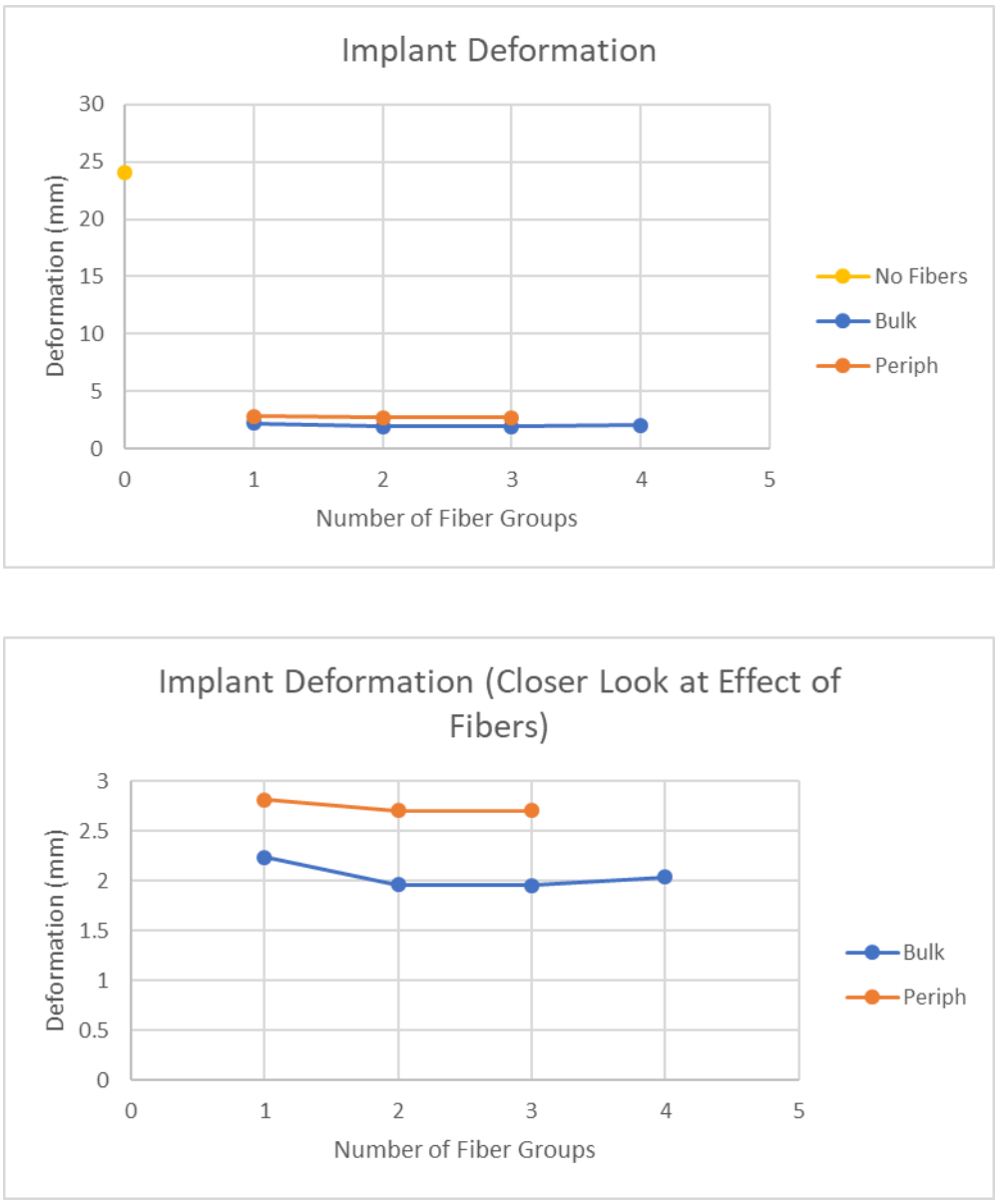

Figure 26: Maximum deformation in the medial direction of implant designs.

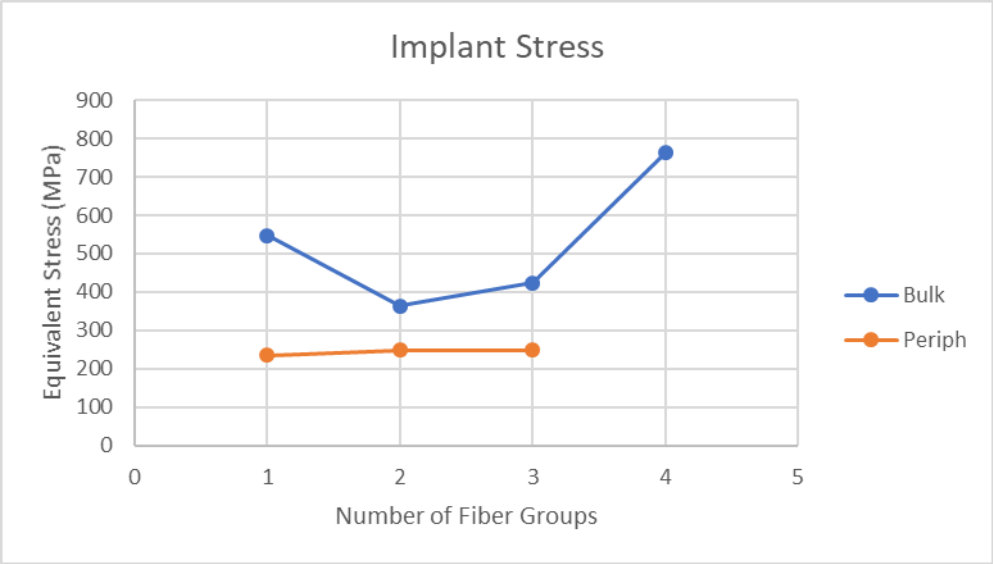

Figure 27: Maximum von mises stress of implant designs.

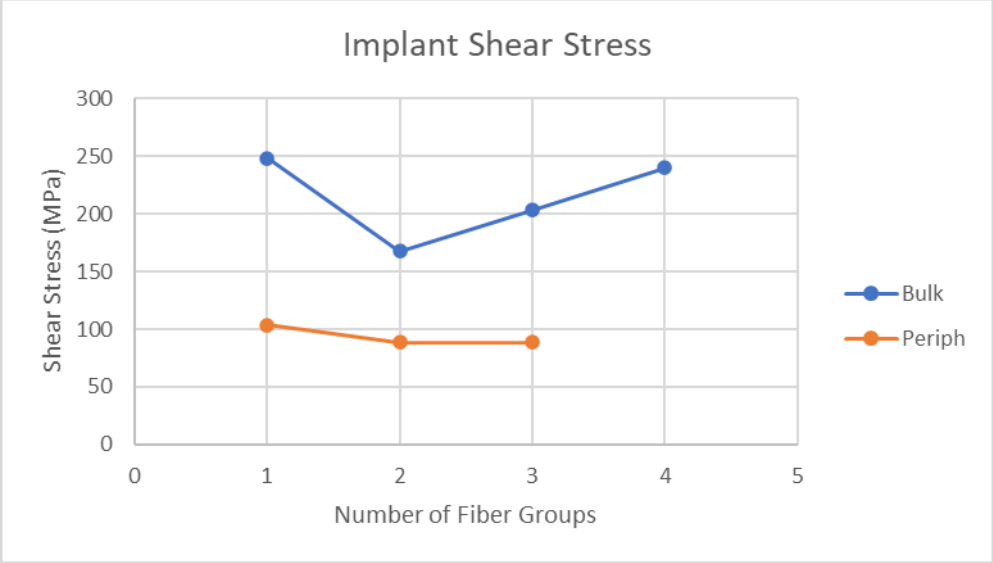

Figure 28: Maximum shear stress of implant designs.

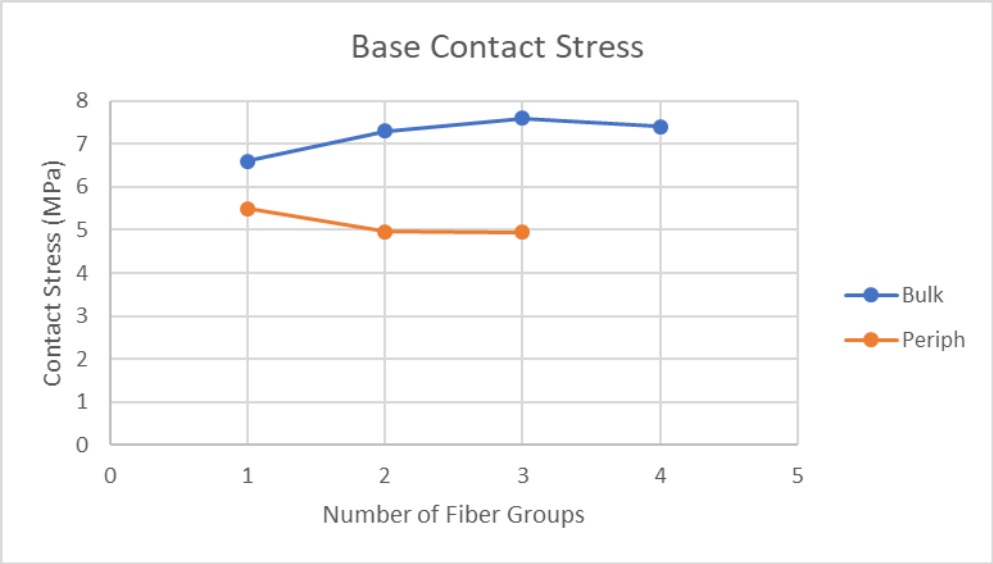

Figure 29: Maximum base contact stress of implant designs.

2.3 Manufacturing

2.3.1 Polyvinyl Alcohol

2.3.1.1 PVA Preparation

PVA was used as the bulk material of the implant. This PVA was made from 50 g of deionized (DI) water mixed with granular PVA (>99% hydrolyzed; molecular weight of 146,000-186,000 g/mol) from Sekisui (Dallas, Texas) to specific weight percentages. 20% PVA was used to best integrate the hydrophilic Kevlar fibers and 40% PVA was used for the bulk of the implant because of its ideal compressive properties shown in the previous work on the implant [69]. This mixture was combined in a beaker and covered with aluminum foil before allowing it to sit for at least 4 hours to ensure the granules absorbed the water. An additional 7 g of DI water was added to the

40% PVA beakers and 10 g of DI water to the 20% PVA beakers to account for the water that would evaporate in the dissolving step.

2.3.1.2 PVA Integration Method Development

Based on the FEA results, one possible implant design involved fibers being placed across both the width and height of the implant. In order to make this fiber spacing possible, a "stacking" approach was needed where several layers were made individually and then assembled. The layers being "stacked" were two different weight percentages of PVA: 20% PVA with 40% PVA. It was decided that the best way to combine the layers without chemically altering the materials was to melt them together. Temperature and time influence melting and were chosen as the variables for the integration method. 200°F was chosen as one of the temperatures because it is the point where PVA begins to rapidly decompose which may allow for material flow between layers as long as the overall hydrogel shape is maintained in a mold [110]. 180°F was chosen as the other temperature because it is the glass transitional temperature for partially hydrolyzed PVA and is well below the boiling point of water to avoid any bubble formation in the hydrogel. The short and long melt times were chosen to be 30 seconds and 2 minutes because they respectively are the rapid and steady state crystallization times of PVA at various temperatures [111].

A shear test across the 20% PVA/40% PVA interface was used to compare the manufacturing methods and identify which resulted in the strongest interface integration. Cylindrical samples were made using the standard operating procedure (SOP) described in the upcoming section but excluded the fiber integration steps. Using this method, three samples were made for each variable combination resulting in a total of 12 samples. An additional three samples were made of continuous 20% PVA and another three made of continuous 40% PVA. These were added to get

an idea of how well the manufacturing methods performed relative to samples made in one piece without an interface simulating two separate layers. The ideal design with complete layer integration was reasoned to be the one as strong as the average strength of the continuous 20% PVA and 40% PVA samples. Samples were tested in shear loading to failure using the setup shown in Figure 39. Each side of the sample was press fit into one of the custom two-piece shear fixtures until the 20% PVA/40% PVA interface was flush to the fixture. The fixture was then clamped to the test frame so that the axial axis of the sample was perpendicular to the machine's actuating axis. Because the shear strength of this material was previously shown to not be rate independent, the samples were tested at a high rate of 2.25 mm/s to limit sample dry-out [69].

Samples were successfully made and tested to failure. Even though the 200°F samples were made below the boiling temperature, all of them contained visible bubbles of varying sizes and locations as shown in Figure 30. The bubble formation did not occur in the 180°F samples regardless of melting time. After testing, the samples were confirmed to have failed in shear across the target interface. The results are shown in Figure 31. The error bars show one standard deviation. The red line shows the average shear strength of the continuous 20% PVA and 40% PVA samples and identifies the minimum shear strength signifying complete layer integration. All manufacturing methods had an average shear strength around the ideal shear strength threshold. The primary distinguishing factor was the variation from each method. The 200°F melting had large enough variation that it could not reliably meet the ideal shear stress threshold and had a much higher chance of performing worse than the continuous 20% PVA. This was likely due to the formation of bubbles within the hydrogel. When these bubbles were not present at the interface, the samples performed better than the 180°F samples, but the ones with bubbles at the interface experienced early failures. For the 200°F samples, the presence of bubbles increased as melting time increased

which resulted in a weaker sample on average. Time had the opposite effect within the 180°F samples. The coefficient of variance stayed very similar from 30 seconds to 2 minutes for the 180°F method (8% for 30 sec and 9% for 2 min), but the average shear strength improved from 100.3 N to 111.0 N by increasing time. To see if this trend continued, another three samples were made at 180°F for 5 minutes. These improvements appeared to plateau and had no added benefit. As a result, integrating the layers by melting them together at 180°F for 2 minutes was chosen as the best manufacturing method.

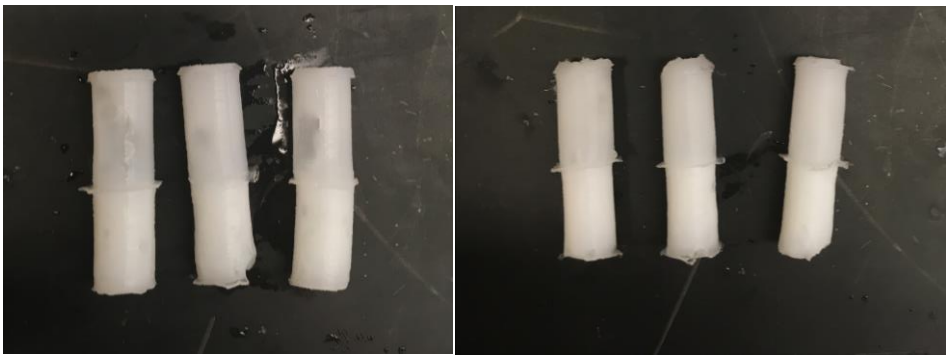

Figure 30: Cylindrical samples with 200°F for 2 min integration method (left) and 180°F for 2 min integration method (right).

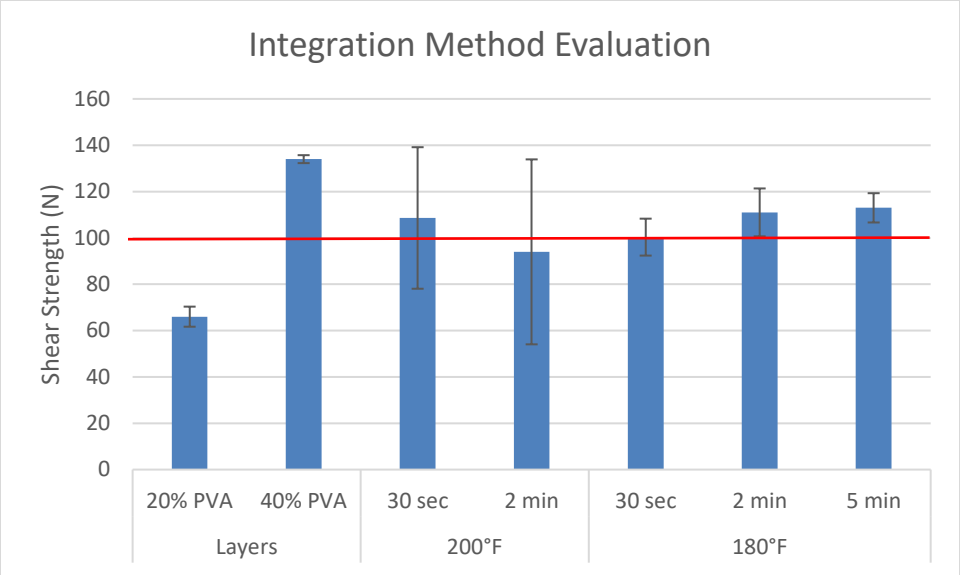

Figure 31: Integration method shear strength.

2.3.2 Implant

This procedure was used to manufacture the final implant design and develop the implants for the extreme and daily compression testing. However, for the design optimization testing, it is important to note that certain steps and quantities of fibers varied depending on the design variable. The molds and stamps used in the implant manufacturing are shown in Figure 32.

2.3.2.1 Kevlar Preparation

Kevlar®-49 obtained from Fibre Glast Developments (Brookeville, Ohio) in plain weave fabric mats with a fiber denier of 1140 was used as the fibers of the implant because of its ideal tensile properties shown in the previous work on the implant [69]. Nine 70 cm long fiber bundles were cut from the Kevlar weave.

2.3.2.2 Inferior Circumferential Fiber Layer

The inferior circumferential fiber layer is a thin layer of 20% PVA used to integrate the fibers into the hydrogel and fix their orientation and spacing. With the aluminum foil still covering the beaker, the 20% PVA mixture was placed in an oven set at 275°F to completely dissolve the PVA granules. After 50 minutes, the beaker was removed from the oven. PVA was scooped from the beaker and spread across the inferior circumferential fiber mold so that it covered the entire base and height of the mold. Excess PVA was wiped away so the PVA was coplanar to the top surface of the mold. Dowel rods were then inserted into each hole in the mold. The rods reflected the points of separate circumferential curves. Two fiber bundles were placed along the peripheral side of each circumferential curve. Tweezers were then used to push the fibers into the PVA until there were fully encapsulated. The layer was then placed in the freezer at -20°C for at least one hour or until the PVA was solid enough to be removed from the mold while retaining its shape.

2.3.2.3 Superior Circumferential Fiber Layer

The superior circumferential fiber layer is a thin layer of 20% PVA used to integrate the fibers into the hydrogel, fix their orientation, and separate them from the circumferential fibers along the inferior surface of the implant. PVA was scooped from the beaker and spread across the superior circumferential fiber mold so that it covered the entire base and height of the mold. This mold followed the curvature of the peripheral edge of the implant. Excess PVA was wiped away so that the PVA was coplanar with top surface of the mold. Two fiber bundles were placed in the circumferential cavity of the mold. Tweezers were then used to push the fibers into the PVA until there were completely embedded. The layer was then placed in the freezer at -20°C for at least one hour or until the PVA was solid enough to be removed from the mold while retaining its shape.

2.3.2.4 Final Implant Assembly

Both the inferior and superior circumferential fiber layers were removed from the freezer and allowed to thaw until the PVA was clear. The composites were removed from the molds and excess PVA was then trimmed from the edges of the layers. With the aluminum foil still covering the beaker, the 40% PVA mixture was placed in an oven set at 275°F to completely dissolve the PVA granules. After 50 minutes, the beaker was removed from the oven. PVA was scooped from the beaker and spread across the final mold so that it covered the entire base. The final mold and intended implant dimensions were the same as those chosen in the previous work on the weave implant. The superior offset stamp was used to evenly spread the PVA across the base of the mold to a specific height. The superior circumferential fiber layer was then placed on top of this 40% PVA layer and slightly inward of the peripheral edge. Additional 40% PVA was scooped from the beaker and spread on top of the superior circumferential fiber layer and across the PVA surface in the mold. The inferior offset stamp was used to evenly spread the PVA across the implant to a specific height. The inferior circumferential fiber layer was then placed on top of this 40% PVA layer and slightly inward of the peripheral edge. Additional 40% PVA was scooped from the beaker and spread on top of the inferior circumferential fiber layer and across the PVA surface. A flat cover was then placed on the top surface of the final mold and was clamped at the anterior, middle, and posterior region of the mold.

2.3.2.5 Layer Integration

The clamped mold was placed in a thin plastic bag to separate the implant from the water in the re-melt step while still allowing for convection. A beaker of water was heated to 180°F using a hot plate. The bag with the mold was placed in the beaker of water for 2 minutes while ensuring the

top of the bag remained above the water. The mold was oriented with the cover of the mold on top and parallel to the hot plate surface to allow any bubbles to escape if formed. After 2 minutes, the bag was removed from the water and placed in an ultrasonic bath for 5 minutes in the same orientation taken in the water bath to allow for dynamic mixing and integration of the layers and to release any bubbles. After 5 minutes, the bag was removed from the ultrasonic bath, and the mold was moved from the bag to a freezer set at -20°C. The mold was subjected to 6 cycles of freezing at -20°C for at least one hour with a thaw cycle at 37°C for 45 minutes following each freeze cycle. After the final thaw cycle, the implant was removed from the mold and submerged in DI water at 25°C for an hour before any flash was trimmed from the edges of the implant. The implant was then submerged again in DI water for at least 24 hours.

2.3.2.6 Radial Fiber Implementation

The radial Kevlar fiber bundle was threaded through the implant using a 0.60 mm diameter sewing needle. It proved helpful to dip one end of the fiber in 10% PVA and allowing it to dry the individual fibers together as one bundle before threading it. A custom-made radial fiber guide fixture was used to sew the fiber bundle into the body of the implant at the desired height and so the turns were evenly spaced along the peripheral edge. Sewing started on the peripheral edge of the posterior horn through to the point on the opposite edge perpendicular to the stroke starting point. This pattern continued moving along the spaces on the radial fiber guide fixture until there was one fiber bundle stroke in each space. At each turn, the fiber bundle was pulled taut. Once all of the turns were completed, the excess fiber at the start and end points was cut flush to the peripheral edge. The implant was then submerged in DI water for at least one hour and until used. Figure 33 shows the final implant.

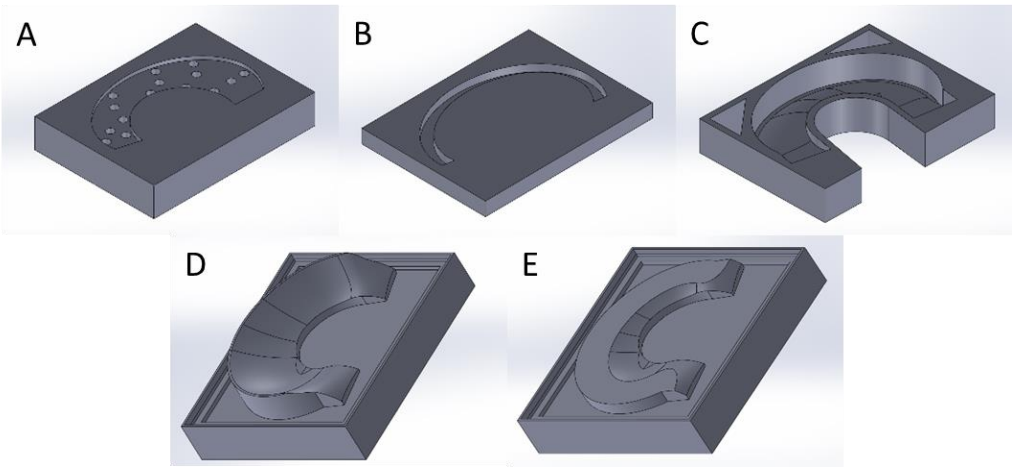

Figure 32: Inferior circumferential fiber mold (A), superior circumferential mold (B), and the final mold. Superior offset stamp (D) and inferior offset stamp (E).

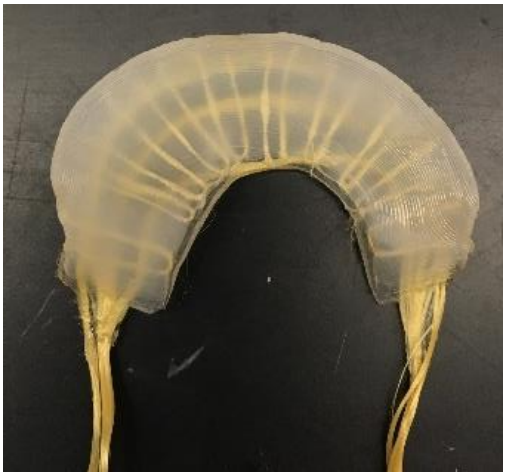

Figure 33: Top view of the final implant.

2.3.3 Cylindrical Sample

This procedure was used to manufacture samples of the 20% PVA/Kevlar/40% PVA interface within the implant. This method was used to develop the samples for the cyclic shear testing.

However, for the design optimization testing, it is important to note that certain steps and quantities of fibers varied depending on the design variable.

2.3.3.1 Kevlar Preparation

Kevlar-49 was used as the fibers of the sample to mimic the properties of the implant. Eight 20 cm long fiber bundles were cut from the Kevlar weave. The fibers were organized into 4 groupings of 2 fiber bundles each. The fibers were pulled tight and taped to the cylindrical sample mold such that 2 groupings spanned across the surface of each row of cylindrical columns as seen in Figure 34. The mold cylinder diameter was 10 mm.

2.3.3.2 20% PVA Side

With the aluminum foil still covering the beaker, the 20% PVA mixture was placed in an oven set at 275°F. After 50 minutes, the beaker was removed from the oven. PVA was scooped from the beaker and pushed into each of the cylindrical columns from the opposite side the fibers were taped to as seen in Figure 35. The mold was then placed in the freezer at -20°C for at least one hour.

2.3.3.3 40% PVA Side

The mold was removed from the freezer and allowed to thaw. The other side of the cylindrical sample mold was attached so that the fibers were positioned in the middle of the height of the mold as seen in Figure 36. With the aluminum foil still covering the beaker, the 40% PVA mixture was placed in an oven set at 275°F. After 50 minutes, the beaker was removed from the oven. PVA was scooped from the beaker and pushed into each of the cylindrical columns from the opposite side of the 20% PVA. The same layer integration steps from the implant manufacturing procedure

were then used for the cylindrical sample manufacturing. The final samples are shown in Figure 37.

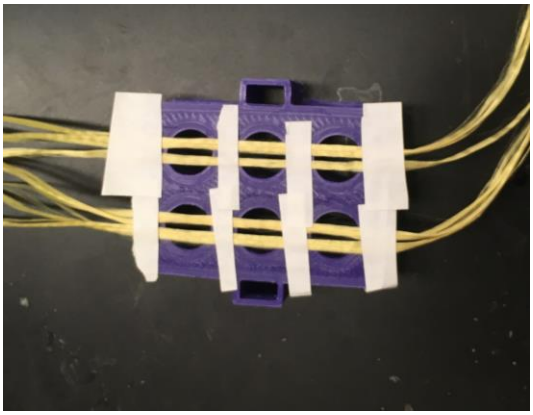

Figure 34: Cylindrical sample mold and fiber placement.

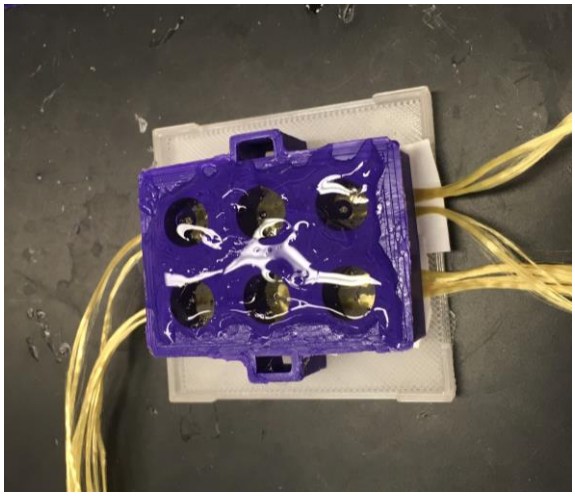

Figure 35: 20% PVA side application.

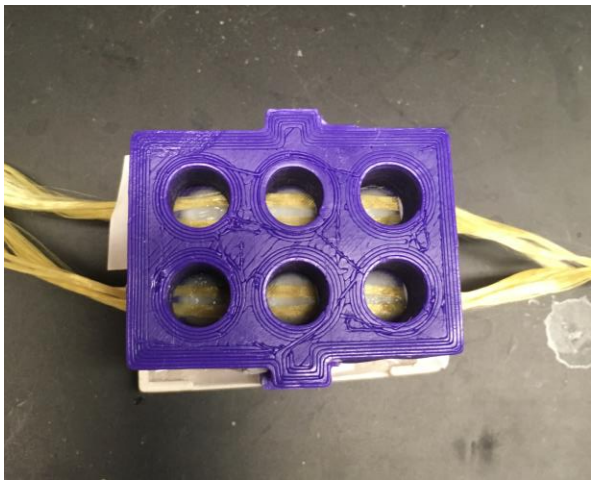

Figure 36: Addition of other side of the cylindrical sample mold.

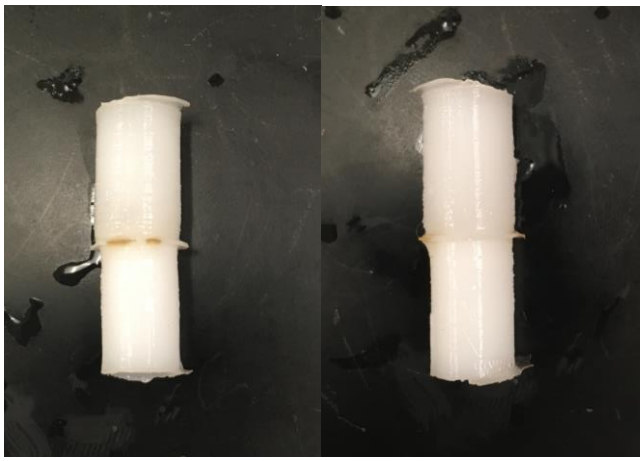

Figure 37: Cylindrical sample with views 90° rotated from each other.

2.4 Design Optimization

2.4.1 Design Variables

It was already shown that PVA and Kevlar encompass the properties desired for a biocompatible, wear resistant, durable, and functional meniscus implant [64, 69, 74-77]. However, the combination of these materials in a design that will survive the environment of the knee while limiting tibial contact pressure has not been identified. As stated before, other groups designed PVA meniscus implants that resulted in tears or composite delamination in vivo [63, 66, 67, 92]. As a result, there is a need to optimize the implant so that there is sufficient reinforcement to prevent the implant from tearing but not an excessive amount that would lead to delamination.

The effects of the number of fibers and their organization were investigated for the circumferential fibers design. Testing done when developing the weave design revealed that the lower range of the natural meniscus circumferential strength (11 MPa) could be achieved with a minimum of 4 circumferential Kevlar fiber bundles [69]. It is important to note that this is a different number that what was reported in the previous work. This is because the previous work used the cross-sectional area of the sample tested to calculate strength, and the new calculation used the cross-sectional area of the largest width of the implant to get the strength of the overall implant. Accordingly, this is the minimum number of circumferential fiber bundles that should be used. However, it may be possible to reinforce the implant as strong as the upper range of the natural meniscus without risking delamination. Additionally, using four fiber bundles as attachment fibers was not able to achieve the same strength as the roots of the native meniscus [83]. Because more fibers are necessary to achieve both of these strengths, yet too many fibers may lead to delamination, doubling the minimum number of circumferential fibers was chosen as the maximum number of circumferential fibers that should be used. As stated previously, it is important to note that even though this will increase the tensile stiffness past that of the native meniscus, this may prove beneficial since it will further limit implant deformation, radial extrusion, and dislocation while

still preserving the compressive compliance that is needed for the shock absorption functionality of the implant. The organization and location of these circumferential fibers may also play a significant role in implant performance. The circumferential fibers of the native meniscus span the bulk of the native meniscus; however, most previously designed meniscus replacements bundle these fibers together along the peripheral edge of the implant, including the previous work done on this implant [66, 69, 94]. As a result, bundled fibers versus spaced fibers were included as variables. The spaced fiber design was chosen to be two peripheral fiber groupings and two bulk fiber groupings based on the FEA work shown previously.

Similar to the circumferential fibers, the effects of the number of radial fibers and their placement were considered. Using the strength of Kevlar data from the weave implant tests, it was calculated that a minimum of 10 Kevlar fiber bundles could be spread across the implant from the anterior horn to the posterior horn for each region (anterior, middle, and posterior) to be as strong as the lower range of the natural meniscus in the radial direction (2 MPa). This calculation is described in the verification test methods section. Accordingly, this is the minimum number of radial fiber bundles that should be used. Similar to the circumferential fibers, the maximum number of radial fibers should not be more than double the minimum amount to allow for enough contact interface between the hydrogel and fibers. These radial fibers in the native meniscus span across the surface they cover. To mimic this, 10 separate fiber bundles cut to the implant width were evenly spread across the implant surface in order to cover it uniformly and entirely. However, the collagen fibers of the native meniscus are much thinner, so an additional radial fiber layout was designed to decrease the density of the fibers in case having a continuous layer of fibers decreased composite integration. Instead of placing 10 individual fibers, one continuous fiber was sewn through the hydrogel in a spline shape from the peripheral to the inner edge so that loops extending from the

peripheral edge of the implant were made. This design had the additional benefit of allowing the surgeon to use these loops to pass a suture through and attach the peripheral edge of the implant to the tibia, which is a common procedure used for allografts. Also, these loops implement additional circumferential strength along the surface they reinforce. The surface these fibers are located on may also play an important role in implant performance. In the native meniscus, the radial fiber layer encapsulates the bulk of the fibers on both the superior and inferior surface. Because the Kevlar fibers are thicker than the collagen in the native meniscus, there is not enough space in the implant to implement both a superior and inferior radial fiber layer. This may also be why most previous meniscus replacements have ignored radial fibers in their designs. As a result, placing the radial fibers along either surface was included a variable. All of the design variables and examples are listed in Table 6. However, it is important to note that no full implants were made for the spanned radial fiber design as explained later, so the example picture may not accurately reflect the design.

Table 6: Design variables.

Circumferential Fiber Placement	Circumferential Fiber Bundle Number	Radial Fiber Layout	Radial Fiber Bundle Number	Radial Fiber Location
Bundled 	Minimum (4)	Spanned 	Minimum (10)	Inferior 
Spaced 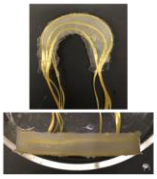	Maximum (8)	Spline 	Maximum (20)	Superior 

2.4.2 Test Methods and Results

The reinforcement design within the hydrogel greatly impacts the integration and strength of the composite implant as well as its functionality. Accordingly, delamination, durability, and tibial contact pressure tests were conducted to determine the best design.

2.4.2.1 Delamination Test

Methods

Similar to the manufacturing methods test, a shear test across the hydrogel/fiber interface was used to identify which designs would likely result in delamination. This was chosen as the first round of testing to eliminate nonideal designs because this was the only failure mode seen in vivo for another PVA/fiber composite design and because the previous weave design of this implant incorporated an unphysiologically high density of fibers [67, 69]. Three samples were made for each variable in Table 6 except for the radial fiber location since the change from the inferior to the superior surface could not be represented by modeling the hydrogel/fiber interface. Additionally, the previously proposed weave design was tested to see if changes to the radial fiber design were necessary. Cylindrical samples isolating the target 20% PVA/Kevlar/40% PVA interface for each variable were made using the cylindrical sample SOP described previously. Each sample was made using the highest density of fibers found in a 5 mm radius across the implant that the sample was representing. Using this method, the maximum fiber number samples had one grouping of 8 fiber bundles, two separate groupings of 2 fiber bundles each, an evenly spread out layer made from 3 fiber bundles, three separate groupings of 1 fiber bundle each, and an unaltered weave for the bundled circumferential, spaced circumferential, spanned radial, spline radial, and weave designs respectively. The minimum fiber number samples followed the same pattern but

with half the number of fibers. Examples of each are shown in Figure 38. The test was designed with a threshold load. As identified in the design inputs, the composite must survive a shear load of 30 N during descending stairs and leg-press and knee-extension machine exercises. In order to reduce this initial test from a cyclic to a monotonic one while giving insight into which designs will survive many cycles at 30 N of shear stress, a shear strength above 60 N, double the maximum cyclic load seen in vivo, was required for a variable to progress to the durability and contact pressure test. Samples were tested in shear loading to failure using the setup shown in Figure 39 under the same methods described in the integration testing methods.

Results

Samples were tested to failure and were confirmed to have failed in shear across the target interface. The overall results of the designs with their average load and standard deviation are shown in Figure 40. The spline radial fiber design performed the best overall regardless of the number of fibers used. This may be because this was the only design made by sewing the fibers into the sample instead of laying them across the interface. The fibers were pulled tighter than was possible for the other designs, which resulted in the fibers taking the smallest area across the target interface. This manufacturing method was not possible with either circumferential fiber design or the spanned radial fiber design. Interestingly, different designs failed in different areas of the interface. Nearly all of the bundled circumferential, spaced circumferential, and spline radial fiber designs failed at the 20% PVA/40% PVA interface with the fibers still embedded in the 20% PVA. These designs all had a shear strength above the threshold. This meant that both of the circumferential fiber designs and the spline radial fiber design progressed to the durability and contact pressure test as final design variables. However, the spanned radial and weave radial designs failed at both the 20%PVA/40% PVA interface and the hydrogel/fiber interface with most

of the fibers exposed. An example of this is shown in Figure 41. These designs had a lower shear strength. Both the weave and the maximum spanned radial designs were below the threshold and at similar values. Even though the minimum spanned radial design was above the threshold, it was not chosen as a final design variable because the maximum spline radial design passed with a higher shear strength while potentially leading to an overall stronger and more durable implant design suggested by the higher number of fibers. In addition to these designs performing the worst, they also had the highest coefficient of variance due to their varying failure mechanisms. It is interesting to note that the bundled circumferential design incorporated twice as many fibers as the spaced circumferential design but resulted in a very similar strength. This may be because even though the cross-sectional area of the fibers across the sample interface was twice as large for the bundled circumferential design, the diameter of this one grouping was the same as the diameter of both of the smaller groupings of the spaced circumferential fiber design combined. This means there was the same ratio of 20% PVA area to fiber area across the shear surface for both designs. This concept may also explain why the spanned radial and weave radial designs had earlier failures at the hydrogel/fiber interface.

2.4.2.2 Durability and Contact Pressure Test

Methods

A compression test of the implant was used to indicate the most durable and best functioning design from the design variables that progressed from the delamination test. These remaining variables were organized into a 2^2 design of experiments (DOE) shown in Table 7. Three implants for each variable combination were made using the implant SOP described previously. Contact pressure and high impact tests were established where the implant underwent compression in a

configuration designed to model the mechanical environment of the knee. This setup can be seen in Figure 42 using the Model 858 MiniBionix II Testing System (MTS, Eden Prairie, MN) with a 15kN load cell. This was chosen as the final test to identify the best overall design because it incorporated every component of the implant as well as the most common mechanics experienced by the native meniscus including bulk compression, hoop stresses in the circumferential fibers, strength of the horns and attachment fibers, resistance to excessive radial extrusion and peak contact pressure, and ability of the radial fibers to hold the implant and circumferential fibers together. The setup included a custom made 303 Stainless Steel femur indenter modeled after the geometry of the Somso NS 50 bone model. The model itself was not used because it began to plastically deform prior to any signs of implant failure during preliminary testing. Similar to the femur indenter, a steel platform was used in place of the bone model tibia due to plastic deformation in preliminary tests. In order to fix the implant to the platform and in line with the femur indenter, a fixture was designed to hold the implant horns flush to a wall by securing the attachment fibers on the distal end of the wall. The attachment fibers were fixed by clamps with teeth resembling the thread height and pitch of a commonly used iFix Interference Screw made by Zimmer Biomet. The rest of the implant was free to translate and extrude across the platform surface. The implant was aligned with the femur indenter so that their contacting surfaces were visually concentric and the peripheral edge of the femur indenter was around 1 mm inside of the peripheral edge of the implant. This positioning also ensured that all of the indenter contacted the implant instead of the platform. This created a more intense test since the native meniscus usually only takes 50% to 70% of the load [1, 2, 112]. For the contact pressure portion of the test, all implants were loaded to 800 N with a Fujifilm (PreScale® Super Low, Pressure Metrics LLC, Whitehouse Station, NJ) pressure film wrapped in plastic for water protection and placed between

the inferior surface of the implant and the platform. The 800 N was held for 5 seconds to allow sufficient color development on the film. After this, the pressure film was removed, and the durability portion of the test was performed. Because the test was designed to induce failure of the implants to clearly differentiate design performance and observe the possible failure modes, the implants were loaded to a high strain of 75% or 5.25 mm of displacement. This is 6.25 times higher than the strain seen in vivo during gait [88]. Zero mm of displacement was identified as the point where around 3 N of preload was applied to the implant. This displacement was applied at high rate of 2.25 mm/s to limit sample dry-out and resemble the loading rate of walking [88]. Performance of the implants was quantified by recording the number and type of failures. The failure modes seen throughout these tests were hydrogel tears, indentations, delamination between PVA layers, circumferential fiber tear out from the hydrogel, and excessive peak pressures, so these became the metrics for evaluating the implants. Because it was previously shown that the PVA/Kevlar composite is able to recover after deformation, indentation was weighted as half as important as tears or delamination [69]. The contact pressures were given a 4, 3, 2, or 1 if the peak pressures were >3 MPa, 3 MPa to 2.75 MPa, 2.75 MPa to 2.5 MPa, and <2.5 MPa respectively. For each implant, the failure modes recorded were multiplied by the weighted severity multiplier of the column the failure was categorized under and then added together. The contact pressure score was also added to this total to arrive at one overall failure incidence score for each implant.

Results

Every sample experienced at least one failure mode from the unphysiologically high compression. This made it easy to quantify the incidence of failures of each design and distinguish them from one another. These results are listed in Table 8. Examples of the failure modes are shown in Figure 43.

Even before any computational analysis was performed, several trends were apparent. Delamination only occurred parallel to the inferior surface and when the radial fibers were placed on the inferior surface. This may be a result of increased stiffness of the reinforced inferior surface relative to the rest of the implant. This delamination plane parallel to the inferior surface was also seen in the FEA work and in vivo as the plane with the highest shear stress. Overall, there were far fewer incidences of delamination than tearing (7 delaminations vs 19 tears). This provided evidence that the shear testing and design variable conclusions helped mitigate delamination and translated from the cylindrical samples to the full implants. Even though tears occurred on both the superior and inferior surface at similar rates (11 superior tears vs 8 inferior tears), placing the radial fibers on the superior surface appeared to be much more effective at mitigating superior surface tears (8 superior tears for inferior surface fibers vs 3 superior tears for superior surface fibers) while not allowing for significantly more inferior surface tears (4 inferior tears for inferior surface fibers vs 5 inferior tears for superior surface fibers). Additionally, placing the radial fibers on the superior surface appeared to help with limiting indentation because all cases of indentation appeared on the superior surface and only for the designs with the radial fibers on the inferior surface. The spaced circumferential fibers appeared to eliminate fiber tear out since this failure mode was only seen in the bundled fiber designs. This type of failure commonly occurred near the posterior horn where the hydrogel began to thin. The circumferential fiber design appeared to play a larger role in pressure distribution and radial fiber location played a larger role in peak contact pressure. The bundled fiber design concentrated all of the contact stress along the peripheral edge of the implant and the spaced fibers spread the contact stress across the width but still retained stress concentrations around the fibers. Placing the radial fibers on the inferior surface led to higher peak contact pressures than superior surface fibers. This stress concentration around the radial

fibers expresses their necessity, because they absorbed some of the load even if it was not from the hoop stresses the other fibers were undergoing.

A DOE computational analysis of these results was conducted using JMP Pro 14 in order to evaluate the effect and significance of these design variables. The failure incidence score was used to create a model for predicting the behavior of the implant design. The strength of the model is shown in Figure 44 with the regression line in red and the average failure incidence score of 8 in blue. This regression yielded a correlation of 0.71, which deemed the model acceptable. The effect summary in Figure 45 identified both the radial fiber location and circumferential fiber design variables as having a significant impact on failure incidence ($P<0.01$ and $P < 0.05$ respectively) and were not confounding.

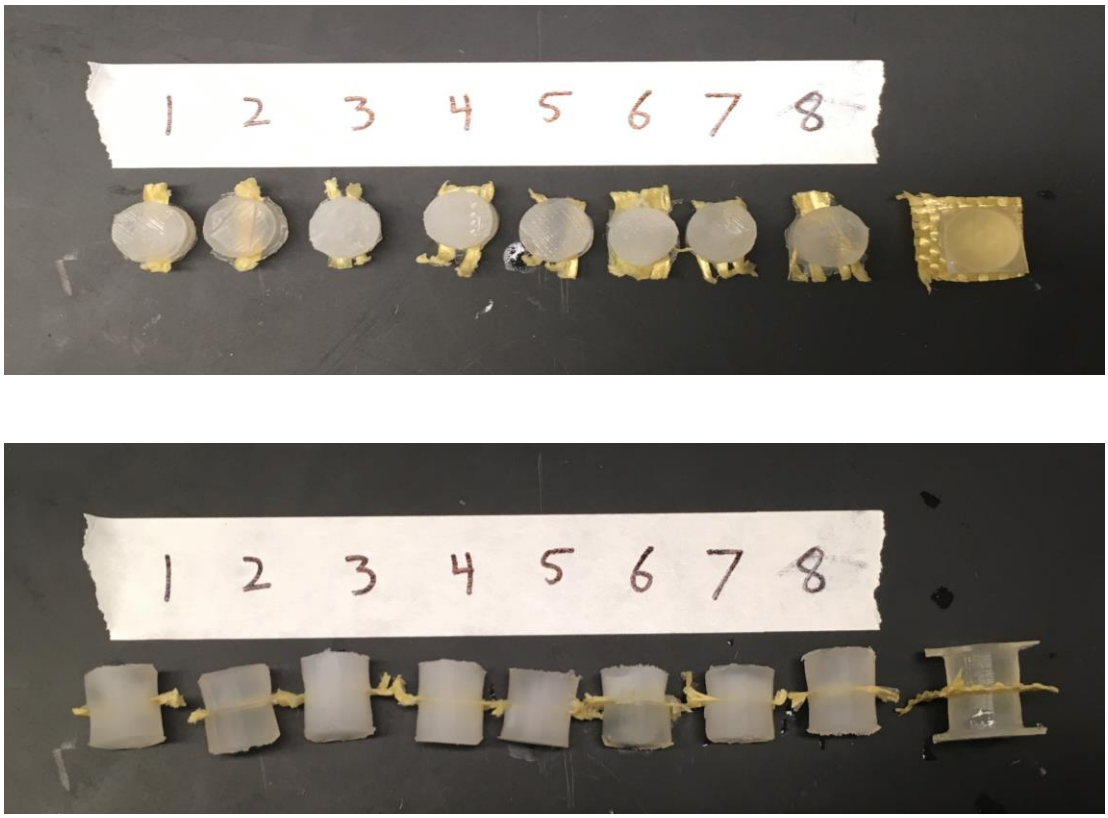

Figure 38: Cylindrical samples for the bundled circumferential minimum (1), bundled circumferential maximum (2), spaced circumferential minimum (3), spaced circumferential maximum (4), spanned radial minimum (5), spanned radial maximum (6), spline radial minimum (7), spline radial maximum (8), and weave designs (right).

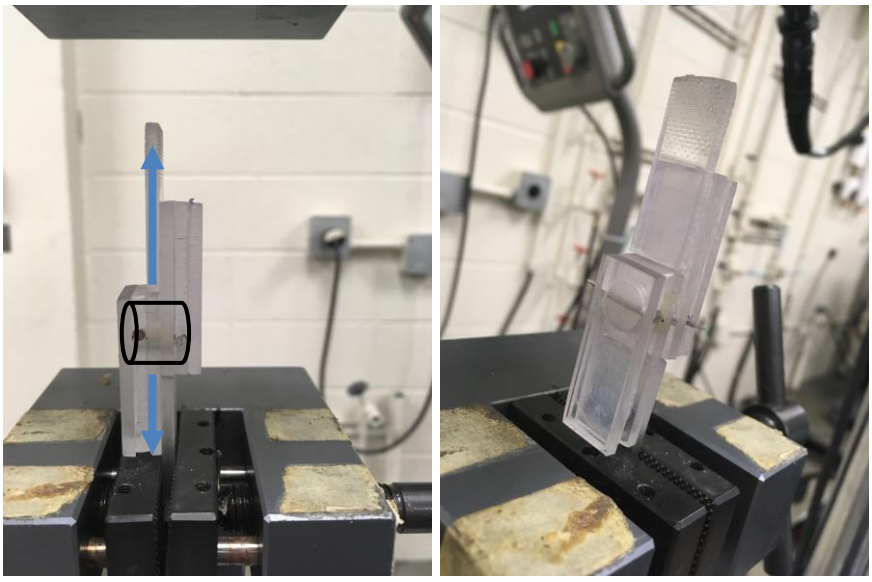

Figure 39: Shear test setup.

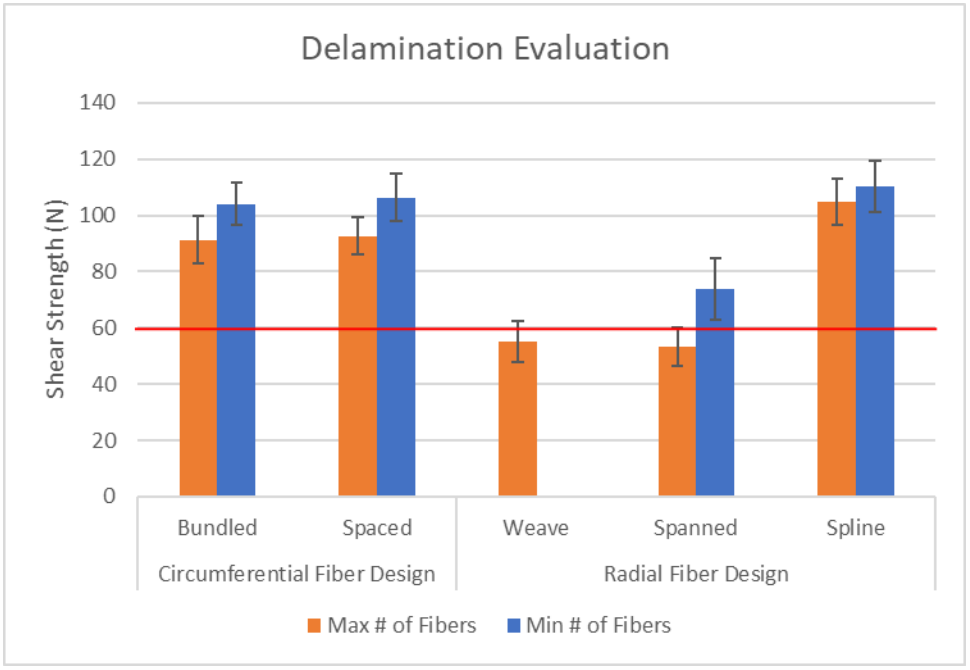

Figure 40: Design variable shear strength.

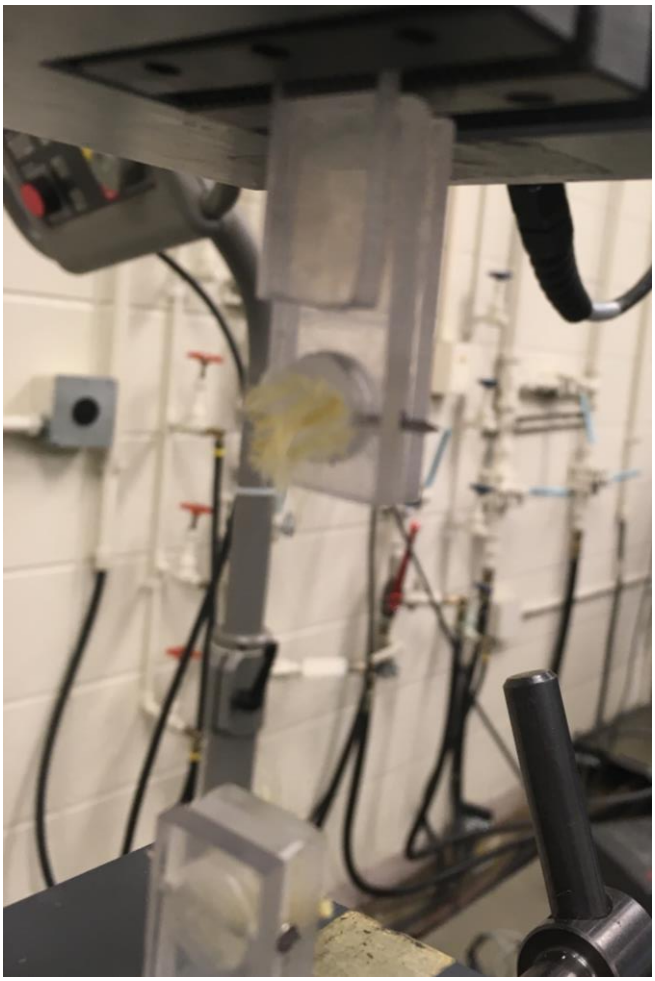

Figure 41: Example of a sample failure at the fiber/hydrogel interface.

Table 7: Design variables tested in the compression tests and used in the 2^2 DOE.

Circumferential Fiber Placement	**Radial Fiber Location**
Bundled	Inferior Surface
Spaced	Superior Surface

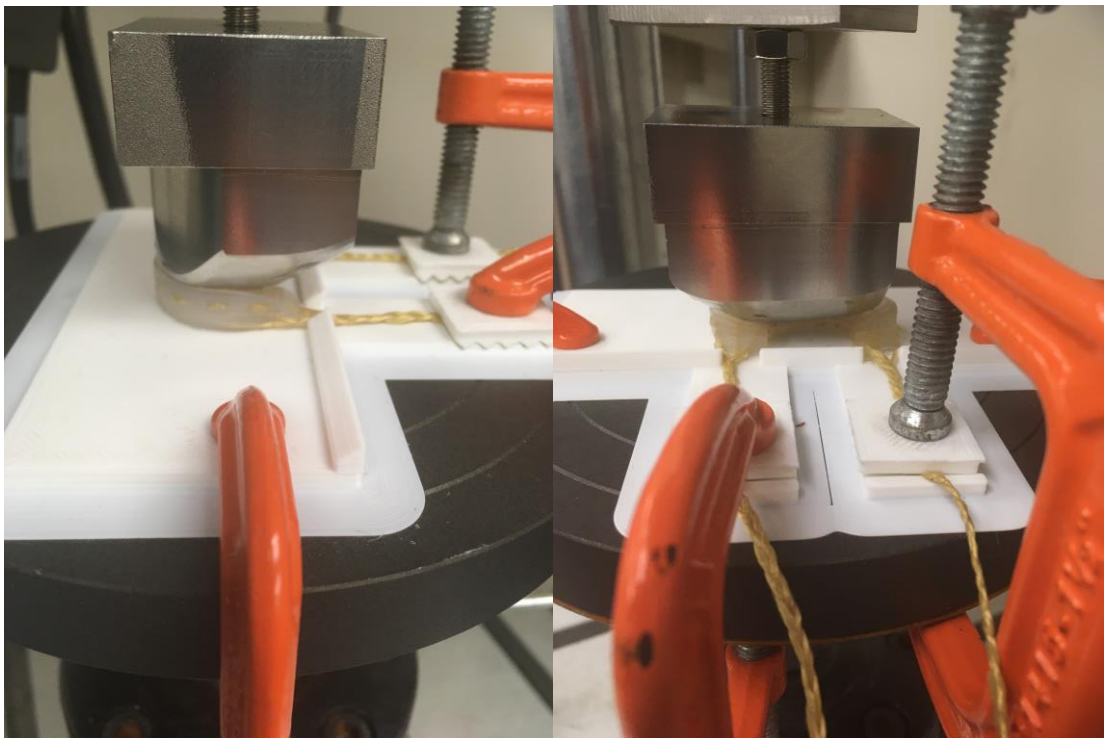

Figure 42: Compression test setup from the posterior (left) and lateral (right) sides of the implant.

Table 8: Compression test raw results.

Full Factorial		**Durability and Contact Pressure Results**						
Circum Design	*Rad Location*	*2*	*2*	*1*	*2*	*2*	*#*	*Weight*
		Superior Tears	Inferior Tears	Superior Indentations	Layer Delaminations	Circum Fiber Tear Outs	Contact Pressure Score	Total
Bundled	Superior		1			1	2	**6**
Bundled	Inferior	2				1	2	**8**
Bundled	Inferior	2	1	1	1		3	**12**
Bundled	Superior		2			1	1	**7**
Spaced	Superior	1					3	**5**
Spaced	Inferior	2		1			4	**9**
Spaced	Inferior	1	1	1	2		3	**12**
Spaced	Superior	1					3	**5**
Bundled	Inferior	1	1	1	2	1	3	**14**
Bundled	Superior	1	1	1		1	2	**9**
Spaced	Inferior			1	2		2	**7**
Spaced	Superior		1	1			1	**4**

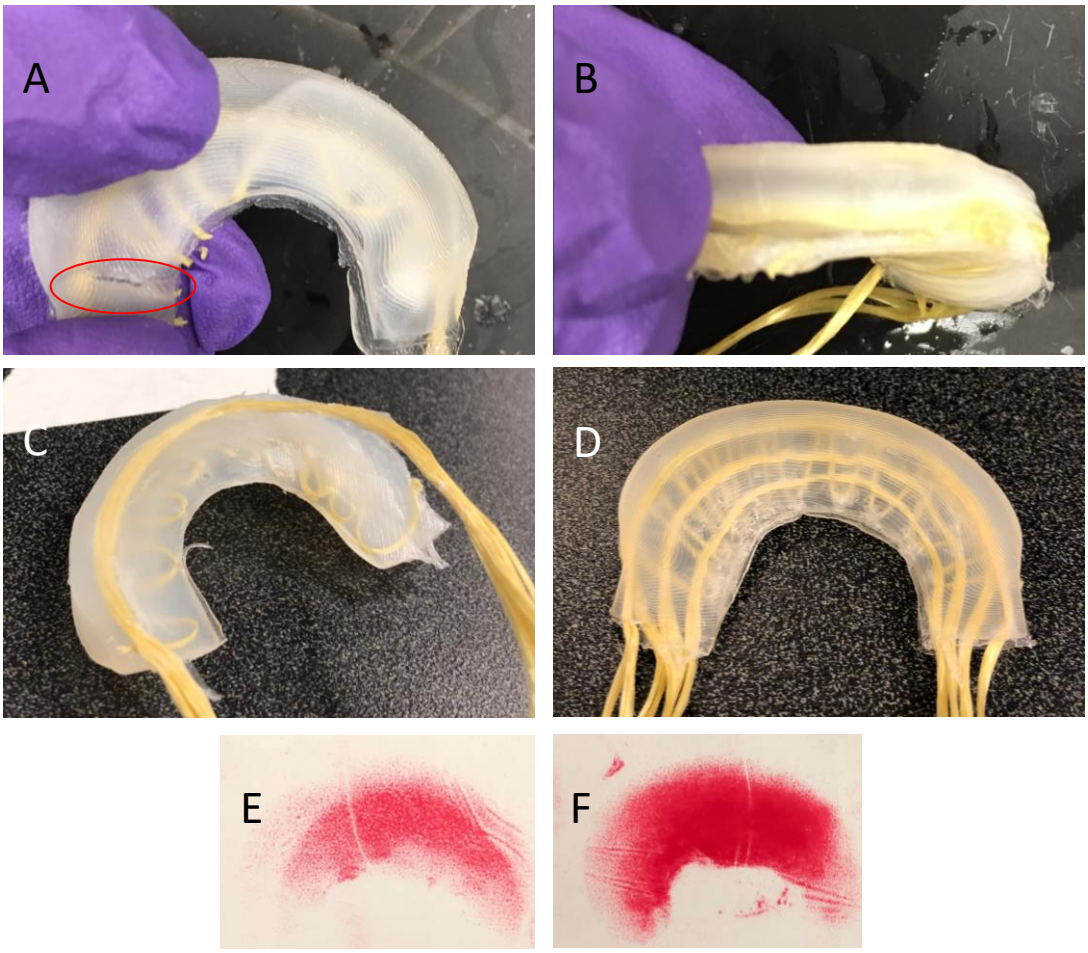

Figure 43: Examples of a superior surface tear (A), layer delamination (B), circumferential fiber tear out (C), superior surface indentation (D), low peak pressure (E), excessive peak pressure (F).

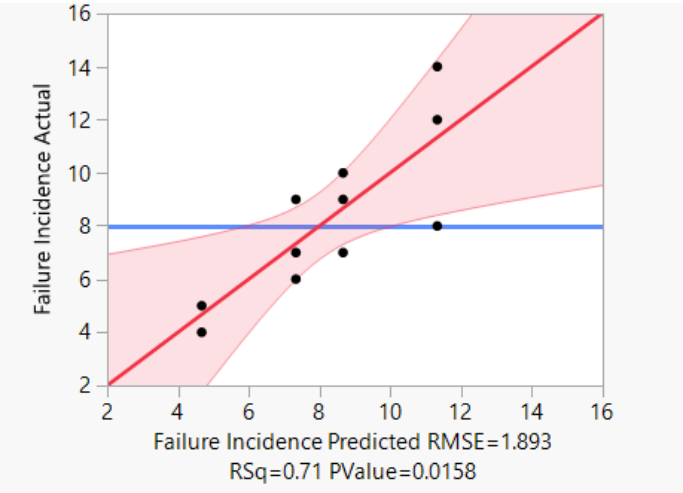

Figure 44: Accuracy of predictive model.

Source	LogWorth	PValue
Radial Location	2.194	0.00640
Circum Design	1.392	0.04057
Circum Design*Radial Location	0.000	1.00000

Figure 45: Design variable effect summary.

2.4.3 Design Choice

Delamination, strength, and contact pressure functionality were the focal points used to evaluate the design variables and determine the best implant. The spline radial fiber design was chosen because it performed significantly better than spanned fiber design in the delamination test. Within the spline radial fiber design, both the minimum and maximum number of radial fibers were around twice the threshold value so the maximum number of spline radial fibers was chosen to increase overall implant strength without introducing concerns of delamination. The remaining variables

for circumferential fiber design and radial fiber location were evaluated using the durability and functionality test because they either had similar results in the delamination test or could not be accurately represented by an interface cylindrical sample. Figure 46 presents the impact of both of these variables on failure incidence. The spaced circumferential fiber design had 2/3 the number of failures as the bundled circumferential fiber design and the superior radial fiber location had half the number of failures as the inferior radial fiber location. The model predicted that optimizing the design by combining the effects of both of these preferred design variables would result in an implant with a 4.67 failure incidence score. This is 2.43 times lower than the predicted failure incidence score for an implant with the opposite design variables (bundled circumferential fibers and inferior radial fibers). As a result, an implant with the maximum number of spline radial fibers placed on the superior surface and the maximum number of spaced circumferential fibers was chosen as the best design.

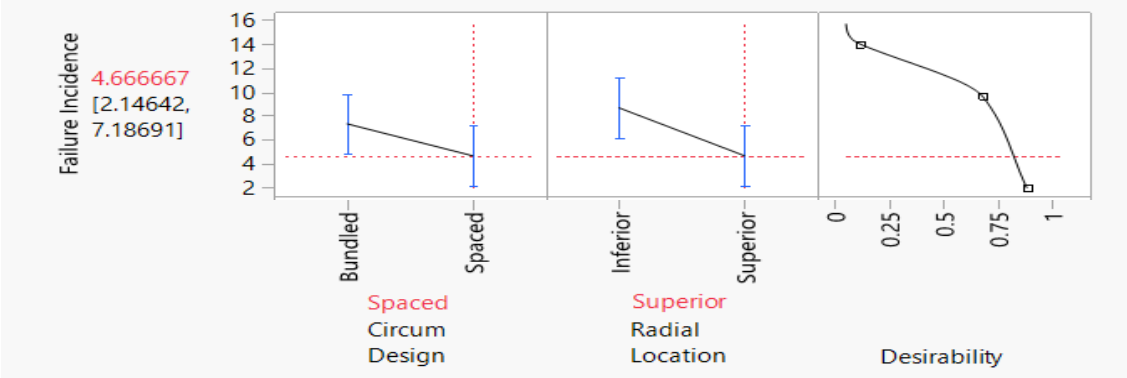

Figure 46: The decrease in failure incidence score for each desired variable (highlighted in red).

CHAPTER 3. VERIFICATION TEST METHODS

3.1 Mechanical Properties

3.1.1 Ultimate Tensile Strengths

As described in the design inputs, the implant needed to have a circumferential strength greater than 19 MPa and a radial strength greater than 4 MPa to pass the criteria. The final design chosen during the design optimization incorporated 8 circumferential fiber bundles and 20 radial fiber turns. Previous testing revealed that the lower range of the circumferential strength can be achieved with a minimum of 4 Kevlar fiber bundles [69]. In this test, all of the samples failed outside of the composite region of the sample and only in the fibers without hydrogel surrounding them as seen in Figure 47. This shows that the hydrogel strengthens the fibers and a conservative estimate of the composite tensile strength could be gathered by calculating just the fiber strength. It was reported in the previous work that the tensile failure force of one fiber bundle was 165 N. Dimensions of the implant were gathered directly from the SolidWorks model without any geometry simplification. Using this data and the largest cross-sectional area of the implant (52.73 mm^2), the circumferential tensile strength of an implant using 8 circumferential fiber bundles could be calculated using Equation 5. A similar approach was used to calculate the strength of the implant in the radial direction. The length of the peripheral edge of the implant was 87.81 mm and the height was 7 mm. Using these dimensions, the radial tensile strength of an implant using 20 radial fiber turns could be calculated using Equation 6.

Figure 47: Composite tensile sample failure mode. [69]

$$8\ fibers\ x\ \frac{T}{A}\ =\ 25\ MPa$$

Individual Fiber Bundle Tensile Failure Force: T = 165 $\frac{N}{fiber}$;

Implant Cross-Sectional Area: A = 52.73 mm^2

Equation 5: Implant strength in the circumferential direction.

$$20\ fibers\ x\ \frac{T}{H\ x\ L}\ =\ 5.4\ MPa$$

Individual Fiber Bundle Tensile Failure Force: T = 165 $\frac{N}{fiber}$;

Implant Peripheral Height: H = 7 mm; Implant Peripheral Length: L = 87.81 mm

Equation 6: Implant strength in the radial direction.

3.1.2 Compressive Modulus

3.1.2.1 Samples

Cylindrical samples were made that reflected the same shape, region, and orientation as the human meniscus samples used for the compressive modulus testing referenced in the design input [88, 89]. The samples were made using the method described in the cylindrical sample SOP. These samples were then cut so the 20% PVA side of the hydrogel was the same height as the 20% PVA layer in the axial direction of the full implant and the 40% PVA layer was cut to the average height of the bulk of the implant. The samples are shown in Figure 48.

3.1.2.2 Setup

The test was run under the same conditions as the human meniscus tests referred to in the design inputs. This means the tests were run in submerged unconfined compression. As described in the design inputs, the sample needed to have a compressive stiffness within 0.35 - 1.13 MPa at 12% strain to pass the input. Tests were conducted using the Model 858 MiniBionix II Testing System. The setup is shown in Figure 49 where the sample was placed between two flat plates. The lower

plate was covered with sandpaper to prevent the sample from sliding and incorporated walls so the sample could be submerged in DI water throughout the test. The samples were preloaded to around 3 N, which was marked as 0% strain. Samples were then cycled to 15% strain at the gait physiological rate of 2.25 mm/s for 10 cycles [88, 97, 98]. The first 3 cycles served as preconditioning to mitigate the high stress the samples experience from initial impact. A linear regression from 2% to 12% strain of the last 7 cycles was run for each sample to calculate the compressive moduli.

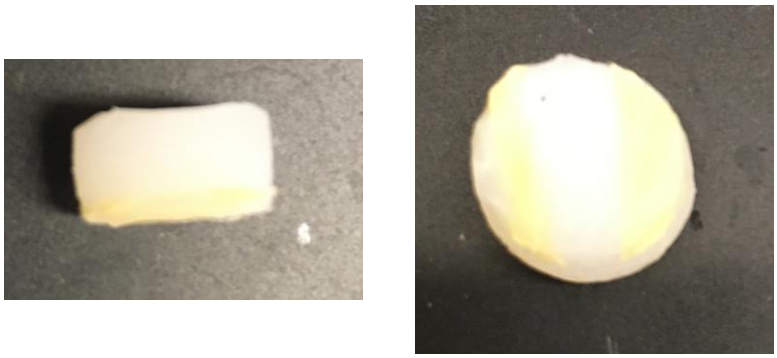

Figure 48: Compressive modulus samples shown from the side (left) and bottom with 20% PVA layer and fiber positioning (right).

Figure 49: Compressive modulus test setup.

3.1.3 Fiber Tear Out Force

Full implants were made to assess both attachment fiber strength and delamination from the bulk implant. As described in the design inputs, attachment fiber tearing or delamination needed to survive 660 N of force to pass the criteria. A custom implant clamp mimicking the curved nature of the femur and flat nature of the tibia was developed to hold the body of the implant in place while allowing the attachment fibers to exit the clamp without any interference. These are seen placed in the Model 858 MiniBionix II Testing System in Figure 50. The implant was positioned so the attachment fibers were pulled taut and in the same plane as the implant base without them crossing. The attachment fibers were secured by looping them around a metal rod that was then clamped to the actuator. The implant clamp was attached to the load cell below. The implant was pretensioned to around 3 N before pulling to failure at 2.25 mm/s. The load rate was previously

shown to not impact strength of this composite, so the fast loading rate seen during gait was chosen to limit hydrogel dry-out [69, 88].

Figure 50: Fiber tear out test setup.

3.2 Durability

3.2.1 Extreme and Daily Compression

3.2.1.1 Cyclic Compression

Full implants were manufactured using the implant SOP to test durability when experiencing axial compression. The implants were setup the same way as the durability and contact pressure test

used in design optimization with the addition of a water bath as shown in Figure 51. The water bath was filled with DI water to fully submerge the implant. To standardize the test further, attachment fibers were pulled to 30-35 N, which was shown in vitro to result in the best contact pressures on a similar hydrogel implant [113].

As described in the design inputs, compressive durability was composed of both a high impact and a longevity component. By using displacement control, both design inputs could be evaluated in the same test. As mentioned in the compressive modulus section, the initial cycle resulted in a much higher stress than the following cycles. Accordingly, there was no preconditioning in the compression test to allow for this initial high impact to occur. Preliminary tests showed that a displacement 3.5 mm or 50% strain resulted in an initial high impact above the extreme compression design input (3,000 N) and a steady state cyclic compression around the daily compression design input (2,300 N). This displacement was adjusted if needed to ensure this occurred. Following a step down stairs, the leg is not in contact with the ground, so a lower load of 5 N was chosen for each cycle to keep the implant in place. The cycles were applied as a 1 Hz sine waveform which resembled the frequency of declining stairs seen in vivo [99]. If the cyclic compression load fell below 2,300 N, the test was stopped and restarted with an adjusted displacement. This meant the implants experienced more than one extreme compression load throughout the test. Because the tests took over 11 hours to complete without any restarting, an entire test could not be run in one day. As a result, each test was run across 3 days and the implant was allowed to recover in DI water overnight twice. Because this test simulated a year of use, allowing only two overnight recoveries was still considered to be a worst-case scenario.

3.2.1.2 Tibial Contact Pressure

After the cyclic test was concluded, the tibial contact pressure from the implant under static/standing loads was evaluated. As described in the design inputs, the implant needed to have a peak contact pressure less than 3 MPa under standing/static loads (800 N) to pass the specification. The test was run using the same methods detailed in the contact pressure test for design optimization as shown in Figure 52. The pressure films were analysed using FPD-8010E software (Fujifilm Corporation, Valhalla, NY) in order to observe the peak contact pressure, average contact pressure, and contact pressure area.

3.2.1.3 Implant Radial Dislocation and Extrusion

After the contact pressure test concluded, the radial dislocation and extrusion of the implant was evaluated. As described in the design inputs, the implant needed to extrude less than 2 mm in the medial direction under standing/static loads (800 N) to pass the criteria. This was tested with the same setup as the tibial contact pressure test excluding the pressure film. Preliminary tests were conducted placing a PVA sheet beneath the implant. The sheet was 2.4 mm thick which is the average thickness of articular cartilage on the tibia in vivo [114, 115]. PVA was chosen as the contacting material because it has a lower coefficient of friction with PVA itself than with cartilage which would lead to greater mobility of the implant and be a more extreme test. However, these tests revealed little radial extrusion because the implant was pushed into the PVA sheet. Because of this, the stiffer tibial platform, which resulted in greater extrusion, was used instead. To lubricate the surface, DI water was spread across the tibial platform to ensure the implant was able to easily slide across the PLA material and the fixture was printed with 100% infill and sanded to ensure the smoothest possible surface. A Model LX500 Laser Exensometer (MTS, Eden Prairie, MN) was used to measure the distance from the horns to the medial most point of the implant both before and after applying 800 N. Reflective strips of tape were placed on the stationary PLA fixture

adjacent to the implant horns and to a fixture attached to the peripheral edge of the implant as seen in Figure 53. Implant radial extrusion was calculated as the difference between these two measurements.

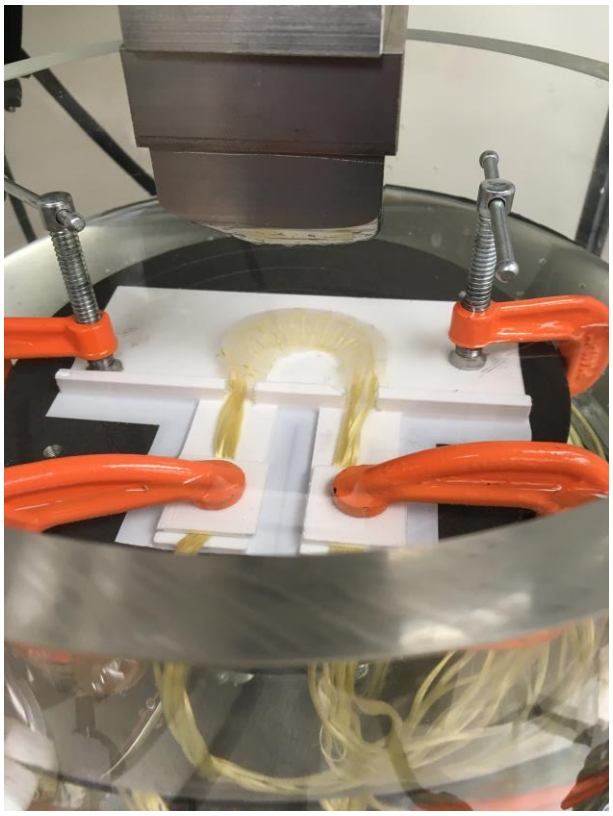

Figure 51: Extreme and daily compression setup.

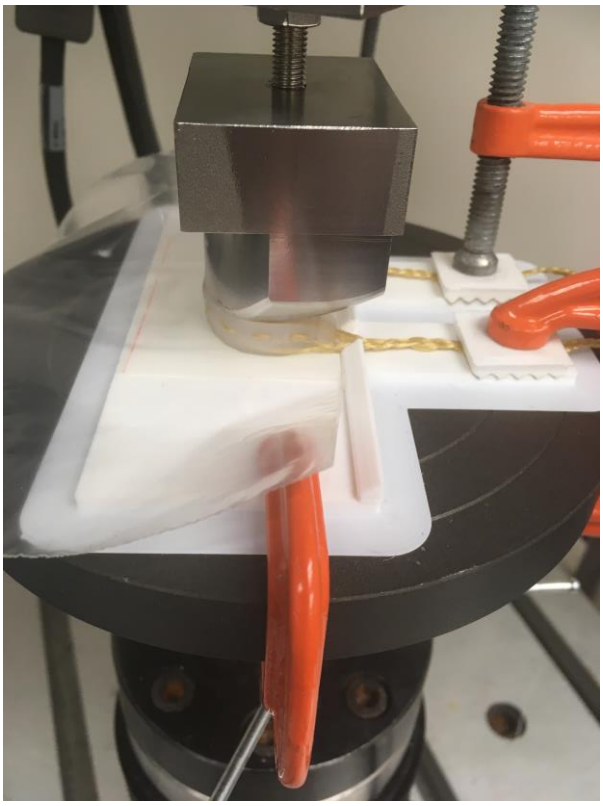

Figure 52: Tibial contact pressure setup with pressure film placed between the implant and tibial platform.

Figure 53: Radial extrusion setup.

3.2.2 Extreme and Daily Shear

Cylindrical samples were made to isolate the target interface for the shear tests. As described in the design inputs, the implant needed to survive 40,000 cycles at 30 N without tearing to pass the input. As seen in Figure 54, the samples were setup the same way as the delamination test used in design optimization. However, the EnduraTEC-ELF 3200 frame with a 100 N load cell was used for its more precise force control. Additionally, the plastic shear fixtures were remade out of aluminum to decrease deformation and were designed to bolt directly into the frame instead of being clamped to avoid any fatigue or slippage issues with the fixturing. Because a water bath could not fit on the load frame, the samples were misted with DI water throughout the test.

As described in the design inputs, both the extreme and daily shear experienced in the knee were the same value, so there was no need for a high impact cycle like what was used in the compression testing. By using force control, the samples could be evaluated at the target cyclic load of 30 N without any excessive forces or need for preconditioning. Following a step down stairs, the leg is not in contact with the ground, so a lower load of 3 N was chosen to keep the frame in tension during force control. Similar to the compression test, the cycles were applied as a 1 Hz sine waveform which resembled the frequency of declining stairs seen in vivo [99]. Because the tests took over 11 hours to complete, an entire test could not be run in one day. As a result, each test was run across 2 days and the implant was allowed to recover in DI water overnight once. Because this test simulated a year of use, one overnight recovery was still considered to be a worst-case scenario.

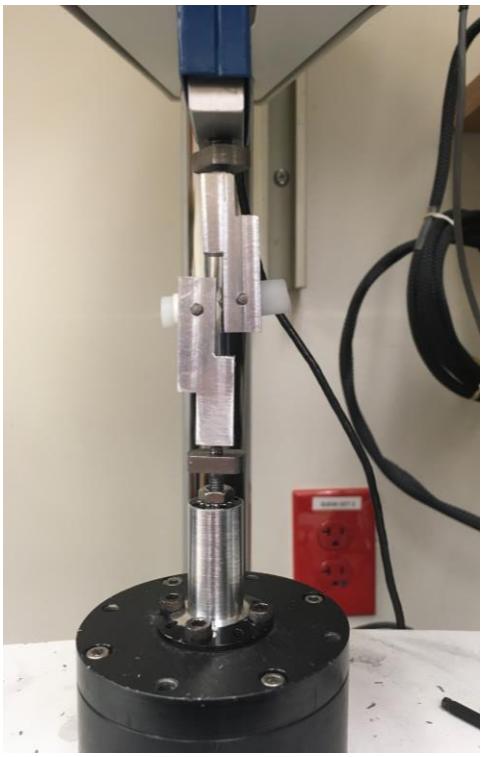

Figure 54: Extreme and daily shear setup.

CHAPTER 4. VERIFICATION TEST RESULTS

4.1 Ultimate Tensile Strengths

The strengths of the circumferential and radial fibers were calculated from tests run during the previous work on this implant. The previous work generated an implant that was only as strong as the lower range of the natural meniscus in the circumferential direction, so the goal of the current work was to incorporate enough fibers to be at least as strong as the higher range of the natural meniscus. As described in the design inputs, this is 19 MPa in the circumferential direction and 4 MPa in the radial direction. The final design chosen included 8 circumferential fiber bundles and 20 radial fiber turns that were used to calculate the strength of the implant in each direction as shown in Equation 5 and Equation 6. The implant circumferential strength was 25 MPa and the radial strength was 5.4 MPa. Both of these passed the design input because they were greater than the strengths of the natural meniscus. While these strengths are stronger than the native meniscus, they remain very close and are on the same order of magnitude. Possible negative effects of this increased strength on compliance of the implant would be seen in the compressive modulus test.

4.2 Compressive Modulus

Three composite samples resembling the makeup of the implant in the axial direction were tested to find the compressive modulus of the implant during physiological strain. As explained in the design inputs, the implant passed the criteria if its average modulus was withing the 0.35-1.13 MPa range of moduli seen in average natural menisci. The data from these tests is shown in Figure 55 along with the dotted regression lines used to calculate the modulus for each sample and the range of the natural meniscus in the red lines. The correlation for each regression line was high and is

shown to verify that the linear assumption was a good fit for a small section of a nonlinear material. The average compressive modulus was 0.94+/-0.037 MPa. This shows that the implant modulus was within the target range up to 5 standard deviations above the average implant modulus, so the implant passed the design input.

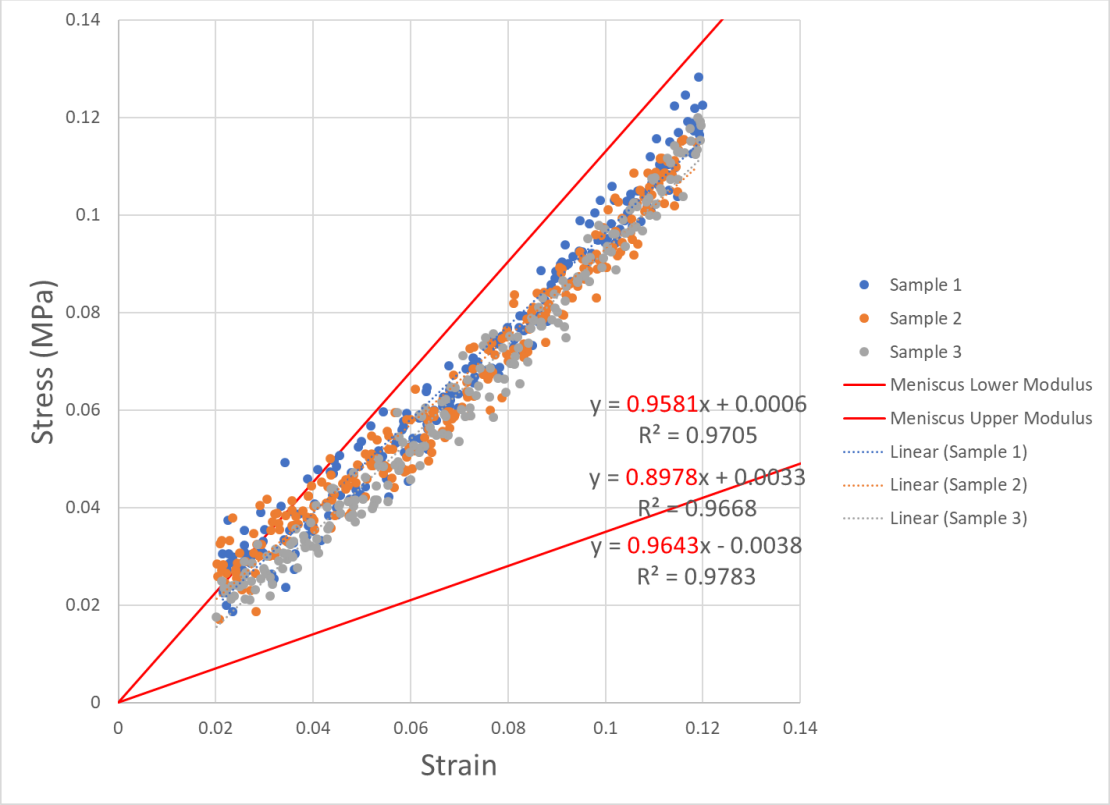

Figure 55: Compressive modulus data and calculated stiffness.

4.3 Fiber Tear Out Force

Three implants were tested to observe the attachment fiber tearing and/or circumferential fiber delamination strength. As discussed in the design inputs, the implant passed the criteria if its average fiber tear out strength was at least as strong as the roots of the average natural meniscus.

Figure 56 shows the failure force of each implant along with the pass criteria of 660 N. All implants failed by delamination of the circumferential fiber layer where all fibers were pulled out of the inferior surface of the implant while still embedded in 20% PVA. Examples of this failure mode are shown in Figure 57. There were small breaks in the load/displacement curve, but these were attributed to slippage of the attachment fibers from the actuator instead of any failure from the implant. This was verified by running an additional test that was loaded to 660 N instead of to failure. These implants were then inspected for any signs of tearing or delamination, of which none were found. The average failure force was 909+/-93 N, which was 1.38 times the root strength of the natural meniscus. Additionally, the failure load was above the design input up to 2.5 standard deviations below the average implant fiber tear out load, so the implant passed the design input.

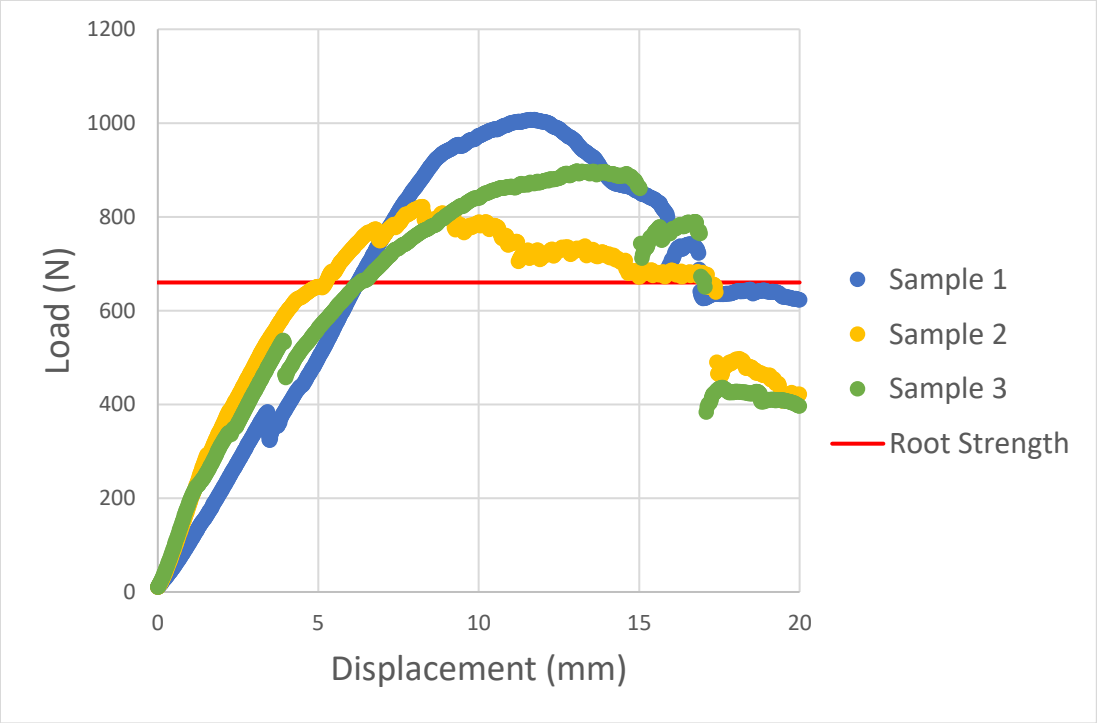

Figure 56: Fiber tear out force.

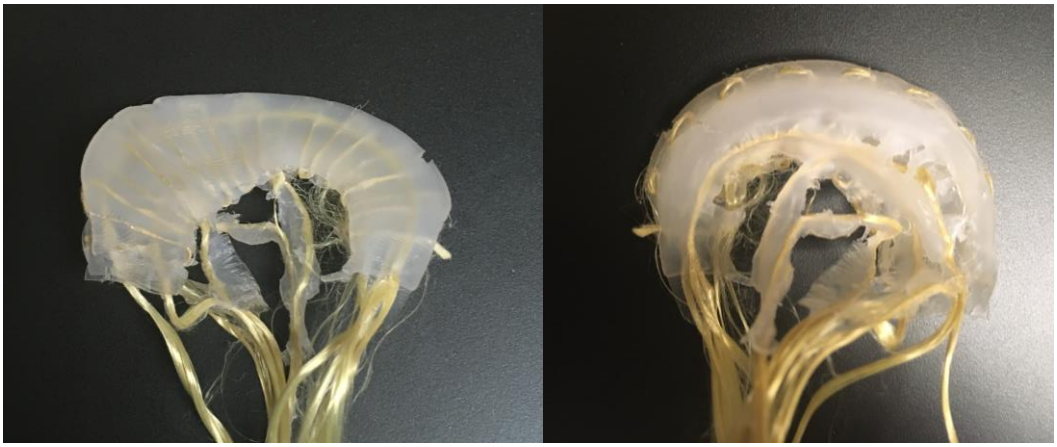

Figure 57: Examples of the fiber tear out failure from the superior view (left) and inferior view (right) of the implant.

4.4 Extreme and Daily Compression

4.4.1 Macroscopic Observation

Three implants were successfully tested with more than one extreme compression and cyclic compressions above the design inputs. The test was run in approximately 2,000 cycle intervals before restarting due to the cyclic compressive load decreasing below the 2,300 N design input. An example of one of these intervals is shown in Figure 58. The initial cycle resulted in a load of 3,395 N on average with a fast drop off, as seen in Figure 59. The initial high impact was nearly 400 N higher than the extreme compression design input and was experienced an average of 21 times by each implant, which was a more extreme scenario than required by the design input. An example of the load vs strain curve from a high impact cycle is shown in Figure 60. Strain was calculated as the ratio of displacement to the height of the peripheral edge of the implant. The curve appears to transition from nonlinear to linear. This is most likely because the hydrogel is allowed to deform more freely during lower strains like those seen during gait, but the reinforcing

fibers limit excessive deformation and become a more significant component of the stiffness as the displacement becomes larger. A similar trend is seen in the natural meniscus. Additionally, the quick recovery seen from the implant resembles the properties of the natural meniscus, which has been shown to become much more compliant from its first to 10^{th} cycle and then gradually continue this trend [89]. The implant appeared to reach a steady state cyclic load around 1,500 cycles, and the average cyclic loads were 2,482 N with a standard deviation of 108 N. The cyclic load was nearly 200 N above the daily compression design input. After completion of each test, the implant was thoroughly examined for any signs of tearing or delamination and none were found. An example of one of the implants after the test is shown in Figure 61. One of the implants felt partially indented on its superior surface. This implant as well as the other two were not allowed to recover in DI water in order to see if any deformation (even if not permanent) would affect tibial contact pressure or radial deformation functionality.

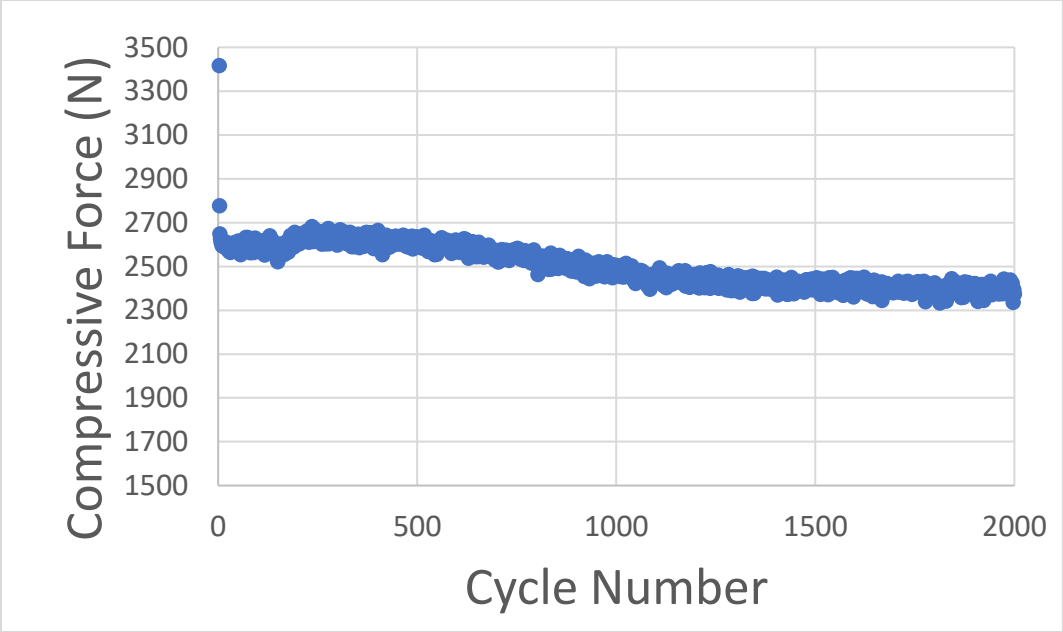

Figure 58: High impact and longevity loading data.

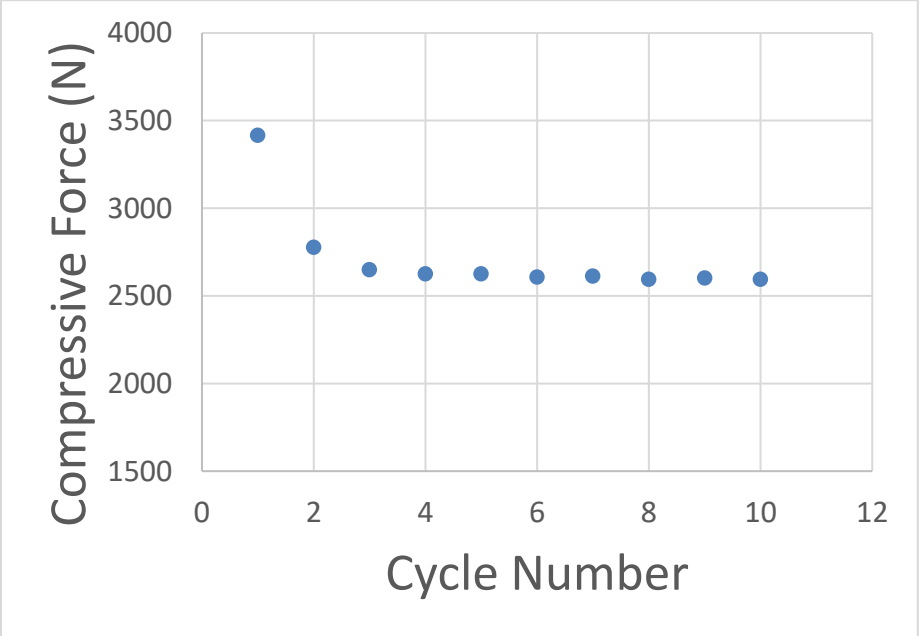

Figure 59: High impact to steady state load.

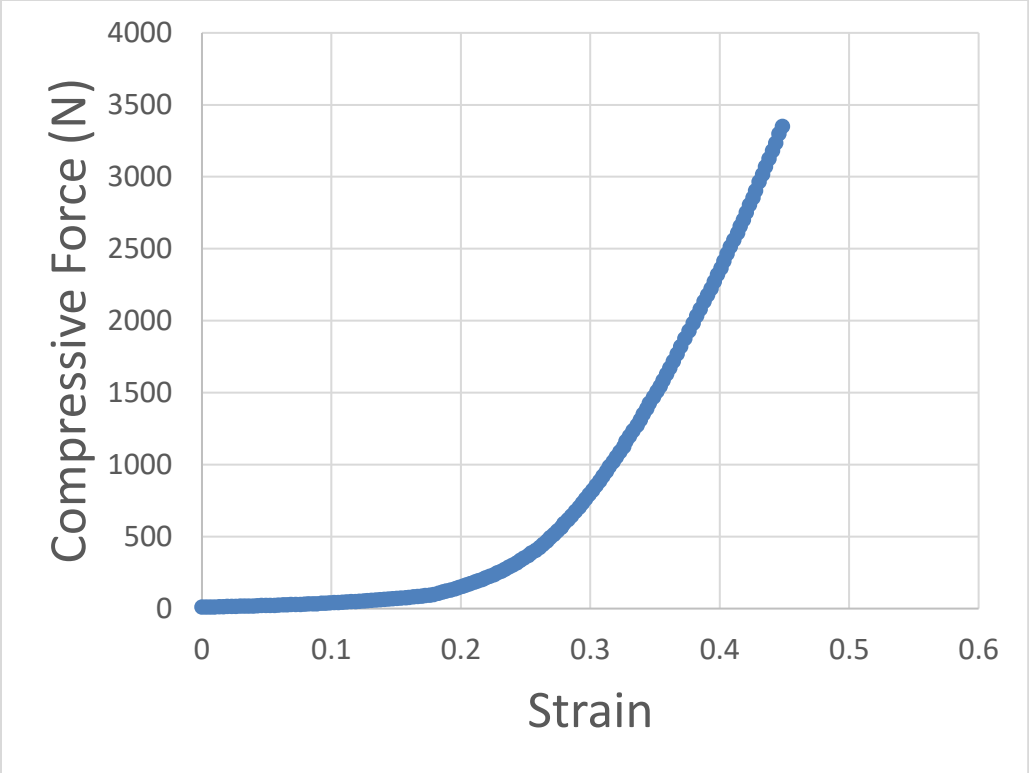

Figure 60: Composite implant stiffness profile.

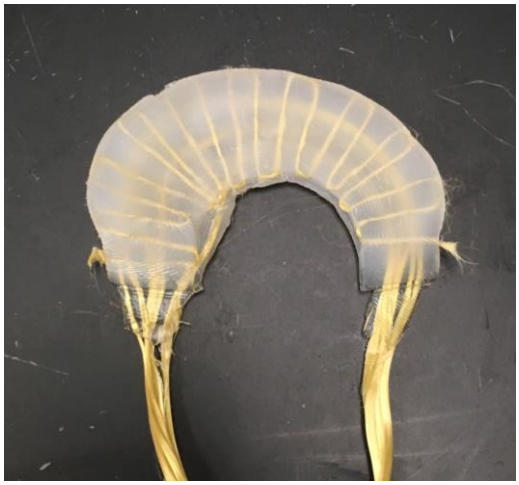

Figure 61: Example of the implant after compression testing (no failures).

4.4.2 Pressure Distribution

The tibial contact pressures were successfully gathered during static/standing loading for all three implants. Pictures of the pressure distributions are shown in Figure 62. The peak contact pressure, average contact pressure, and area of contact are shown in Table 9. Interestingly the indented implant identified during the macroscopic evaluation did not perform worse than the remaining two implants. This may be because the indentation was found only on the superior surface and did not affect the inferior surface. It may have even made the implant superior surface more concentric to the femur and enhanced load transmittance into hoop stresses. Similar to the trends discovered during design optimization and FEA, the spaced circumferential fibers along the inferior edge of the implant stiffened the implant to prevent excessive deformation but result in a higher stress concentration around the fibers, especially the middle and lateral circumferential fibers. The average peak contact pressure was 2.21+/-0.38 MPa, which was two standard deviations below the peak contact pressure of the natural meniscus, so the implant passed the design input.

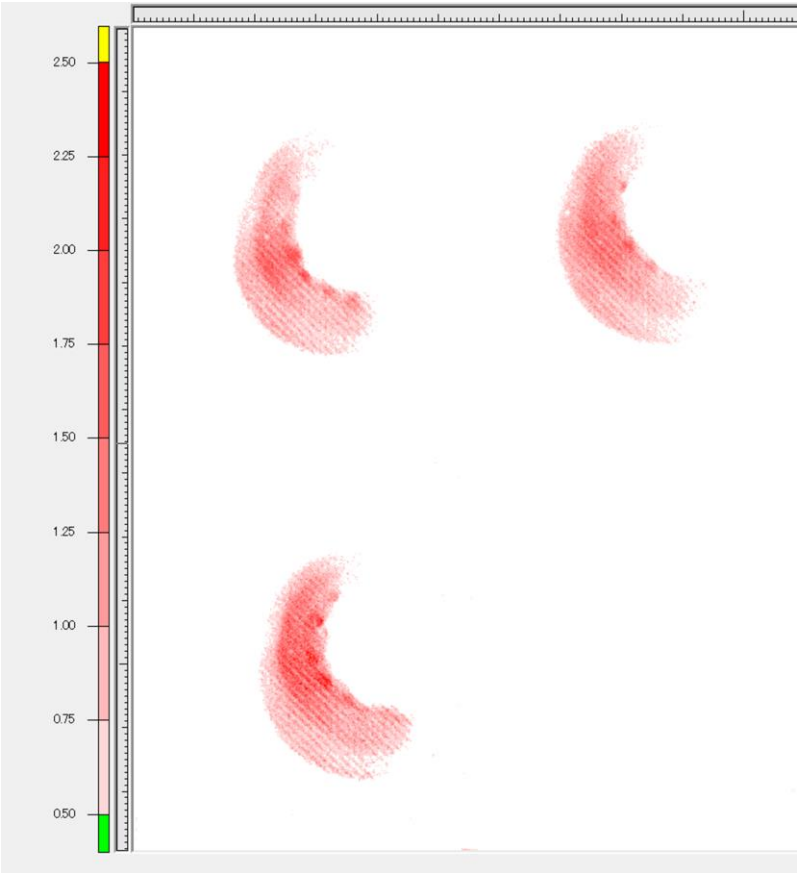

Figure 62: Pressure distributions and contact pressure of the implants after compression testing.

Table 9: Average contact pressure, peak contact pressure, and contact area.

Sample	Max Pressure(MPa)	Ave Pressure(MPa)	Pressed Area(mm2)
1	2.05	0.89	364
2	1.94	0.91	387
3	2.65	1	422
Average	2.21	0.93	391.00
SD	0.38	0.06	29.21

4.4.3 Implant Radial Dislocation and Extrusion

The deformation in the medial direction was successfully gathered before and after static/standing loading for all three implants. The average and standard deviation of the radial extrusions are shown in Table 10. Interestingly the indented implant identified during the macroscopic evaluation did not perform worse than the remaining two implants. This may be because the radial extrusion of the implant is limited by the Kevlar fibers creating the hoop stresses instead of the bulk hydrogel of the implant, so even when the bulk of the implant becomes temporarily deformed before recovery, the circumferential fibers remain in their designed position. The average extrusion was 1.05+/-0.08 mm, which is nearly half the radial extrusion of the natural meniscus. Additionally, the extrusion was below the design input up to 11.89 standard deviations above the average implant radial extrusion, so the implant passed the design input.

Table 10: Radial extrusion data.

Sample	**1**	**2**	**3**
Initial Distance (mm)	42.28	42.3	42.5
Final Distance(mm)	43.32	43.43	43.47
Radial Extrusion (mm)	1.04	1.13	0.97
Average	1.05		
SD	0.08		

4.5 Extreme and Daily Shear

Three cylindrical samples were successfully tested in cyclic shear above the design input. The test was run in approximately 20,000 cycle intervals before restarting due to the length of the test. An example of a 2,000 cycle interval is shown in Figure 63. As seen in the example data, there were no high impacts and load drop offs like what was seen in the compression test. The average peak load was 30.07+/-0.01 N across all three tests, which was above the design input load of 30 N. An example of the load vs strain curve from one of the cycles is shown in Figure 64. Strain was calculated as the ratio of displacement to the diameter of the sample cross section. Interestingly, the profile appears more linear than the hydrogel stiffness profile in compression. After completion of each test, the sample was thoroughly examined for any signs of tearing or delamination and none were found. An example of one of the implants after the test is shown in Figure 65. The 20% PVA/Kevlar/40% PVA interface of the samples shrunk by the end of the test, but this was likely because of sample dry-out since the fixturing holding the sample blocked this region from receiving the DI water mist.

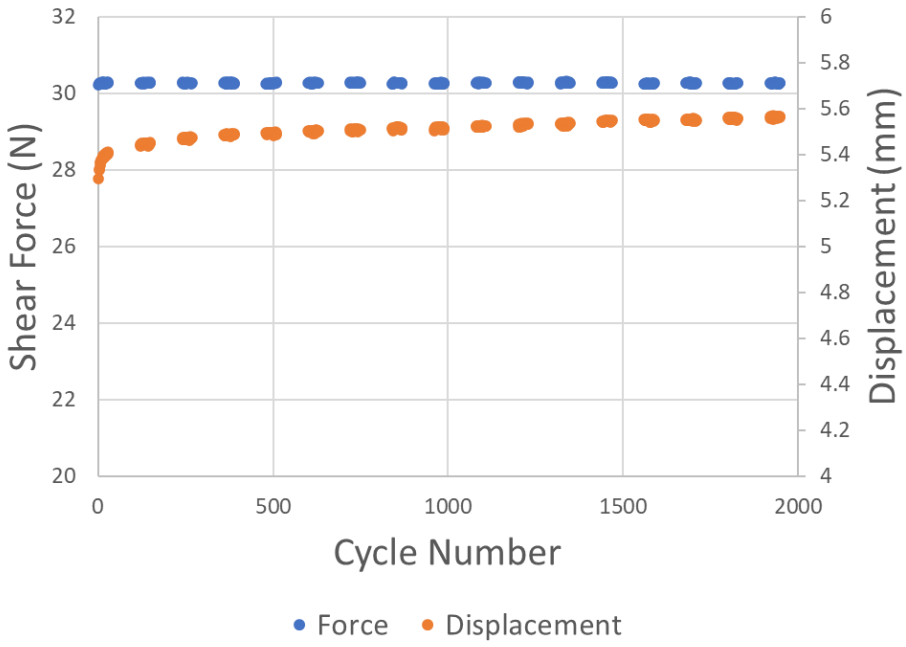

Figure 63: Example of the peak shear load over 2,000 cycles.

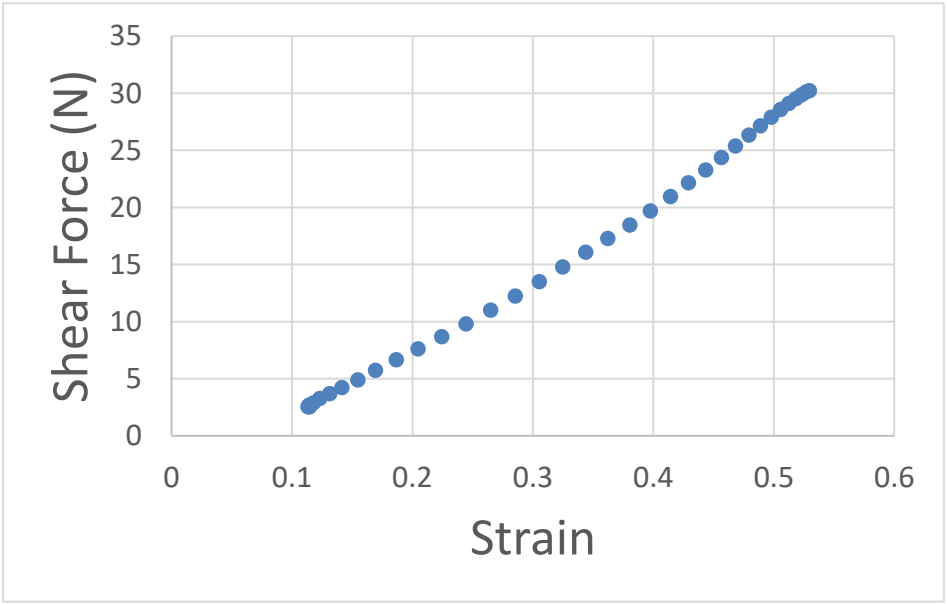

Figure 64: Shear sample stiffness profile of the initial cycle.

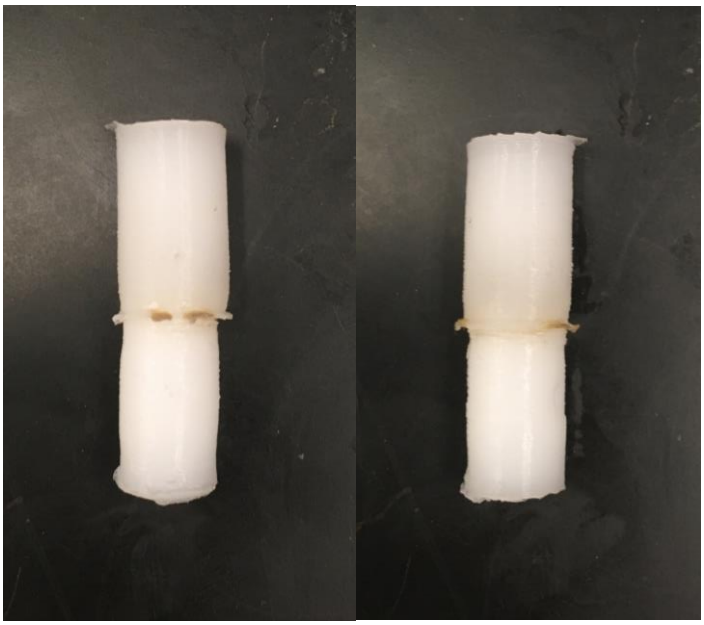

Figure 65: Examples views of a sample after shear testing (no failures).

CHAPTER 5. DESIGN VALIDATION

5.1 User Needs

The design verification ensured that the implant was being built correctly and in accordance to the test specifications, but design validation is needed to check that the implant has the correct design and functionality for the needs of its intended users. In order to verify this, a list of user needs for both the patients receiving the device and the orthopaedic surgeons implanting the device was assembled.

5.1.1 Patient

The patient user needs were derived from the surveys of people who had received a total knee replacement. These surveys were chosen because unicompartmental and total knee replacements are the most commonly implanted devices for patients with an osteoarthritic knee. Additionally, total knee replacements focus on durability, which was a primary focus of the design verification tests for this implant, but they are still not a favorable device and are typically only used on patients 50 years old or above. Looking at these surveys can give insight into additional features beyond durability that patients want devices to offer. Table 11 shows the reorganized and condensed results of a review of over two hundred of these surveys in the columns of the left, and the solutions provided by the artificial implant on the right [116].

Table 11: User needs of the patient.

Overall Needs	Test Specifics	Implant or Test Solution
Quick recovery	Arthroscopy	• Same size or smaller than allograft • Flexible material

No reoperation	No implant failure	• Long term strength
		  ○ No tears
		• No excessive wear
		• Long term fixation
		  ○ No dislocation

	No inflammation	• Biocompatible material • No infection
	Minimize progression of osteoarthritis	• No excessive contact stresses

5.1.2 Surgeon

The orthopedic surgeon user needs were derived from input from Dr. Kyle Hammond (head team physician for the Atlanta Falcons, head orthopedic surgeon for the Atlanta Hawks, associate team physician for the Atlanta Braves, Georgia Tech, Emory University, and several metro Atlanta High Schools) and Dr. Jeremiah Easley (ACVS founding fellow for large animal minimally invasive surgery, co-director of the Preclinical Surgical Research Laboratory, and assistant professor in the Department of Clinical Sciences at Colorado State University). Suggestions from both professionals and ovine cadaveric work of the implantation procedure by Dr. Easley were used to arrive at the surgeon user needs. Table 12 shows the results in the columns on the left and the solutions provided by the artificial implant on the right.

Table 12: User needs for the surgeon.

Overall Needs	Test Specifics	Implant or Test Solution
Simple implantation	Similar procedure as used for allografts	• Condense the attachment fibers into one grouping ○ Braided attachment fibers
Secure fixation	Similar attachment to allografts	• Boney fixation • Interference screws not possible because of width of attachment fibers compared to bone tunnel (not enough room for interference screw) • Knot attachment fibers around endobutton and then secure
	Peripheral edge of tibia attachment	• Radial fiber loops extending outside peripheral edge

5.2 Methods

5.2.1 Study Endpoints

The goal of the pilot animal study was to supply initial evidence that the implant could meet the required user needs of both the patient and surgeon. The needs of both stakeholders could be addressed by focusing on the procedure and in vivo outcomes. This required an animal model that would give insight into the effectiveness of the implant durability, biocompatibility, and chondroprotective functionality.

5.2.1.1 Durability

Not only is durability of the implant a primary concern of the patient because it is a major factor in reoperation, but it was also the most common shortcoming of nearly every meniscus replacement that has reported clinical or animal trials [63, 66, 67]. Similar to the in vitro tests, the durability of the implant could be checked by macroscopically observing any tears or delamination after being explanted. Additionally, the fixation of the implant could become compromised, allowing it to dislocate. This could be evaluated by observing if the horns of the implant were detached or were no longer flush to their attachment point on the tibial plateau. The implant may also experience excessive wear that could compromise its mechanical properties. Wear could be evaluated using the histology outlined in the upcoming endpoint. The implant gives positive insight into being durable and satisfying the user needs if there are no macroscopically observable tears in the implant and if the implant receives a histology score of 1 or less for signs of implant degradation and particulate debris.

5.2.1.2 Biocompatibility

Biocompatibility of the implant within the knee is another major factor for reoperation. Inflammation could arise from either the nature of the materials themselves or from the wear particles they produce within the knee environment. Even though PVA is an FDA approved material and aramid fibers have been used in sutures, neither have been FDA approved for use in the knee which raises new concerns. To check for inflammation, 5 mm long slice sections of the tibial plateau, femoral condyle, and synovial membrane would be collected for histology. H&E stain on the synovial membrane and H&E and safranin-O fast green stain on the articular cartilage samples could be used to identify and quantify the cells in Table 13. This table is an expansion of the ASTM F981-04 (Standard Practice for Assessment of Compatibility of Biomaterials for Surgical Implants with Respect to Effect of Materials on Muscle and Insertion into Bone). The

implant gives positive insight into being biocompatible and satisfying the user needs if it receives a histology score of 1 or less for polymorphonuclear cells, lymphocytes, plasma cells, macrophages, giant cells, necrosis, neovascularization, and fibrosis.

5.2.1.3 Chondroprotection

Chondroprotection evaluation could be used to give insight into the implant's ability to minimize progression of osteoarthritis as well as provide a secondary evaluation method for fixation compromise that results in increased contact pressures [29, 30]. After the study has concluded, scoring of the femoral and tibial articular cartilage would be conducted using India ink to monitor surface cartilage cracking following the frequently used modified Modified Mankin system. It is important to note that none of the commercial or experimental meniscus replacements detailed in the background section showed significantly improved chondroprotection over meniscectomy and even allografts have been shown clinically to not significantly provide chondroprotection compared to meniscectomy [59, 63, 66, 67, 117, 118]. As a result, chondroprotection was a secondary endpoint used to better quantify the functionality of the implant but was not the focus of the study. As stated in the previous two endpoints, because nearly all previous implants mechanically failed in animal studies and because the implant material biocompatibility has not been shown in the knee, these remained the two primary endpoints of the study.

Table 13: Histological evaluation of defect site sections for cell type and response.

	Score				
Cell type/response	**0**	**1**	**2**	**3**	**4**
Polymorphonuclear cells	None	Rare, 1-5/HPF*	5-10/HPF	Heavy infiltrate	Packed
Lymphocytes	None	Rare, 1-5/HPF	5-10/HPF	Heavy infiltrate	Packed
Plasma cells	None	Rare, 1-5/HPF	5-10/HPF	Heavy infiltrate	Packed
Macrophages	None	Rare, 1-5/HPF	5-10/HPF	Heavy infiltrate	Packed
Giant cells	None	Rare, 1-2/HPF	3-5/HPF	Heavy infiltrate	Sheets
Necrosis	None	Minimal	Mild	Moderate	Severe
Neovascularization[&]	None	Minimal	Mild	Moderate	Severe
Fibrosis	None	Minimal	Mild	Moderate	Severe
Signs of implant degradation	None	Minimal	Mild	Moderate	Severe
Particulate debris	None	Minimal	Mild	Moderate	Severe

** HPF – per high powered field*

[+] Osteoblastic cells – severe suggests numerous OB Cells

[#] Signs of bone remodeling by osteoclasts – severe suggests abundant bone remodeling present

[&] Neovascularization – severe suggests numerous neovascular vessels

5.2.2 Model

Sheep were chosen for the animal model because of their similarity to humans in meniscus strength, general size, and compressive properties [119-121]. Additionally, the contact stresses transmitted to the tibial plateau for sheep are within the range of that found in human knees, sheep menisci have a layer of radial fibers similar to humans that is absent in other species, and their onset of OA is similar to that of humans unlike some species with spontaneous OA after surgery [121-126]. Based on previous animal studies with synthetic total meniscus replacements, a 3-month study was decided. This was because studies have shown chondroprotection differences between initial and 3-month endpoints but no difference between 3 and 6 month endpoints [94, 127]. It has been shown that the fastest rate of wear for PVA is within the initial cycles of use and

then plateaus so the most significant period of wear would be experienced during the beginning of the animal study [128]. A similar implant experienced wear and tear of its attachment fibers in all seven implants after 3 months of use [92]. A PVA implant with reinforcing fibers showed complete delamination of its fibers at 4 months [67]. Even though this study was a month longer than the proposed study, the failed implants were torn in half due to delamination, so it is believed that initial signs of delamination or tearing are likely to appear by 3 months if the proposed implant is not durable enough. Because this is a pilot study, one sheep was chosen to get an idea of the implant performance and identify possible failure modes for redesigns if applicable.

5.2.3 Procedure

Animals will be placed in dorsal recumbency following induction of general anesthesia. Anesthetic medications and monitoring are outlined below. The wool will be clipped from one stifle and it will be prepped for aseptic surgery using alternating scrubs of povide-iodine and alcohol. All of the instruments, gowns and drapes are properly heat or chemically sterilized prior to use on this study. The surgeons perform an aseptic prep for at least 5 minutes and use a topical disinfectant (Avagard) prior to sterile gowning and gloving.

A medial parapatellar arthrotomy of the stifle will be performed (without patellar subluxation) and the medial collateral ligament exposed. The medial collateral ligament will be released from its attachment to the femur by creating an osteotomy and reflecting the medial collateral ligament to expose the medial meniscus. A partial meniscectomy will be performed to remove part of the meniscus. A bone tunnel with a diameter of 3 mm will be drilled at each tibial attachment point of the natural meniscus. The removed portion will be replaced with one of the meniscal implants. The implant will be secured by feeding the attachment fibers of the implant through the bone tunnels

and tying them together on the distal end. This fixation method is to be used instead of interference screws in the pilot study because of its familiarity and because it was deemed sufficient from a cadaveric study when cycling the joint with the implant through the full range of motion 15 times. Using a screw, the bone block with the medial collateral ligament will be reattached to the femur. The incisions will then be closed. The joint capsule will be closed with #2/0-polysorb suture material in an interrupted pattern. The overlying fascia of the tensor fascia lata will be closed using #2/0-Polysorb suture material. The subcutaneous tissues will be closed in a simple continuous pattern using #2/0-polysorb suture material, while skin closure will be in an interrupted pattern using stainless steel staples (Proximate; Ethicon).

Immediately after surgery, sheep will be transferred from the operating table to a Sheep Jeep and returned to the prep area in the PSRL where they will be monitored until their swallow reflex returns, at that time they will be taken to the stock trailer where they will be propped in sternal recumbency and monitored periodically. At the end of the day, all animals that were operated upon that day will be moved to the research barn at the VTH. The sheep will be housed indoors for the first two weeks of the study to monitor healing of the incision sites.

5.3 Sheep Implant

5.3.1 Geometry and Sizing

The implant is intended to be an off the shelf product instead of custom made to each patient's anatomy, so different implant sizes were developed to give the surgeon options and the patient cheaper and quicker service. To ensure the sheep implant resembled the human implant, the shape was generated using the same dimensions identified to construct the human implant shape. This meant the inferior and peripheral surfaces of the implant remained flat while the width (posterior,

middle, and anterior), height, A-P length, arc length of the peripheral edge, and curvature of the superior surface were adjusted to sheep dimensions found in literature [120, 129]. These dimensions were verified to be representative of the sheep used in the animal study through computed tomography (CT) imaging and cadaver knees generously provided by the Preclinical Surgical Research Laboratory (PSRL) at Colorado State University. CT images of the sheep used in prior knee device studies at PSRL were analysed using ITK-SNAP. Because the actual meniscus cannot be captured by CT, the available space between the femur and tibia was dimensioned and is shown in Figure 66. All of these dimensions besides the available height fell within one standard deviation of the literature values, so the three implant sizes decided upon for cadaveric work were the average sheep dimensions, one standard deviation smaller in each dimension, and one standard deviation larger in each dimension from the literature values. This ended up being around a 5% change in the A-P and M-P dimensions, which was the same tolerance that is used for allograft sizing [40].

Cadaveric work using sheep stifle joints was used to ensure proper fit and fixation of the implant and identify additional design improvements. The native medial meniscus was explanted, and bone tunnels were drilled into the tibia starting where the native meniscus root attachment points were found. For this study, the implant was attached to the tibia by tying the attachment fibers together at the distal end of the bone tunnels. After implantation, the knees were cycled through their full range of motion several times. The braided attachment fibers condensed the loose attachment fibers into a tight bundle which made it easier to feed the fibers through the bone tunnels. They also led to a more secure knot than the free fibers when submerged in water. This was possibly because of increased friction due to the grooves between braids or because the tighter structure prevented the hydrophilic fibers from absorbing water, expanding, and loosening the knot.

Additionally, PVA extensions were added to the horns of the implant to allow for more secure and consistent placement as well as to protect the fibers from wear at the bone interface where fiber failures were shown in previous hydrogel implants [92]. Pictures of the tibia with the native meniscus are shown in Figure 67. Figure 68 shows the implant fit within the knee. It is important to note that the radial fibers are not shown in this sheep implant picture because they did not affect the implant shape or fixation method in this work. The femoral condyle fit entirely within the rim of the implant from all sides and the attachment fibers were able to be inserted into the bone tunnels so that the PVA extensions protected the fibers at the tunnel entrance.

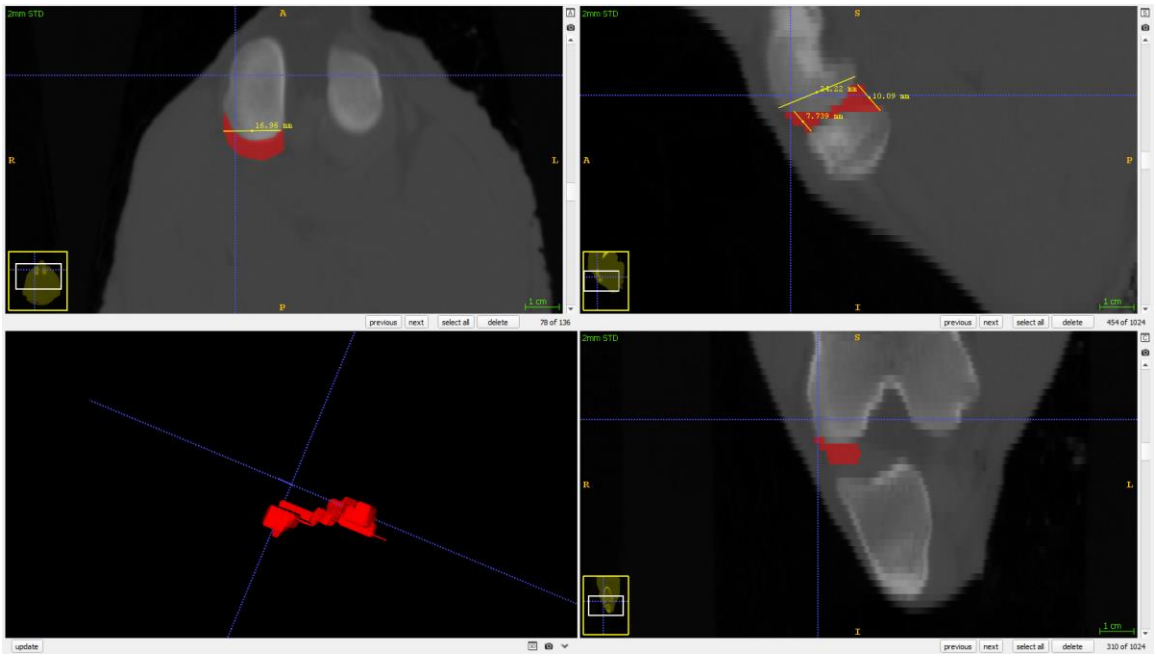

Figure 66: CT scan of sheep stifle joint with the available space outlined in red and the dimensions taken shown by the yellow lines.

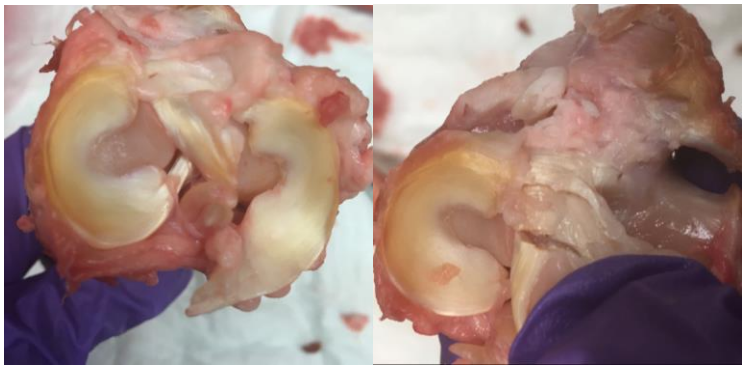

Figure 67: Native sheep medial meniscus showing the posterior attachment (left) and anterior attachment (right).

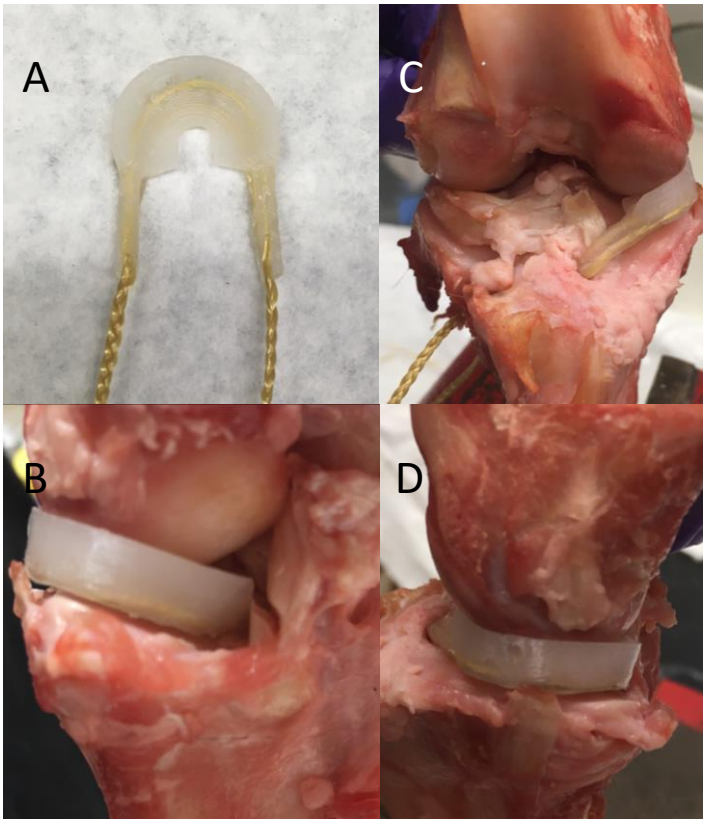

Figure 68: Sheep implant (A) implanted in the knee with views from the posterior (B), anterior (C), and medial (D) sides.

5.3.2 Fiber Reinforcement

The number of fibers reinforcing the sheep implant was decided using the same logic used for the human implant. The human implant used enough fibers to be stronger than the average human meniscus. At the same time, this number was limited to two groupings of two fiber bundles within a 5 mm radius of the implant to protect against delamination. The average sheep meniscus has a circumferential strength of 36 MPa and the sheep implant has a maximum cross sectional area of 23.54 mm^2 [96]. Using Equation 7, the sheep implant must have at least 6 circumferential fiber bundles. This meant two groupings of two circumferential fiber bundles each could be spread across the width and an additional grouping along the height resulting in the same density of fibers used during the shear verification test. As an additional check, the maximum circumferential tensile load of sheep menisci was found to be 572.6 N, which is the strength of 4 Kevlar fiber bundles [129]. No strengths were found for sheep menisci in the radial direction, so the radial fibers were scaled from the human design by the same ratio as the circumferential fibers (6/8). As a result, 15 radial fibers were used in the sheep implant.

$$6\ fibers\ x\ \frac{T}{A} = 42\ MPa$$

Individual Fiber Bundle Tensile Failure Force: T = 165 $\frac{N}{fiber}$;

Cross-sectional Area of the Sheep Implant: A = 23.54 mm^2

Equation 7: Sheep implant strength in the circumferential direction.

5.3.3 Sheep Implant Manufacturing

The sheep implants were made using the same method outlined in the implant SOP with adapted molds and additional steps to ensure the implant was sterile. In order to sterilize the materials, 75 g of dry PVA granules and 6 Kevlar fiber bundles each 30 cm in length were autoclaved at 120°C and 15 psi for 15 minutes. The fibers were then removed and placed in a sterile bag. Sterile saline 0.9% from Medline (Mundelein, Illinois) was used instead of DI water to make the 20% and 40% PVA. The remaining steps remained the same as those found in the implant SOP. The implants were made in a biosafety cabinet, and an overview of adapted the sheep molds used in the steps is shown in Figure 69. Following the 6 freeze/thaw cycles, the attachment fibers were braided tightly together. The implant was then submerged again in sterile saline for at least 24 hours and then the 15 radial fibers were sewn into the superior surface. The implants were then stored in sterile saline until use. The implant body and attachment fibers will be briefly dipped in 70% ethanol immediately prior to implantation within the sheep.

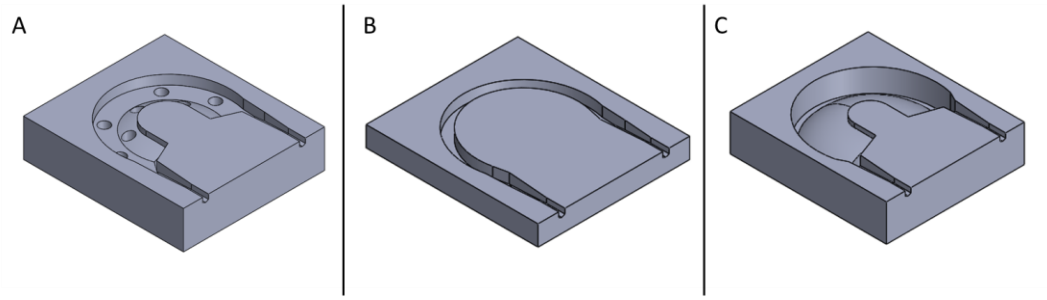

Figure 69: Inferior circumferential fiber mold (A), superior circumferential mold (B), and the final mold.

CHAPTER 6. IMPLANT AND TESTING EVALUATION

6.1 Mechanical Testing Limitations

The goal of this thesis was to design an implant that would survive the environment of the knee for at least one year. Because nearly every previous implant failed due to mechanical problems centered around implant strength, the mechanical tests were designed to resemble the harsh environment of the knee and, in some tests, emulate a worst-case scenario to inspire further confidence in the device.

All of the design specifications were from measured properties explicitly of the natural meniscus or from in vivo sensors measuring forces directly experienced in the knee. Stresses were chosen as the design inputs for the majority of the implant mechanical properties, but forces were chosen as the evaluation criteria for the durability of the implant. This was because cross sectional areas for stresses can be dimensioned from an explanted meniscus during mechanical property evaluation, but no literature was found that detected the stresses within the meniscus during various activities in vivo. The highest loads during extreme and daily activities were used as design inputs, but it is a possible that that largest stresses within the meniscus are actually seen during times with lower loads but higher degrees of flexion and thus less interfacing area between the femur and meniscus. However, because no literature was found concerning force and contact area between the femur and meniscus across extreme or daily activities, the highest loads were used. Additionally, it was beneficial to test the entire implant in a situation with zero degrees of flexion as opposed to only testing the posterior region to simulate high flexion activities.

The compression tests were conducted with an indenter and platform made to resemble the geometry of the femur and tibia. In addition to the geometries being simplified, they were also far stiffer than the articular cartilage directly contacting the meniscus. The stiffer material was deemed acceptable because it led to a worst-case scenario. In an intact knee, the articular cartilage would deform and absorb some of the force in the knee; however knees with severe cartilage degeneration may have direct contact between the meniscus and the bone leading to a more direct load transmission. The geometry of the femur indenter was modeled after a 3D scan of the Somso NS 50 bone model to ensure it closely resembled the human femoral condyle shape. However, no model was used when generating the flat platform the implant rested on. This most likely impacted the pressure distribution results. In the design optimization, this method was used for all designs, so it was acceptable to compare across these results. This also standardized the test because there were concerns that using the bone model tibia would introduce greater variation because the pressure distribution changed based on where exactly the implant was placed on the uneven bone model tibia. This would make it even harder to decipher any pressure distribution trends between designs. Additionally, similar implants were tested using the anatomical Somso NS 50 bone model itself and resulted in a peak contact pressure only 0.3 MPa higher than with the platform tibia [69].

The shear tests were conducted on a sample instead of the entire implant. This was because the superior and inferior surfaces of the implant could not successfully be clamped. The sample designed for this test resembled the plane parallel to the tibial plateau that was identified in vivo to experience the largest shear force in the knee. It isolated the 20% PVA/Kevlar/40% PVA interface in the final design that had the lower shear strength identified in design optimization and thus would most likely fail first. It was manufactured using the same methods as those used for the whole implant, and it resembled the internal aspect of the implant where shear tears are believed

to originate [22]. Because of this, the shear test using a sample shows how the overall implant would perform in shear and may even be a worst-case scenario without the additional reinforcement of the radial fibers and 40% PVA exterior of the implant.

6.2 Implant Design Limitations

The implant was designed based on limiting the number and occurrence of failure modes based on previous findings from synthetic implants and allografts. Because nearly every previous implant failed due to mechanical problems centered around implant strength, this became the focus area of the design during its optimization.

The Kevlar fibers are much stronger than the PVA hydrogel and thus contribute more to the overall strength of the implant. Accordingly, the fibers were chosen as the focus for designing a strong implant. Most design variables were chosen to resemble the fiber arrangement of the natural meniscus. However, the bundled circumferential fiber design and spline (sewn in) radial fiber design were chosen because of either previous use or ease of manufacturing. Previous versions of the implant attempted integrating the spline radial fiber design in its own 20% PVA hydrogel layer and then assembling all of the layers together in a similar manner to how the spaced circumferential fibers were integrated. However, the radially aligned fibers would shift and no longer retain their original orientation once the whole implant was melted together. As a result, the sewing technique was implemented so the fibers could be added after implant re-melting. Additionally, the radial fibers could not be placed on both the superior and inferior surface due to the thickness of the Kevlar fibers. Previous versions of the implant tried to integrate both a superior and inferior radial fiber layer but resulted in notable overlap of fibers within the hydrogel which led to insufficient fiber/hydrogel interfacing and early delamination. However, it was shown that reinforcing the

superior surface was more effective at preventing tears. Other versions of the implant attempted to use PVA fibers that were smaller and better integrated with the PVA hydrogel to further limit delamination and possibly allow for even greater fiber spacing. However, these implants could not be successfully tested because the attachment fibers were too elastic and would allow the implant to radially extrude out from under the femur indenter.

Optimization was performed on fibers, but implant shape could potentially be improved as well. When the implant has sufficient strength, shape and size become the primary variables influencing tibial contact pressure. This was not conducted in this work because the implant revealed contact pressures similar to the natural meniscus and studies have already been conducted observing size and shape trends of the natural meniscus and their impact on contact pressure and internal stresses [130-133]. Surprisingly, these reveal that a smaller implant leads to better contact pressures. This also results in higher internal stresses. Because the implant is reinforced more than the average natural meniscus, it may be able to withstand these higher internal stresses, so decreasing the size of different aspects of the implant may be of future interest. However, a smaller than anatomical implant may increase valgus/varus motion and decrease knee stability, so it was not changed for this implant. Along with the shape of the implant, the size was not adjusted. However, the implant was reinforced so that it was stronger in the circumferential and radial directions and at the attachment fibers than the natural meniscus. Additionally, the extreme compression test exceeded the load that would be seen in a 75% percentile weight man over 20 in the US. This gives confidence that the reinforcement of the implant may be sufficient for the majority of people so the implant size can be adjusted while keeping the number of fibers the same.

The sheep implant designed for device validation may have some shortcomings as well. Even though, the sheep implant was designed using the same methods as the human implant in terms of

matching fiber reinforcement to the strength of the natural meniscus, this could only be done for the circumferential fibers since no literature was found on radial fiber strength of the sheep meniscus. As a result, these fibers were simply scaled to the human radial fiber number by the same ratio as the circumferential fibers. Additionally, the shape of the sheep implant was chosen based on what best resembled the shape of the sheep meniscus instead of scaling all dimensions of the human meniscus down to a smaller size. As a result, the more symmetric anterior and posterior sides as well as the flatter nature of the sheep implant may result is tibial contact pressure or durability outcomes that do not resemble those of the implant when used in a human. Regardless, because the same materials and design methods were used for both the human and sheep implants, the pilot study should provide valuable insight into implant performance.

6.3 Improvements over Previous Implants

There are other groups that have experimented with PVA meniscus replacements. Earlier PVA implants developed by Kobayashi et al. did not include reinforcement and had sufficient strength to survive in a rabbit knee. However, they experienced radial tears in all devices when implanted in a sheep knee, which is likely to translate to the human knee where joint forces are also large [65, 66].

Another PVA implant developed by Holloway implemented reinforcement to strengthen the implant. These implants were reinforced with polyethylene weaves that were chosen for their strength and FDA approval for other devices used in the knee. Mechanical properties such as the tensile and compressive moduli and tibial contact pressure were focused on in the development process. Additionally, successful individual fiber pull out tests were performed on fiber/hydrogel samples; however, no tests were run modeling integration of an entire fiber weave. When the

implants were tested in a sheep model, complete delamination of the weave reinforcement from the hydrogel occurred in two of the three implants along with excessive radial extrusion [67].

Previous work on this implant lead to the development of the weave design. Kevlar fibers were used instead of polyethylene because of their strength and hydrophilic nature to better integrate with the PVA. Similar to the Holloway implant, development of the weave design focused on tensile strength and compressive moduli as well as fiber pull out strength and contact pressures. In this implant, the fibers were separated into circumferential fibers and general reinforcement, where the circumferential fibers were bundled together along the periphery of the implant and the general reinforcement was a weave of fibers spanning the body. An entire implant fiber pull out test was performed on the circumferential fibers. However, there was no delamination test performed on the weave fibers, which were the cause of delamination in the Holloway implant. Additionally, the bundled circumferential fibers did survive to loads experienced during gait, but they were not tested to higher loads or while integrated into the implant. These fibers were only as strong as the lower range of the natural meniscus, which raised concern for tearing and delamination.

The goal of the proposed implant was to optimize the fiber reinforcement to create an implant as strong as the natural meniscus, with the same compressive modulus, and that would not fail or lose functionality in the knee environment. More intense compression and delamination tests were developed to design the strongest implant across several variables chosen based on physiology and manufacturability. Additionally, the tests used the entire implant whenever possible, and when a sample had to be used, the area with the highest chance of failure was tested. Spacing the circumferential fibers throughout the body of the implant and sewing in radial fibers along the superior surface resulted in a stronger implant that was less likely to delaminate. Also, because the fibers were more evenly spread and because a smaller number were required, the compressive

modulus decreased to be within the range of the natural meniscus, which was not possible with the weave design. The durability and functionality of this new design were then tested using cyclic tests at higher loads than the gait simulations used for the other commercial and experimental implants.

Additional improvements were made with the sheep implants that may translate to the human design as well. Adding horn extrusions that went into the bone tunnels may increase fixation and protect the attachment fibers from wear at the bone tunnel entrance. Braiding the attachment fibers may also lead to more secure and easier attachment of the implant.

6.4 Future Directions

A next iteration of the FMECA was used to identify future steps for the development of the implant. The results are shown in Table 14. Unaddressed or partially covered failure modes were identified by RPN scores above 20. These were given recommended future actions that are highlighted. All of the mechanical properties of the implant itself were address and had low RPN scores. The majority of the high RPN scores are addressed by the animal study outlined in the design validation methods. In fact, this FMECA was used in addition to the user needs to design the animal study. Outside of the labeling and training, the remaining recommended actions were to provide implant size variations, implement boney fixation of the attachment fibers via biological or chemical additives, and adapt the horn design of the implant to standardize implantation so the device would be placed in the correct location on the tibia and a consistent distance from the bone tunnels. Most of these recommendations were performed for the sheep implant so the effectiveness of the chosen sizes and implant horn design could be evaluated in vivo before applying the same methodology to the human implant. Training of the surgeons and labeling the packaging for the

implant were also addressed during the cadaveric study; however, this was only for the application of a pilot study and should be thoroughly tested in future development.

Table 14: FMECA for future steps.

Design Function	Potential Failure Mode	Potential Effect(s) of Failure	S	Potential causes of failure	O	Current Design Controls	D	RPN	Recommended actions
Bulk meniscus strength	Partial radial tear	Slight mechanical impairment (popping, catching) from unsmooth implant surface	3	Insufficient radial longevity	2	Fiber cyclic testing; Implant design with radial reinforcement	1	6	None
			3	Insufficient radial strength	2	Fiber strength testing; Implant design with radial reinforcement	1	6	None
		Propagation risk to large size	4	Insufficient radial reinforcements throughout hydrogel	2	Fiber cyclic testing; Implant design with radial reinforcement near surface where tear originates; Implant compression and shear cyclic testing	1	8	None
	Large radial tear (90% or more)	Accelerated cartilage degeneration from increased contact pressure	4	Insufficient radial longevity/ strength/ reinforcement	2	Fiber cyclic and strength testing; Implant design with radial reinforcement near surface where tear originates; Implant high impact testing	1	8	None
		Pain/tenderness from increased contact pressure	4	Insufficient radial longevity/ strength/ reinforcement	2	Fiber cyclic and strength testing; Implant design with radial reinforcement near surface where tear originates; Implant high impact testing	1	8	None

Table 14 Continued

		Mechanical impairment (locking, buckling)	4	Insufficient radial longevity/ strength/ reinforcement	2	Fiber cyclic and strength testing; Implant design with radial reinforcement near surface where tear originates; Implant high impact testing	1	8	None
	Partial longitudinal tear	Slight mechanical impairment (popping, catching)	3	Insufficient longitudinal longevity/ strength	3	Circumferential cyclic and strength testing; Implant design with reinforcement	1	9	None
		Propagation risk to large size	4	Insufficient circumferential reinforcement throughout hydrogel	3	Circumferential cyclic and strength testing; Implant design with circumferential reinforcement throughout hydrogel cross-section; Implant compression and shear cyclic testing	1	12	None
	Complete longitudinal tear (bucket handle)	Accelerated cartilage degeneration from increased contact pressure	4	Insufficient longitudinal longevity/ strength/ reinforcement	3	Circumferential cyclic and strength testing; Implant design with circumferential reinforcement throughout hydrogel cross-section; Implant high impact testing	1	12	None
		Pain/tenderness from increased contact pressure	4	Insufficient longitudinal longevity/ strength/ reinforcement	3	Circumferential cyclic and strength testing; Implant design with circumferential reinforcement throughout hydrogel cross-section; Implant high impact testing	1	12	None
		Mechanical impairment	4	Insufficient longitudinal longevity/ strength/ reinforcement	3	Circumferential cyclic and strength	1	12	None

Table 14 Continued

		(locking, buckling)				testing; Implant design with circumferential reinforcement throughout hydrogel cross-section; Implant high impact testing			
	Horizontal tear	Meniscal cysts and local swelling	3	Insufficient hydrogel longevity/ strength	2	Composite shear cyclic testing	1	6	None
	Oblique tears	Mechanical impairment (flap catching)	4	Insufficient longitudinal or radial longevity/ strength/ reinforcement	3	Fiber cyclic and strength testing; Implant design with reinforcement spaced across hydrogel; Implant high impact testing	1	12	None
		Propagation risk to complete longitudinal	4	Insufficient longitudinal or radial reinforcement	3	Fiber cyclic and strength testing; Implant design with circumferential reinforcement throughout hydrogel cross-section; Implant compression and shear cyclic testing	1	12	None
	Compressive deformation	Joint space narrowing – potential increase in contact stress and cartilage damage	3	Insufficient hydrogel longevity/ compressive strength and stiffness	3	Compressive and cyclic testing for modulus and deformation; Implant compression cyclic testing	1	12	None
	Reinforcement/ attachment fiber tear out (partial)	Slight mechanical impairment (popping, catching) from loose fibers	3	Insufficient strength or number of reinforcing fibers	2	Tensile strength testing of composites	1	6	None
			3	Improper layout of reinforcing fibers	2	Fiber tear out testing of implants	1	6	None
		Reduced strength; risk of additional fibers breaking	4	Insufficient strength / number / improper layout of reinforcing fibers	2	Tensile strength and fiber tear out testing	2	16	None

Table 14 Continued

	Reinforcement/ attachment fiber tear out (complete)	Mechanical impairment (locking, buckling) from implant dislocation	4	Insufficient strength or number of reinforcing fibers	2	Tensile strength testing of composites	1	8	None
	Delamination of composite	Reduced stress transfer – potential increase in contact stress, cartilage damage, and hydrogel tear	3	Insufficient interfacial adhesion of reinforcing fibers and hydrogel	3	Fiber tear out testing of implants; Hydrophilic fibers; Shear cyclic testing	1	9	None
			3	Improper integration of fibers into hydrogel matrix	2	Fiber tear out testing of implants; Optimize reinforcement to increase fiber/ hydrogel surface interaction; Shear cyclic testing	2	12	None
		Mechanical impairment from dislocation of hydrogel component	4	Insufficient interfacial adhesion of reinforcing fibers and hydrogel	3	Fiber tear out testing of implants; Shear cyclic testing	1	12	None
			4	Improper integration of fibers into hydrogel matrix	2	Fiber tear out testing of implants; implant Optimize reinforcement to increase fiber/ hydrogel surface interaction; Shear cyclic testing	2	16	None
	Unnatural tibial pressure distribution	Accelerated cartilage degeneration from increased contact pressure	4	Insufficient tibial/femoral interfacing/strengths/fixation/geometry	3	Anatomic implant shape and fiber orientation for pressure distribution and implant tensile properties; Pressure distribution testing with reinforced/fixed implant	2	24	In vivo articular cartilage analysis
		Pain/tenderness from increased contact pressure	4	Insufficient tibial/femoral interfacing/strengths/fixation/geometry	3	Anatomic implant shape and fiber orientation for pressure distribution	2	24	In vivo articular cartilage analysis

Table 14 Continued

						and implant tensile properties; Pressure distribution testing with reinforced/fixed implant			
Fixation	Attachment tear at horns	Accelerated cartilage degeneration from insufficient tibial plateau coverage; Pain/tenderness from excessive extrusion	4	Insufficient attachment fiber strength	2	Attachment fiber tensile testing; Implant design with all circumferential fibers as attachment fibers	1	8	None
			4	Insufficient horn strength/reinforcement	3	Attachment fiber tensile testing; Implant design with slightly increased horn area; Implant high impact testing	1	12	None
	Radial extrusion	Accelerated cartilage degeneration from insufficient tibial plateau coverage; Pain/tenderness from excessive extrusion	4	Insufficient circumferential strength / reinforcement	3	Implant design with circumferential fibers; Tensile testing	1	12	None
			4	Improper layout of reinforcing fibers	3	Anatomic fiber orientation for implant tensile properties; Radial extrusion testing	2	24	In vivo macroscopic dislocation analysis
	Bone tunnel widening	Slight fixation impairment	1	Insufficient implant anchoring stiffness	3	Surgical design option specs from literature	4	12	None
	Implant dislocation	Slight fixation impairment	2	Insufficient implant anchoring stiffness	3	Fix implant using interference screws	3	18	In vivo macroscopic dislocation analysis
		Accelerated cartilage degeneration from insufficient tibial plateau coverage; Pain/tenderness from excessive extrusion	4	Implant anchoring slippage	3	Fix implant using interference screws	3	36	In vivo macroscopic dislocation analysis

Table 14 Continued

			4	Improper implant geometry	2	Implant design with anatomic geometry; Pressure distribution testing with reinforced/fixed implant	2	16	None
Implant/cartilage interface	Extensive wear of implant	Joint space narrowing – potential increase in contact stress and cartilage damage	3	Insufficient contact stress distribution	2	Pressure distribution testing with reinforced/fixed implant; Implant design with maximized contact area (curvature)	2	12	None
			3	Insufficient shear/tensile strength near surface (of hydrogel only)	2	Tensile and shear strength testing of hydrogel	2	12	None
		Inflammation from wear particles	4	Excessive number of wear particles from composite roughness and lubricity	1	PVA literature wear rate values	4	16	None
			4	Excessive size of wear particles from composite roughness	2	PVA literature wear particle sizes and in vivo performances	4	32	In vivo inflammation analysis
	Extensive wear of articular cartilage	Accelerated cartilage degeneration from wear	4	Insufficient contact stress distribution	2	Pressure distribution testing with reinforced/fixed implant; Implant design – maximized contact area (curvature)	3	24	In vivo macroscopic and histological articular cartilage analysis
		Slight mechanical impairment (popping, catching) from unsmooth implant surface	3	Excessive implant surface roughness	2	PVA literature roughness values	3	18	In vivo macroscopic and histological articular cartilage analysis; Implant design with surface roughness similar to that or articular cartilage
	Increased joint friction	Slight motion impairment	2	Insufficient lubricity/excessive roughness and stiffness	2	Implant design with stiff reinforcements further from interface and hydrogel material to maintain lubricity	3	12	None

Table 14 Continued

	Incompatible geometry with tibial and femoral surfaces	Excessive contact stresses from decreased contact area resulting in wear and accelerated cartilage degeneration	3	Inaccurate curvature of implant articulating surfaces.	2	Implant design with curved superior implant surface and hydrogel material will conform to interacting surface geometry	2	12	None
Compatibility	Host rejection	Inflammation from bulk composite	4	Insufficient biocompatibility of PVA	2	PVA literature in vivo results	2	16	In vivo inflammation analysis
		Bony reactions (Osteolysis)	4	Insufficient biocompatibility of PVA and Kevlar	2	PVA and Kevlar literature in vivo results	2	16	In vivo inflammation analysis
	Implant not compatible with adjunctive therapies	Altered physical properties or dimensional changes of implant	3	Inadequate labeling/training	2	None	4	24	Labeling/training
Packaging	Implant/package damaged during shipping	Procedure cannot be performed	2	Insufficient package strength/material	2		4	16	Sterilization validation, package testing
		Mechanically faulty implant inserted in patient	3	Insufficient package strength/material; insufficient fixation of implant in package	2		4	24	Sterilization validation, package testing
		Implant no longer sterilized	4	Insufficient package strength/material/insulation	2		4	32	Sterilization validation, package testing
	Packaging material contamination	Infection	4	Improper packaging material	2	Current packaging material literature review	3	24	Packaging must be EU accepted packaging
	No implant present in package	Procedure cannot be performed	2	Inadequate process qualification, inspection test plans	2		4	16	Process qualification and specifications, inspection test plans
	Implant package labeled incorrectly or wrong product in package	Improper implantation	4	Inadequate process qualification, inspection test plans	2		4	32	Process qualification and specifications, inspection test plans
	Package does not maintain shelf life	Implant performance degradation	3	Insufficient implant/package longevity	2		4	24	Implant/package mechanical aging studies
		Implant no longer sterilized	4	Insufficient package material/insulation longevity	2		4	32	Implant/package sterilization aging studies
	Implant installed following exposure to temperatures in excess of 49 C	Implant experiences degradation in performance	3	Inadequate labeling/training	2		4	24	Labeling/training

Table 14 Continued

	Packaging labels fall off	Temperature: Implant experiences degradation in performance	3	Insufficient package with label longevity	2		4	24	Package with label aging studies
		Implant type: Improper implantation	3	Insufficient package with label longevity	2		4	24	Package with label aging studies
Sterilization	Implant not sterile	Infection	4	Implant material not compatible with sterilization	2	PVA literature sterilization results	3	24	Sterilization validation, package testing
			4	Insufficient sterilization	2	Literature general sterilization results	4	32	Sterilization validation, package testing
Implantation	Internal exposure to environment during surgery	Infection	4	Excessively invasive procedure (not arthroscopic)	2	Implant design – flexible material; similar implantation as allografts	2	16	None
	Improper surgical technique - Physician damages implant during installation	Degradation of implant performance, premature failure	3	Inadequate training	2	Implant design – flexible, elastic material; similar implantation as allografts	3	18	Training
	Improper implant placement	Accelerated cartilage degeneration from insufficient tibial plateau coverage; Pain/tenderness from excessive extrusion	4	Incorrect surgical orientation/anchoring location	2	None	4	32	Adapt horn design to fit in desired location (bone tunnels); labeling/training
	Improper patient selection	Subjected to repetitive excessive loadings that could damage implant	3	Inadequate inspection test plans/labeling/training	2	None	4	24	Labeling/training
	Improper implant size selected	Pain/tenderness from excessive extrusion; limits range of motion	4	Implant size too large; inadequate training/labeling	2	Implant design - average meniscus geometry; Visualization during surgical procedure	4	32	Variety of size options; Labeling/training
		Accelerated cartilage degeneration from insufficient tibial plateau coverage; limits range of motion	4	Implant size too small; inadequate training/labeling	2	Implant design - average meniscus geometry	4	32	Variety of size options; Labeling/training

Table 14 Continued

	Physician modifies implant	Alters function of the device	3	Inadequate labeling/training	2	None	4	24	Labeling/training
	Osteophytes not properly removed	Unable to place device; premature implant compromise	3	Inadequate training	2	None	4	24	Training

6.5 Conclusion

The PVA reinforced with an 8 circumferential Kevlar fiber bundles spanning the width and height and 20 radial fibers spanning the A-P length of the superior surface of the implant was shown to be suitable as a meniscus replacement. The fiber layout was designed to mimic the natural meniscus and be durable and functional based on the design variables chosen, delamination tests, and compression and pressure distribution tests. The final design was tested and proved to be as compliant as the natural meniscus as well as have stronger attachment fibers. Further testing showed that the implant could survive the extreme and daily environment of the knee up to at least a year of use via high impact and cyclic compression and shear tests. Following these tests, the implant remained functional with tibial peak pressures below those experienced with the natural meniscus and radial extrusion less than that observed by a health meniscus. A sheep meniscus was designed using the same methods in order to evaluate the durability, biocompatibility, and chondroprotective function of the implant in vivo. Successful cadaveric studies were conducted to ensure the implant shape, size, and fixation was appropriate. Upon completion of this animal study, evidence will be provided whether this implant could provide a superior treatment option for patients in need of a meniscus replacement.

REFERENCES

1. Verma, N., et al., *The Effects of Medial Meniscal Transplantation Techniques on Intra-Articular Contact Pressures.* J Knee Surg. , 2008. **21**: p. 20-26.

2. Baratz, M.E., F.H. Fu, and R. Mengato, *Meniscal tears: the effect of meniscectomy and of repair on intraarticular contact areas and stress in the human knee: a preliminary report.* Am J Sports Med, 1986. **14**(270).

3. Fox, A.J., A. Bedi, and S.A. Rodeo, *The basic science of human knee menisci: structure, composition, and function.* Sports Health, 2012. **4**(4): p. 340-51.

4. Fox, A.J., et al., *The human meniscus: a review of anatomy, function, injury, and advances in treatment.* Clin Anat, 2015. **28**(2): p. 269-87.

5. Makris, E.A., P. Hadidi, and K.A. Athanasiou, *The knee meniscus: structure-function, pathophysiology, current repair techniques, and prospects for regeneration.* Biomaterials, 2011. **32**(30): p. 7411-31.

6. Messner, K. and J. Gao, *The menisci of the knee joint. Anatomical and functional characteristics, and a rationale for clinical treatment.* J. Anat., 1998. **193**: p. 161-178.

7. Krause, W.R., et al., *Mechanical changes in the knee after meniscectomy.* J. Bone Joint Surg. Am., 1976. **58**(5): p. 599-604.

8. Jones, R.S., et al., *Direct measurement of hoop strains in the intact and torn human medial meniscus.* Clinical Biomechanics, 1996. **11**(5): p. 295-300.

9. Skaggs, D.L., W.H. Warden, and M. V.C, *Radial tie fibers influence the tensile properties of the bovine medial meniscus.* J. Orthop. Res., 1994. **12**(2): p. 176-185.

10. McDermott, I.D., S.D. Masouros, and A.A. Amis, *Biomechanics of the menisci of the knee.* Current Orthopaedics, 2008. **22**(3): p. 193-201.

11. Bullough, P., et al., *The Strength of the Menisci of the Knee as it Relates to Their Fine Structure.* J. Bone and Joint Surgery, 1970. **52-B**(3).

12. Beaupré, A., et al., *Knee menisci. Correlation between microstructure and biomechanics.* Clin. Orthop. Relat. Res., 1986. **5**(208).

13. Petersen, W. and B. Tillmann, *Collagenous fibril texture of the human knee joint menisci.* Anat Embryol, 1998. **197**: p. 317-324.

14. Masouros, S.D., et al., *Biomechanics of the meniscus-meniscal ligament construct of the knee.* Knee Surg Sports Traumatol Arthrosc, 2008. **16**(12): p. 1121-32.

15. Jones, J.C., et al., *Incidence and Risk Factors Associated with Meniscallnjuries Among Active-Duty US Military Service Members.* J. ofAthletic Training, 2012. **47**(1): p. 67-73.

16. Majewski, M., H. Susanne, and S. Klaus, *Epidemiology of athletic knee injuries: A 10-year study.* Knee, 2006. **13**(3): p. 184-8.

17. Garrett, W.E., et al., *American Board of Orthopaedic Surgery Practice of the Orthopaedic Surgeon: Part-II, Certification Examination Case Mix.* J. Cone and Joint Surgery, 2006. **88-A**(3).

18. Vrancken, A.C., P. Buma, and T.G. van Tienen, *Synthetic meniscus replacement: a review.* Int Orthop, 2013. **37**(2): p. 291-9.

19. Pekkerman, B., P. Ralhan, and R. Chang, *Meniscus Injuries of the Knee.* American Academy of Physical Medicine and Rehabilitation, 2013.

20. Dangelmajer, S., et al., *Meniscal Transplants and Scaffolds: A Systematic Review of the Literature.* Knee Surg Relat Res, 2017. **29**(1): p. 3-10.

21. Post, E.G., et al., *The Association of Sport Specialization and Training Volume With Injury History in Youth Athletes.* Am J Sports Med, 2017. **45**(6): p. 1405-1412.

22. Schepsis, A.A. and B.D. Busconi, *Lower Extremity.* Sports Medicine, 2006.

23. Browner, B.D., et al., *Skeletal Trauma.* Basic Science, 2003(3).

24. Drosos, G.I. and J.L. Pozo, *The causes and mechanisms of meniscal injuries in the sporting and non-sporting environment in an unselected population.* The Knee, 2004. **11**(2): p. 143-149.

25. Terzidis, I.P., et al., *Meniscal tear characteristics in young athletes with a stable knee: arthroscopic evaluation.* Am J Sports Med, 2006. **34**(7): p. 1170-5.

26. Kijima, H., et al., *Relationship between Pain and Medial Meniscal Extrusion in Knee Osteoarthritis.* Adv Orthop, 2015. **2015**: p. 210972.

27. Yanagisawa, *Population-based study of the relationship between medial meniscus radial displacement, determined by use of ultrasound screening, and knee pain.*

28. Roos, H., et al., *Knee Osteoarthritis after Meniscectomy.* ARTHRITIS & RHEUMATISM, 1998. **41**(4): p. 687-693.

29. Swamy, N., et al., *Medial meniscal extrusion: Detection, evaluation and clinical implications.* Eur J Radiol, 2018. **102**: p. 115-124.

30. Vrancken, A.C., et al., *Functional biomechanical performance of a novel anatomically shaped polycarbonate urethane total meniscus replacement.* Knee Surg Sports Traumatol Arthrosc, 2016. **24**(5): p. 1485-94.

31. Lecouvet, F., et al., *Magnetic resonance imaging (MRI) of the knee: Identification of difficult-to-diagnose meniscal lesions.* Diagn Interv Imaging, 2018. **99**(2): p. 55-64.

32. Cannon, W.D. and J.M. Vittori, *The incidence of healing in arthroscopic meniscal repairs in anterior cruciate ligamentreconstructed knees versus stable knees.* Am J Sports Med, 1992. **20**: p. 176-181.

33. Daniel, D.M., et al., *Fate of the ACL-injured patient. A prospective outcome study.* Am J Sports Med, 1994. **22**: p. 632-644.

34. Shelbourne, K.D. and C. Klotz, *What I have learned about the ACL: utilizing a progressive rehabilitation scheme to achieve total knee symmetry after anterior cruciate ligament reconstruction.* J Orthop Sci, 2006. **11**(3): p. 318-25.

35. Taylor, S.A. and S.A. Rodeo, *Augmentation techniques for isolated meniscal tears.* Curr Rev Musculoskelet Med, 2013. **6**(2): p. 95-101.

36. Montgomery, S.R., et al., *Cross-sectional analysis of trends in meniscectomy and meniscus repair.* Orthopedics, 2013. **36**(8): p. e1007-13.

37. Fukubayashi, T. and H. Kurosawa, *The contact area and pressure distribution pattern of the knee. A study of normal and osteoarthrotic knee joints.* Acta Orthop Scand, 1980. **51**(6): p. 871-9.

38. Henning, C.E., M.A. Lynch, and J.R. Clark, *Vascularity for Healing of Meniscus Repairs.* J. Arthroscopic and Related Surgery, 1987. **3**(1): p. 13-18.

39. Englund, M., E.M. Roos, and L.S. Lohmander, *Impact of type of meniscal tear on radiographic and symptomatic knee osteoarthritis: a sixteen-year followup of meniscectomy with matched controls.* Arthritis Rheum, 2003. **48**(8): p. 2178-87.

40. Verdonk, R., et al., *Indications and limits of meniscal allografts.* Injury, 2013. **44**: p. S21-S27.

41. McCormick, F., et al., *Survival and reoperation rates after meniscal allograft transplantation: analysis of failures for 172 consecutive transplants at a minimum 2-year follow-up.* Am J Sports Med, 2014. **42**(4): p. 892-7.

42. Kazi, H.A., et al., *Meniscal allograft with or without osteotomy: a 15-year follow-up study.* Knee Surg Sports Traumatol Arthrosc, 2015. **23**(1): p. 303-9.

43. Abat, F., et al., *Prospective comparative study between two different fixation techniques in meniscal allograft transplantation.* Knee Surg Sports Traumatol Arthrosc, 2013. **21**(7): p. 1516-22.

44. Gonzalez-Lucena, G., et al., *Meniscal allograft transplantation without bone blocks: a 5- to 8-year follow-up of 33 patients.* Arthroscopy, 2010. **26**(12): p. 1633-40.

45. Kempshall, P.J., et al., *Outcome of meniscal allograft transplantation related to articular cartilage status: advanced chondral damage should not be a contraindication.* Knee Surg Sports Traumatol Arthrosc, 2015. **23**(1): p. 280-9.

46. Hergan, D., et al., *Meniscal allograft transplantation.* Arthroscopy, 2011. **27**(1): p. 101-12.

47. Vundelinckx, B., J. Bellemans, and J. Vanlauwe, *Arthroscopically assisted meniscal allograft transplantation in the knee: a medium-term subjective, clinical, and radiographical outcome evaluation.* Am J Sports Med, 2010. **38**(11): p. 2240-7.

48. Lubowitz, J.H., et al., *Meniscus allograft transplantation: a current concepts review.* Knee Surg Sports Traumatol Arthrosc, 2007. **15**(5): p. 476-92.

49. Brophy, R.H. and M.J. Matava, *Surgical options for meniscal replacement.* J Am Acad Orthop Surg, 2012. **20**(5): p. 265-72.

50. Zaffagnini, S., et al., *Prospective long-term outcomes of the medial collagen meniscus implant versus partial medial meniscectomy: a minimum 10-year follow-up study.* Am J Sports Med, 2011. **39**(5): p. 977-85.

51. Monllau, J.C., X. Pelfort, and M. Tey, *Collagen Meniscus Implant: Technique and Results.* Springer Berlin Heidelberg, 2010: p. 373-382.

52. Monllau, J.C., et al., *Outcome after partial medial meniscus substitution with the collagen meniscal implant at a minimum of 10 years' follow-up.* Arthroscopy, 2011. **27**(7): p. 933-43.

53. Ginés, A., et al., *Collagen Meniscus Implant. Outcomes After 4 to 7 Years.* Orthop. Proc., 2006. **88-B**(2): p. 329.

54. Spencer, S.J., et al., *Meniscal scaffolds: early experience and review of the literature.* Knee, 2012. **19**(6): p. 760-5.

55. Rodkey, W.G., et al., *Comparison of the collagen meniscus implant with partial meniscectomy. A prospective randomized trial.* J Bone Joint Surg Am, 2008. **90**(7): p. 1413-26.

56. Tienen, T.G., R.G. Heijkants, and G. J.H., *Replacement of the knee meniscus by a porous polymer implant: a study in dogs.* Am J Sports Med, 2006. **34**(1): p. 64-71.

57. Welsing, R.T., T.G. Van Tienen, and N. Ramrattan, *Effect on tissue differentiation and articular cartilage degradation of a polymer meniscus implant: a 2-year follow-up study in dogs.* Am J Sports Med, 2008. **36**(10): p. 1978-1989.

58. Verdonk, R., et al., *Tissue ingrowth after implantation of a novel, biodegradable polyurethane scaffold for treatment of partial meniscal lesions.* Am J Sports Med., 2011. **82**(39).

59. Van Der Straeten, C., et al., *Short- and Medium-Term Results of Artificial Meniscal Implants.* Orthopaedic Proceedings, 2018. **98-B**(4).

60. Leroy, A., et al., *Actifit((R)) polyurethane meniscal scaffold: MRI and functional outcomes after a minimum follow-up of 5 years.* Orthop Traumatol Surg Res, 2017. **103**(4): p. 609-614.

61. Verdonk, P., et al., *Successful treatment of painful irreparable partial meniscal defects with a polyurethane scaffold: two-year safety and clinical outcomes.* Am J Sports Med, 2012. **40**(4): p. 844-53.

62. Pederson, A., *First 'Artificial Meniscus' Wins FDA Breakthrough Device Designation.* Med Device and Diagnostic Ind, 2019.

63. Vrancken, A.C.T., et al., *In Vivo Performance of a Novel, Anatomically Shaped, Total Meniscal Prosthesis Made of Polycarbonate Urethane: A 12-Month Evaluation in Goats.* Am J Sports Med, 2017. **45**(12): p. 2824-2834.

64. Kobayashi, M., J. Toguchida, and M. Oka, *Preliminary study of polyvinyl alcohol-hydrogel (PVA-H) artificial meniscus.* Biomaterials, 2003. **24**(4): p. 639-647.

65. Kobayashi, M., Y.S. Chang, and M. Oka, *A two year in vivo study of polyvinyl alcohol-hydrogel (PVA-H) artificial meniscus.* Biomaterials, 2005. **26**(16): p. 3243-3248.

66. Kelly, B.T., et al., *Hydrogel meniscal replacement in the sheep knee: preliminary evaluation of chondroprotective effects.* Am J Sports Med, 2007. **35**(1): p. 43-52.

67. Holloway, J.L., *Development and Characterization of UHMWPE Fiber-Reinforced Hydrogels For Meniscal Replacement.* Drexel University, 2012.

68. Medical, A., *Meniscus of the knee.* 2020.

69. Schwartz, J.W., *Design and Mechanical Evaluation of an Artificial Meniscus Implant.* Georgia Institute of Technology, 2018.

70. Lozinsky, V.I., et al., *Study of cryostructuring of polymer systems: 28. Physicochemical properties and morphology of poly(vinyl alcohol) cryogels formed by multiple freezing-thawing.* Colloid J., 2008. **70**(2): p. 189-198.

71. Ricciardi, R., et al., *Investigation of the Crystallinity of Freeze/Thaw Poly(vinyl alcohol) Hydrogels by Different Techniques.* Macromolecules, 2004. **37**(25): p. 9510-9516.

72. Peppas, N.A., *Turbidimetric studies of aqueous poly(vinyl alcohol) solutions.* Die Makromol. Chemie, 1975. **176**(11): p. 3433-3440.

73. Stauffer, S.R. and N.A. Peppas, *Poly(vinyl alcohol) hydrogels prepared by freezing-thawing cyclic processing.* Polymer (Guildf). 1992. **33**(18): p. 3932-3936.

74. Holloway, J.L., A.M. Lowman, and G.R. Palmese, *Mechanical evaluation of poly(vinyl alcohol)-based fibrous composites as biomaterials for meniscal tissue replacement.* Acta Biomater., 2010. **6**(12): p. 4716-4724.

75. Spiller, K.L., et al., *Superporous hydrogels for cartilage repair: Evaluation of the morphological and mechanical properties.* Acta Biomater., 2008. **4**(1): p. 17-25.

76. Baker, M.I., et al., *A review of polyvinyl alcohol and its uses in cartilage and orthopedic applications.* J Biomed Mater Res B Appl Biomater, 2012. **100**(5): p. 1451-7.

77. Chang, Y.S., et al., *Comparison of the bony ingrowth into an osteochondral defect and an artificial osteochondral composite device in load-bearing joints.* Knee, 1998. **5**(3): p. 205-213.

78. Oliveira, A.S., et al., *Tough and Low Friction Polyvinyl Alcohol Hydrogels Loaded with Anti-inflammatories for Cartilage Replacement.* Lubricants, 2020. **8**(3).

79. Goldberg, A., et al., *Association Between Patient Factors and Outcome of Synthetic Cartilage Implant Hemiarthroplasty vs First Metatarsophalangeal Joint Arthrodesis in Advanced Hallux Rigidus.* Foot Ankle Int, 2017. **38**(11): p. 1199-1206.

80. Baumhauer, J.F., et al., *Prospective, Randomized, Multi-centered Clinical Trial Assessing Safety and Efficacy of a Synthetic Cartilage Implant Versus First Metatarsophalangeal Arthrodesis in Advanced Hallux Rigidus.* Foot Ankle Int, 2016. **37**(5): p. 457-69.

81. Glazebrook, M., et al., *Midterm Outcomes of a Synthetic Cartilage Implant for the First Metatarsophalangeal Joint in Advanced Hallux Rigidus.* Foot Ankle Int, 2019. **40**(4): p. 374-383.

82. Zimmerman, M. and K.E. Gordon, *Tendon cell outgrowth rates and morphology associated with kevlar-49.* J. Biomed. Mater. Res.: Applied Biomaterials, 1988. **22**(A3): p. 339-350.

83. Ellman, M.B., et al., *Structural Properties of the Meniscal Roots.* Am J Sports Med, 2014. **42**(8): p. 1881-7.

84. Fithian, D.C., M.A. Kelly, and V.C. Mow, *Material properties and structure-function relationships in the menisci.* Clin. Orthop. Relat. Res., 1990(252): p. 19-31.

85. Tissakht, M. and A.M. Ahmed, *Tensile stress-strain characteristics of the human meniscal material.* J. Biomech, 1995. **28**(4): p. 411-422.

86. Bruni, D., et al., *Unicompartmental knee replacement: A historical overview.* Joints, 2013. **1**(2): p. 45-47.

87. McDowell, M., et al., *Anthropometric reference data for children and adults: United States, 2003-2006.* Natl. Health Stat. Report., 2008(10).

88. Chia, H.N. and M.L. Hull, *Compressive moduli of the human medial meniscus in the axial and radial directions at equilibrium and at a physiological strain rate.* J Orthop Res, 2008. **26**(7): p. 951-6.

89. Fischenich, K.M., et al., *Dynamic compression of human and ovine meniscal tissue compared with a potential thermoplastic elastomer hydrogel replacement.* J Biomed Mater Res A, 2017. **105**(10): p. 2722-2728.

90. Franceschini, F. and M. Galetto, *A new approach for evaluation of risk priorities of failure modes in FMEA.* International Journal of Production Research, 2001. **39**(13): p. 2991-3002.

91. Elattar, M., et al., *Twenty-six years of meniscal allograft transplantation: is it still experimental? A meta-analysis of 44 trials.* Knee Surg Sports Traumatol Arthrosc, 2011. **19**(2): p. 147-57.

92. Vrancken, A.C., et al., *Short Term Evaluation of an Anatomically Shaped Polycarbonate Urethane Total Meniscus Replacement in a Goat Model.* PLoS One, 2015. **10**(7): p. e0133138.

93. Straeten, C.V.D., *SHORT- AND MEDIUM-TERM RESULTS OF ARTIFICIAL MENISCAL IMPLANTS.*

94. Zur, G., et al., *Chondroprotective effects of a polycarbonate-urethane meniscal implant: histopathological results in a sheep model.* Knee Surg Sports Traumatol Arthrosc, 2011. **19**(2): p. 255-63.

95. Drakos, M. and A. Allen, *Meniscal Structure, Function, Repair, and Replacement.* Oncology and Basic Science, 2016.

96. Peloquin, J.M., M.H. Santare, and D.M. Elliott, *Advances in Quantification of Meniscus Tensile Mechanics Including Nonlinearity, Yield, and Failure.* J Biomech Eng, 2016. **138**(2): p. 021002.

97. SWEIGART, M.A., et al., *Intraspecies and Interspecies Comparison of the Compressive Properties of the Medial Meniscus.* Ann. Biomed. Eng., 2004. **32**(11): p. 1569-1579.

98. Joshi, M.D., et al., *Interspecies variation of compressive biomechanical properties of the meniscus.* J Biomed Mater Res, 1995. **29**(7): p. 823-8.

99. Kutzner, I., et al., *Loading of the knee joint during activities of daily living measured in vivo in five subjects.* J Biomech, 2010. **43**(11): p. 2164-73.

100. Heinlein, B., et al., *ESB Clinical Biomechanics Award 2008: Complete data of total knee replacement loading for level walking and stair climbing measured in vivo with a follow-up of 6-10 months.* Clin Biomech (Bristol, Avon), 2009. **24**(4): p. 315-26.

101. Kumar, D., K.T. Manal, and K.S. Rudolph, *Knee joint loading during gait in healthy controls and individuals with knee osteoarthritis.* Osteoarthritis Cartilage, 2013. **21**(2): p. 298-305.

102. Fryar, C.D., et al., *Anthropometric reference data for children and adults: United States, 2011–2014.* National Center for Health Statistics. Vital Health Stat, 2016. **3**(39).

103. Bassett, D.R., A.L. Cureton, and B.E. Ainsworth, *Measurement of daily walking distancequestionnaire versus pedometer.* MEDICINE & SCIENCE IN SPORTS & EXERCISE, 1999.

104. Boxheimer, L., et al., *MR Imaging of the Knee: Position Related Changes of the Menisci in Asymptomatic Volunteers.* Investigative Radiology, 2004. **39**(5): p. 254-263.

105. Muzaffar, N., et al., *Meniscal Extrusion in the Knee: Should only 3 mm Extrusion be Considered Significant? An Assessment by MRI and Arthroscopy.* Malays Orthop J, 2015. **9**(2): p. 17-20.

106. D'Lima, D.D., et al., *The 2011 ABJS Nicolas Andry Award: 'Lab'-in-a-knee: in vivo knee forces, kinematics, and contact analysis.* Clin Orthop Relat Res, 2011. **469**(10): p. 2953-70.

107. Hull, M.L., *A Finite Element Model of the Human Knee Joint for the Study of Tibio-Femoral Contact.* Journal of Biomechanical Engineering, 2002. **124**(3).

108. Elsner, J.J., et al., *Design of a free-floating polycarbonate-urethane meniscal implant using finite element modeling and experimental validation.* J Biomech Eng, 2010. **132**(9): p. 095001.

109. Shemesh, M., et al., *Viscoelastic properties of a synthetic meniscus implant.* J Mech Behav Biomed Mater, 2014. **29**: p. 42-55.

110. Yan, Y., *Developments in fibers for technical nonwovens*, in *Advances in Technical Nonwovens*. 2016. p. 19-96.

111. Peppas, N.A. and P.J. Hansen, *Crystallization Kinetics of Poly(viny1 Alcohol).* Journal of Applied Polymer Science, 1982. **27**: p. 4787-4797.

112. Ahmed, A.M. and D.L. Burke, *In-vitro measurement of static pressure distribution in synovial joints - Part I: Tibial surface of the knee.* J. Biomech. Eng., 1983. **105**(3): p. 216-225.

113. Elsner, J.J., et al., *DESIGN OPTIMIZATION OF A POLYCARBONATE-URETHANE MENISCAL IMPLANT IN THE SHEEP KNEE: IN-VITRO STUDY.* ASME 2010 Summer Bioengineering Conference, 2019.

114. Cohen, Z.A., et al., *Knee cartilage topography, thickness, and contact areas from MRI: in-vitro calibration and in-vivo measurements.* Osteoarthritis and Cartilage, 1999. **7**: p. 95-109.

115. Shepherd, D. and B. Seedhom, *Thickness of human articular cartilage in joints of the lower limb.* Ann Rheum Dis, 1999. **58**: p. 27-34.

116. Kahlenberg, C.A., et al., *Patient Satisfaction After Total Knee Replacement: A Systematic Review.* HSS J, 2018. **14**(2): p. 192-201.

117. Cook, J.L., *The current status of treatment for large meniscal defects.* Clin. Orthop. Relat. Res., 2005(435): p. 88-95.

118. Hede, A., E. Larsen, and H. Sandberg, *The long term outcome of open total and partial meniscectomy related to the quantity and site of the meniscus removed.* Int. Orthop., 1992. **16**(2): p. 122-125.

119. Arnoczky, S.P., et al., *Translational Models for Studying Meniscal Repair and Replacement: What They Can and Cannot Tell Us.* Tissue Eng Part B, 2010. **16**(1).

120. Takroni, T., et al., *Anatomical study: comparing the human, sheep and pig knee meniscus.* J Exp Orthop, 2016. **3**(1): p. 35.

121. Sandmann, G.H., et al., *Biomechanical comparison of menisci from different species and artificial constructs.* BMC Musculoskeletal Disorders, 2013. **14**.

122. Maher, S.A., et al., *A pre-clinical test platform for the functional evaluation of scaffolds for musculoskeletal defects: the meniscus.* HSS J, 2011. **7**(2): p. 157-63.

123. Chevrier, A., et al., *Meniscus structure in human, sheep, and rabbit for animal models of meniscus repair.* J Orthop Res, 2009. **27**(9): p. 1197-203.

124. Burger, C., et al., *The sheep as a knee osteoarthritis model: early cartilage changes after meniscus injury and repair.* Lab Anim, 2007. **41**(4): p. 420-31.

125. Little, C.B., et al., *The OARSI histopathology initiative - recommendations for histological assessments of osteoarthritis in sheep and goats.* Osteoarthritis Cartilage, 2010. **18 Suppl 3**: p. S80-92.

126. Gregory, M.H., et al., *A review of translational animal models for knee osteoarthritis.* Arthritis, 2012. **2012**: p. 764621.

127. Aagaard, H. and R. Verdonk, *Function of the normal meniscus and consequences of meniscal resection.* J Med Sci Sports, 1999. **9**: p. 134-140.

128. Covert, R.J., R.D. Ott, and D.N. Ku, *Friction characteristics of a potential articular cartilage biomaterial.* Wear, 2003. **255**(7-12): p. 1064-1068.

129. Brzezinski, A., et al., *The Ovine Model for Meniscus Tissue Engineering: Considerations of Anatomy, Function, Implantation, and Evaluation.* Tissue Eng Part C Methods, 2017. **23**(12): p. 829-841.

130. Huang, A., et al., *Identification of Cross-Sectional Parameters of Lateral Meniscal Allografts That Predict Tibial Contact Pressure in Human Cadaveric Knees.* Journal of Biomechanical Engineering, 2002. **124**(5).

131. Khoshgoftar, M., et al., *The sensitivity of cartilage contact pressures in the knee joint to the size and shape of an anatomically shaped meniscal implant.* J Biomech, 2015. **48**(8): p. 1427-35.

132. Vrancken, A.C., et al., *3D geometry analysis of the medial meniscus--a statistical shape modeling approach.* J Anat, 2014. **225**(4): p. 395-402.

133. Meakin, J.R., et al., *Finite element analysis of the meniscus: the influence of geometry and material properties on its behaviour.* The Knee, 2003. **10**(1): p. 33-41.